Ultrasonic technique for vibration measurement of immersed primary components in FBRs

by

V. PRAKASH

Enrollment No: ENGG02200804006

Indira Gandhi Centre for Atomic Research
Kalpakkam

Thesis Submitted to Board of Studies in Engineering Sciences

for Total Fulfillment to the Requirements of

Doctor of Philosophy

of

Homi Bhabha National Institute, Mumbai

August, 2015

Homi Bhabha National Institute

Recommendations of the Viva-Voce Committee

As members of the Viva-Voce Committee, we certify that we read the dissertation prepared by V. Prakash entitled **"Ultrasonic technique for vibration measurement of immersed primary components in FBRs"** and recommend that it may be accepted as fulfilling the thesis requirement for the award of Degree of Doctor of Philosophy.

Chairman	- Dr. M. Sai Baba	Date: 29-8-16
Guide	- Prof. Krishnan Balasubramanian	Date: 29/8/16
Examiner	- R.I.K. Moorthy	Date: 29/8/16
Member- 1	- Dr. B.P.C. Rao	Date: 29/8/16
Member- 2	- Dr. K. Velusamy	Date: 29/8/2016

Final approval and acceptance of this dissertation is contingent upon the candidate's submission of final copies of the thesis to HBNI.

I hereby certify that I have read this thesis prepared under my direction and recommend that it may be accepted as fulfilling the thesis requirement.

Place : Kalpakkam

Date : 29/8/16

Prof. Krishnan Balasubramanian
(Guide)

Homi Bhabha National Institute

Certificate

I, Krishnan Balasubramanian, certify that all the corrections suggested by the external examiner for the dissertation by Shri. V. Prakash titled **"Ultrasonic technique for vibration measurement of immersed primary components in FBRs"** have been duly incorporated in the revised version of the thesis. Therefore, the revised thesis report has been bound and submitted to HBNI for the Degree of Doctor of Philosophy.

Kalpakkam

29 August 2016

Prof. Krishnan Balasubramanian

(Guide)

Statement by Author

This dissertation has been submitted in partial fulfillment of requirements for an advanced degree at Homi Bhabha National Institute (HBNI) and is deposited in the library to be made available to borrowers under the rules of HBNI.

Brief quotations from this dissertation are allowable without special permission provided that accurate acknowledgement of source is made. Requests for permission for extended quotation from or reproduction of this manuscript in whole or in part may be granted by competent authority of HBNI when in his or her judgment the proposed use of materials in the interest of scholarship. In all other instances, permission must be obtained from the author.

Place: Kalpakkam

Date : 25.08.2015

(V. Prakash)

Declaration

I declare that the thesis entitled "Ultrasonic technique for vibration measurement of immersed primary components in FBRs" submitted to Homi Bhabha National Institute for the award of Doctor of Philosophy in Mechanical Engineering is original research carried out by me under the supervision of Prof. Krishnan Balasubramanian, Indian Institute of Technology, Chennai.

The work reported in this thesis has not been used for the award of any other degree or diploma.

Place: Kalpakkam

Date : 25.08.2015

(V. Prakash)

List of publications arising from the thesis

Journal Publications

1) **V.Prakash**, P.Anup Kumar, K.K.Rajan, Dr.Krishnan Balasubramanian, "Ultrasonic Technique for vibration measurements on PFBR fuel subassemblies", Accepted for publication in Journal of Vibration Engineering and Technologies (2015).

2) **V.Prakash**, M.Thirumalai, M.Anandaraj, P.Anup Kumar, D.Ramadasu, G.K.Pandey, G.Padmakumar, C.Anandababu, and K.K.Rajan "Experimental qualification of subassembly design for Prototype Fast Breeder Reactor", Nuclear Engineering and Design 241 (2011) 3325– 3332.

3) **V.Prakash**, P.Anup Kumar, M.Anadaraj, M.Thirumalai,C.Anandababu and K.K.Rajan "Flow induced vibration studies on PFBR control plug components", Nuclear Engineering and Design, Vol. 250, Sep 2012, pp. 725–734

4) **V.Prakash,** M.Thirumalai, R.Prabhakar and G.Vaidyanathan "Assessment of flow induced vibration in sodium-sodium heat exchanger, Nuclear Engineering and Design, Vol. 239, 2009, pp. 169-179.

5) P. Anup Kumar, R. Vidhyalakshmi, M. Thirumalai, S. Chandramouli and **V. Prakash**, "Development of SONAR device for fuel subassembly vibration measurement in PFBR", Journal of Acoustic Society of India, Vol 41, No. 3, 2014 (pp. 137-143).

6) R. Ramakrishna, P. Anup Kumar, M. Anandaraj, M. Thirumalai, **V. Prakash**, C. Anandbabu and P. Kalyanasundaram, NDE Technique for Reactor Core Vibration Measurement in FBRs, Journal of Non destructive Testing & Evaluation, Vol. 10, Issue 2 September 2011.

7) M. Thirumalai, M. Anandaraj, P. Anup Kumar, **V. Prakash**, C. Anandbabu, P. Kalyanasundaram, G. Vaidyanathan, Experimental investigation of weir instability in main vessel, Nuclear Engg. & Design, Volume 240 (2010), 84-91.

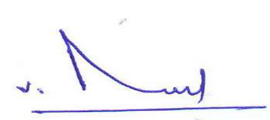

(V. Prakash)

Seminars and conferences

1. P. Anup Kumar, R. Vidhyalakshmi, Sudheer Patri, S. Chandramouli, **V. Prakash**, et. al., Vibration measurements on PFBR fuel subassemblies, Int. Conf. VETOMAC X 2014, September 9-11, 2014, Manchester, UK.
2. P. Anup Kumar, R. Vidhyalakshmi, S. Chandramouli, **V. Prakash**, et. al., Development of SONAR device for fuel subassembly vibration measurement in PFBR, Acoustics 2013 Conference, New Delhi, India.
3. **V.Prakash**, P.Anup Kumar, M.Anandraj, M.Thirumalai, G.K.Pandey, Piyush Agarwal, Indranil banerjee, G.Padmakumar, C.Anadbabu, K.K.Rajan, Thermal hydraulics and FIV experiments simulating the reactor assembly of FBR, SMiRT Post conference Seminar on Fast Reactor Design, 14-15, November, 2011, Kalpakkam, India
4. R.Ramakrishna, P.Anup kumar, M.Anandraj, M.Thirumalai, **V.Prakash**, C.Anandababu and P.Kalyanasundram, NDE Technique for Core vibration measurement in FBRs, NDE 2010, Kolkata, India.
5. M. Anandaraj, P. Anup Kumar, R. Ramakrishna, M. Thirumalai, **V. Prakash**, C. Anandbabu and P. Kalyanasundaram, Flow induced vibration studies on PFBR fuel subassembly, 2nd Int. Conference on Asian Nuclear Prospects 2010, ANUP-2010, 11-13 Oct 2010, Chennai, Tamilnadu, India.
6. M.Thirumalai, **V.Prakash**, M.Anandaraj, P.Anupkumar, D.Ramdasu, G.K.Pandey, G.Padmakumar, C.Anandbabu, P.Kalyanasundaram, G.Vaidyanathan, Subassembly Hydraulic Experiments, THEME Meeting on Challenges in Thermal Hydraulics of Nuclear Reactors; TM-CTHNR 2010, Feb 18-19, 2010; Kalpakkam, India.
7. R.Ramakrishna, M.Anandaraj, M.Thirumalai, P.Anup Kumar, P.Anitha, C.Asokane, **V.Prakash**, P.Kalyanasundaram, Flow Induced Vibration measurement using Ultrasonic Technique, International Conference on Sensors & Related Networks, SENNET 09, Dec 07-10, 2009; VIT, Vellore, India.

(V. Prakash)

Dedicated to my Parents,

Wife and Children

Acknowledgement

I am immensely grateful to my Research Guide Prof. Krishnan Balasubramanian, Indian Institute of Technology, Chennai, for his invaluable guidance in the right direction to complete this work.

I am thankful to Chairman of my Doctoral Committee Dr. M. Sai Baba and members of my Doctoral Committee Dr.B.P.C.Rao and Dr.K.Velusamy for their useful suggestions in my research work.

I owe my sincere thanks to Dr. Baldev Raj, Former Director, IGCAR for granting permission to do Ph.D and allowing me to use various facilities in IGCAR.

I am grateful to Dr. P. Kalyanasundaram, Former Director, FRTG for helping me to get permission and showing interest in my research work. I am thankful to Shri. R Prabhakar Former Director (Technical), BHAVINI for very useful discussions during the course of this research work. I am also thankful to Dr. K.K. Rajan, Director, FRTG for the encouragement given during the manufacture and testing of SONAR device.

I acknowledge the help rendered by my colleagues Shri. P. Anup Kumar, Shri. Hemanth Prakash Agnihotri and Shri. J. Jaikanth in various studies carried out as part of this research work. I also acknowledge the contributions of Shri. C. Asokane, Shri. M.R. Jayan and Shri. Saju Abraham for their help in the development and testing of ultrasonic sensors and SONAR device.

I place on record my thanks to Ms. K. Kavitha for providing typing, printing and other supports.

(V. Prakash)

Synopsis

The backbone of India's future energy resources is the nuclear energy. The second stage of the India's nuclear programme envisages development and operation of a series of Fast Breeder Reactors (FBRs) which uses plutonium as their fuel. FBRs are compact and hence power density is high. Higher power density calls for an efficient heat removal medium and hence sodium has emerged as the preferred choice based on its better physical and neutronic properties. Various advantages of sodium coolant in the context of FBRs are excellent heat transfer characteristics, high boiling point, low neutron absorption etc. In spite of the above advantages of sodium as coolant, various phenomena associated with sodium pose challenges related to process and component design, structural integrity, in-service inspection and thermal hydraulics. Due to the opaque nature of sodium, under sodium inspection/diagnostics in fast reactors is quite a challenge.

The primary circuit of FBRs, which is contained in the main vessel comprises of core subassemblies, primary sodium pumps, intermediate heat exchangers and control plug. Pool type design facilitates the compact containment of all primary radioactive components in a single chamber, on the other hand it demands development of structural components with close tolerances and also results in complex flow pattern in the primary vessel. The fission heat generated in the core is picked up by the primary sodium and is transported to the secondary circuit in the intermediate heat exchanger, which is a shell and tube type heat exchanger with primary sodium in the tube side and secondary sodium in the shell side. The primary sodium pumps in the pool provide the necessary head to drive sodium through the core, hot pool and the intermediate heat exchangers. For the safe and reliable operation of a nuclear power plant for a period of 40 years or 60 years, non-destructive examination practices for in-service inspection is very essential.

Ultrasound waves find applications in various engineering fields for cleaning, flaw detection, thickness measurement, object detection, navigation systems etc. Development of ultrasonic sensors, processing techniques, signal analysis methods etc have come to such a level of maturity that its application is inevitable in the field of Non-Destructive Testing (NDT). The challenges pertaining to under sodium viewing applications are also well addressed in these days and ultrasonic technique emerged as a key diagnostic tool for in-service inspection of components in fast reactors.

The focus of this research is on the development of ultrasonic technique for the vibration measurement of immersed components in FBRs. NDT techniques using ultrasound waves are in common use in various industries. However, their applications related to nuclear industry are not fully developed. The limiting factors are the high temperature environment and the medium (sodium coolant) in FBRs. Not many attempts are reported on the application of ultrasonic techniques for anomaly detection in FBRs. Economic and safety implications for conducting studies in sodium etc are the major reasons for these setbacks. However, it is required to explore the application of acoustic and ultrasonic techniques for certain challenging problems currently faced in FBRs. One such application identified is the measurement of vibration of immersed components. In a pool type reactor with all the primary components immersed in a sodium pool, the complex coolant flow results in component vibration. As such no technology is available for measuring the vibration of immersed components in sodium, hence it is decided to carry out an investigation oriented in this direction using the ultrasonic technique.

In the research work of this thesis, a challenging problem currently faced in FBR in-service inspection is addressed. The study is aimed at developing a technique as an NDT tool for vibration measurement of sodium immersed components in FBRs. Towards this, following are the key areas where research work is focused on:

a) Development of ultrasonic technique for subassembly vibration measurement in FBRs

b) Development of wave guides for high temperature in-sodium vibration measurements.

Flow induced vibration studies of Fuel subassemblies

The turbulent flow through the core of Prototype Fast Breeder Reactor (PFBR) can cause flow induced vibration, which is an undesirable phenomenon which can cause reactivity noise and can also lead to the failure of components due to fatigue, wear and vibration induced fretting. Flow induced vibration measurements were carried out in a water test facility on full scale dummy subassembly and the overall strain level and its resulting stress levels are checked with the design limits to qualify the subassembly design for its use in reactor. However, it is a safety requirement to measure the amplitude and frequency of vibration of subassembly during pre-commissioning tests of PFBR. The major challenges involved were sodium environment, and high temperature (200^0C). Since conventional sensors like accelerometers, LVDT, strain gages etc cannot be used under sodium at high temperature, alternate methods with non-contact type measurement technique were investigated. Due to the opacity of sodium to light, optical methods are not considered. Due to accessibility issues, probe positioning issues, modification in subassembly geometrical profile etc, eddy current methods were also not useful. The ultrasonic technique was explored and feasibility studies were conducted. Non-contact measurement technique using ultrasound waves was planned and extensive experiments were carried out in various test facilities and measurement technique was established and demonstrated.

FIV studies were carried out on PFBR fuel subassembly in water test loop and subassembly was qualified for reactor applications. During this out-of-pile testing vibration measurements were carried out to determine the amplitude and frequency of vibration. First natural frequency of subassembly was measured as 3.6 Hz and overall amplitude of vibration displacement in the frequency range of 0.3 Hz to 100 Hz at the subassembly top is 0.2 mm (rms).

Development of ultrasonic technique for vibration measurement

Ultrasonic sensors in pulse echo mode are used for the detection of target vibration. The ultrasound waves emitted by the sensors are focused on the target and measures the time delay between each emitted and echo pulses. So continuous triggering of the sensor yields the time of flight corresponding to the subassembly movement. By suitably extracting the time of flight data from the train of ultrasonic pulses target movement/vibration is measured.

During preliminary studies, a dummy subassembly was mounted in a test section in water with ultrasonic sensors focused on top of the subassembly. LVDT was used as the reference probe for this study. To induce vibration in the subassembly, an electro-dynamic exciter was used. The ultrasonic signal was recorded using commercially available equipment and extraction of vibration signal was attempted. The results were encouraging and the target vibration frequency and amplitude were measured from the ultrasonic signal.

To have a deep insight into the technique based on the preliminary experimental results, a prototype mechanism was designed and manufactured. The mechanism was tested in water and in sodium for its performance. The target used in the study was the crown region of the actual subassembly head. The target is excited using an electro-dynamic exciter connected to the target suspended from the top of the vessel. The target was excited for different input frequencies and the ultrasonic train of pulses were measured and analyzed. From the recorded signal, vibration of target was extracted using the developed software. The test results obtained from water and sodium testing were very promising. It was observed that the input vibration time signal is reliably recovered from the train of pulses. This study gave a clear indication of the possibility of using this measurement technology in sodium for reactor applications. Moreover, performance of the sensors was also established during this study.

Various measurement and acquisition parameters involved in the development of ultrasonic technique for vibration measurement, which can highly influence the accuracy of measurements are:- a) Ultrasonic sensor operating frequency, b) Pulse repetition frequency (PRF) of ultrasonic pulser, c) Target vibration frequency, which is to be measured and d) Ultrasonic signal acquisition frequency. All measurement parameters are optimised during the study for the vibration measurement. The sensor used for the measurement was developed using a special grade PZT-crystal with an operating temperature of 230^0C. The casing material of the ultrasonic sensor was made up of Nickel so as to have better wetting in sodium as compared to stainless steel casing. Sensors were also tested in sodium for the rated temperature.

Development of SONAR device for FBRs

With the confidence obtained from the testing, a device was designed and manufactured for FBR applications. Since the principle of operation is sound navigation and ranging, the device is named as SONAR device. The major challenges involved in this measurement is the development of device with proper leak tightness, mounting in the central canal of FBR, focusing the target inside sodium, self vibration of sonar device itself in sodium flow etc. The designed sonar device is equipped with three numbers of ultrasonic sensors namely, S1, S2 and S3. Sensor S1 and sensor S2 are mounted at an angle of 60^0 so as to focus on the crown region of the subassembly, whereas sensor S3 is used to measure the self vibration of the sonar device itself. The device is capable of movement in two axis, Theta-axis/rotational motion and Z-axis/vertical movement. The control panel of the sonar device is equipped with ultrasonic pulser-receivers to excite the sensors, a high frequency data acquisition system for capturing the signals from the sensors and application software to process the acquired signal and to extract the vibration signal. The developed device was assembled.

For carrying out the studies, a water test vessel was used with subassembly heads arranged to simulate reactor core top region. Extensive studies were carried out in water using the device to understand various aspects of the measurement technique in detail. Before assembling the sensors, axial and cross sectional beam profiling of the ultrasonic sensors were carried out by the immersion technique using a standard pinducer to qualify the sensors.

After assembling the device in a test vessel, focusing trials were carried out by rotating the spinner tube (Theta movement) and moving it up and down (Z-movement). Subassembly heads were arranged in the vessel so as to simulate the reactor core top. Subassembly head (crown region) was suspended from the top and was connected to the stinger rod of the exciter to facilitate its required movement. The first phase of studies was conducted by exciting the target with known frequencies. The ultrasonic sensor S1 was excited using the pulser-receiver and signal from the sensor S1 was recorded. Using the developed software vibration signal was extracted from the ultrasonic signal and the results were compared with the reference LVDT mounted on the target. The experiments were repeated with different sinusoidal frequencies and with random excitation. It was observed from the test results that the developed algorithm reliably extracted the vibration signal from ultrasonic signal. The time signal and frequency spectra were analyzed and were compared with the reference LVDT and were found to be matching well. Apart from this, the signals were recorded using an oscilloscope to study phase change in the reflected echo, if any, during the movement of target. No phase shift was observed in the signal. In all the studies, it was also observed that the vibration of target was accurately recovered from the ultrasonic signal.

In the second phase of experiments, target was made stationary and sonar device was excited using electro-dynamic exciter. The experiment was conducted for various excitation frequencies and signal from side viewing Sensor S3 was recorded and analyzed. Analysis of the data from Sensor S3 clearly indicated the movement of sonar device and the measured vibration data was matching with the reference LVDT mounted on the sonar device. This study was conducted to assess the performance of Sensor S3, which in the case of reactor, is focused on the shroud tube of the central canal which is the stationary reference target for vibration measurement. During the vibration measurements inside the primary pool of a FBR, there can be random movement of the sonar device in the turbulent coolant flow, hence this study was conducted towards developing the vibration compensation technique.

In the third phase of measurements, both the target subassembly head and the sonar device were excited using electro-dynamic exciter and simultaneous measurements were carried out using Sensors S1 and S3. Signals from the Sensors S1 and S3 were recorded and analyzed. Sensor S1 measured the vibration of the target whereas sensor S3 measured the vibration of the sonar device. Studies were carried out with various excitation frequency combinations. Experiments were repeated with different excitations to the target as well as to the Sonar device. In all the measurement campaigns the device was able to accurately measure the vibration of the target as well as the sonar device.

Sensor S1 measures the amplitude of vibration of target with respect to the sonar device at an angle of 30^0 with the horizontal, whereas Sensor S3, which is at 0^0 to the horizontal, measures the amplitude of vibration of sonar device. Sensor S3 is located at an elevation of 688 mm above sensor S1. The sensors S1 and S3 are installed in the same vertical plane. In order to exactly measure the vibration of the target, sonar device vibration needs to be compensated. The correction is applied for obtaining the vibration compensation for the sonar device. After measuring both the amplitudes of vibration, vibration compensation was implemented by applying suitable correction factor. Amplitudes measured during the study was tabulated after applying the correction factor and were found to be matching well with the reference sensor signal. It was also observed that the technique used for vibration compensation for Sonar device is effective and can be applied for extracting the actual vibration of target in a turbulent primary pool of reactor where the measurement device itself is subjected to flow disturbance/vibration. Using this developed technique it is planned to measure the vibration of fuel subassemblies in PFBR, which is in the final stage of commissioning. Measurements are planned during the isothermal run of the reactor at 200^0C with dummy subassemblies in the core.

Development of wave guide for high temperature in-sodium vibration measurements

Ultrasonic techniques for under sodium imaging, core protrusion detection, core mapping etc are well matured for low temperature applications whereas measurements at still higher temperatures are yet to be demonstrated and are still emerging. High temperature ultrasonic sensors for reactor applications are commercially not available, hence development of suitable waveguides as an alternative is very important for various measurement techniques. Vibration measurement technique developed for FBR primary pool applications cannot be extended as such for high temperature applications (550^0C) due to limitations in high temperature sensor availability. In order to facilitate vibration measurements under operating conditions (rated flow and high temperature 550^0C), waveguide (SS316 strip) based measurement system was developed as an extension to the project. The ultrasonic signal is generated outside the hostile environment and transmitted to and from the reactor using a waveguide. The principal advantage of this arrangement is that the source of sound is located in a low temperature environment at one end of the waveguide. Hence, conventional low temperature ultrasonic sensors/piezoelectric crystals can be used to generate ultrasonic pulse.

Development of wave guides for under water or under sodium applications demands the propagation of ultrasonic waves through the waveguide (metal) and then through the liquid medium. To achieve a single pulse as a result of a single excitation pulse the guide must be operated such that only a single mode may exist. Dispersion curves plotted for SS strip (1.6 mm) using DISPERSE software show the different Lamb wave modes that could actually propagate in the plate waveguide. 'A0' Lamb wave mode was selected based on the high out-of-plane displacement component required for it to leak into the liquid sodium efficiently. Also, the point on the 'A0'dispersion curve was chosen away from the dispersive region, which allows the energy to propagate long distances in the waveguide with minimum losses. Hence, a suitable working point for generation of 'A0' mode was selected as 1.6 MHz-mm. 'A0' Lamb wave modes are generated by sending longitudinal waves, by exciting a piezoceramic element on specifically designed angle wedge made of Aqualene material.

For preliminary studies, the length of waveguide is fixed as 10 m and thickness as 1.6 mm. A cover tube of length 1 m is provided at the end of the waveguide at the immersed portion such that only one face of the plate waveguide is exposed to the liquid. The leaked signal propagating in the liquid is directed towards the target to obtain echo signals. A test vessel of 5 m diameter is used for testing the waveguide. Water is used as the test fluid. A target rectangular plate is kept at a distance of 3m from the waveguide and connected to an electro-dynamic exciter using a stinger rod. The output from the pulser-receiver is recorded using a high frequency oscilloscope and various studies were carried out. In order to understand the beam pattern and its angle of travel, further studies were conducted using the developed waveguide. To observe the beam pattern axial beam profiling was carried out. The wave guide was installed inside a water test tub and by immersion technique, the axial beam profile was studied using a pinducer to study the symmetry of beam intensity distribution. After these studies cross sectional beam profiling of the waveguide sensor was also carried out. To measure the variation in the beam exit angle, waveguide was operated for different frequencies and the angle at which maximum amplitude occur was measured. These studies also revealed the possibility of using the waveguides for beam steering applications. Towards the end of studies with waveguides, vibration measurements were attempted using various target objects in the test vessel. Ultrasonic waveguide sensor was used in pulse-echo mode at a pulse repetition frequency of 50 Hz for the detection of target vibration. The target plate was excited with a known frequency and the ultrasonic train of pulses from the target for 2 second duration was recorded using the oscilloscope. The extracted vibration data was compared with the reference LVDT signal. The results indicate that vibration signals are faithfully detected and extracted from the ultrasonic signals. This developed waveguide technology is promising and it can find application in FBRs for vibration measurement of components like inner vessel, control plug and pump shells, CSRDM and DSRDM etc. under normal operating conditions at high temperature.

The research work of this thesis has been focused on vibration measurement of immersed components in the primary pool of FBRs. Coolant sodium and high temperature environment poses the challenges of direct measurement techniques, hence calls for alternative solutions like ultrasonic techniques. Extensive studies were carried out and a measurement methodology was developed and optimized. Using the technique measurements were carried out with simulated targets and a system named SONAR was developed for FBRs. All the challenging issues were successfully addressed and the end results are very promising for applications in FBRs.

Ultrasonic technique was studied and implemented for subassembly vibration measurement in PFBR and a measurement device (sonar) was developed for PFBR for subassembly vibration measurement during commissioning. Studies were also carried out for development of ultrasonic waveguide sensors for FBR applications. A waveguide system was developed and tested successfully. The wave guide sensor was also used for vibration measurement of a target plate. The performance of the waveguide system was satisfactory and encouraging. The technique proved to be very promising for under sodium vibration measurements inside the reactor primary vessel without the use of high temperature sodium immersible ultrasonic sensors.

List of Figures

CHAPTER-4 **Page No.**

CHAPTER-5 **Page No.**

List of Tables

Nomenclature

δ	-	Displacement
D_h	-	Hydraulic diameter
ρ	-	Density
V	-	Velocity
E	-	Modulus of elasticity
I	-	Moment of inertia
μ	-	Viscosity
ω	-	Angular frequency
f_n	-	Natural frequency
M	-	Mass per unit length
R_e	-	Reynolds number
pC	-	Pico-Coulomb
g	-	Acceleration due to gravity
f_v	-	Vortex shedding frequency
S	-	Strouhal number
λ	-	Wavelength

Abbreviations

ARDM	-	Absorber Rod Drive Mechanism
CCP	-	Core Cover Plate
CP	-	Control Plug
CSRDM	-	Control and Safety Rod Drive Mechanism
DAS	-	Data Acquisition System
DHX	-	Decay Heat Exchanger
DSRDM	-	Diverse Safety Rod Drive Mechanism
FBRs	-	Fast Breeder Reactors
FFLM	-	Failed Fuel Localization Modules
FFT	-	Fast Fourier Transform
IGCAR	-	Indira Gandhi Centre for Atomic Research
IHX	-	Intermediate Heat Exchanger
LRP	-	Large Rotating Plug
LSP	-	Lower Stay Plate
LVDT	-	Linear Variable Differential Transformer
MI	-	Mineral Insulated
NI	-	National Instruments
PDF	-	Probability Density Function
PFBR	-	Prototype Fast Breeder Reactor
PHWR	-	Pressurized Heavy Water Reactor
PRF	-	Pulse Repetition Frequency
PSP	-	Primary Sodium Pump
PZT	-	Lead Zirconate Titanate
SAMRAT	-	Scaled Model of Reactor Assembly for Thermal Hydraulics
SRP	-	Small Rotating Plug
US	-	Ultrasonics
USP	-	Upper Stay Plate

Contents

CHAPTER-3
ULTRASONIC TECHNIQUE FOR VIBRATION MEASUREMENT

CHAPTER-4
DEVELOPMENT OF SONAR DEVICE

CHAPTER-1

INTRODUCTION AND LITERATURE SURVEY

1.1 Energy scenario in India

At present, the primary source of electricity generation in India is coal. It is adequate to meet the energy demand for about 50-60 years. Potential of other renewable and non-renewable energy resources like gas, oil, wind, solar etc. is not fully developed and very limited. Uranium resource in India is moderate, whereas Thorium reserve exists in abundance [1]. Relying on the large thorium reserve, a three stage nuclear program was put forward by Dr. Homi Jahangir Bhabha. Pressurized Heavy Water Reactor (PHWR) fuelled by natural uranium, which are currently in operation and in construction constitutes the first stage. The spent fuel from the first stage reactors is reprocessed for the recovery of plutonium. Plutonium fuelled FBRs represents the second stage of nuclear program. This will facilitate launching of a large scale Th-U_{233} fuel cycle in the third stage. FBRs utilize natural uranium fuel very effectively through breeding and thus provide a rapid energy growth potential. The nuclear energy is a clean source of power unlike fossil fuels. The major advantages of nuclear power over other sources of energy are-

- Nuclear power is clean as it produces no carbon dioxide or sulfur dioxide.
- One gram of uranium yields as much energy as about a ton of coal and oil.
- Correspondingly nuclear waste is also million times smaller than fossil fuel waste. Nuclear waste can be totally confined and spent fuel can be used again by its reprocessing.
- Nuclear power is safe and the same is proved by record of many commercial nuclear reactors.

- Nuclear reactors are reliable as they are having good capacity factors. With advance in technology, intervals between refueling can be extended and down time can be reduced further.
- Cost of electricity produced in nuclear power plants is competitive and stable. Cost of electricity produced in nuclear power plants reduces with increase in power plant life.
- Nuclear reactor is very compact and nuclear radiation can be confined.

1.2 Indian Fast Breeder Reactors

The backbone of India's future energy resources is the nuclear energy. The second stage of India's nuclear energy program envisages setting up of FBRs, backed up by reprocessing plants and plutonium based fuel fabrication plants. These reactors produce more fuel than they consume. Indira Gandhi Centre for Atomic Research (IGCAR) is responsible for the design and development of fast breeder reactors, along with the development of the associated fuel cycle technologies. The construction of 500MWe Prototype Fast Breeder Reactor (PFBR) has been commenced at Kalpakkam and is in the advanced stage of commissioning. Fig. 1 shows the schematic of PFBR. PFBR is a pool type FBR with a power output of 500 MWe [2]. Pool type design facilitates the containment of all primary radioactive components within the vessel. Fission heat produced in the core is picked up by the coolant and transported to the secondary sodium in the intermediate heat exchanger (IHX). The secondary sodium exchanges heat to the steam water system, which in turn produces steam to rotate the turbine. PFBR uses Pu-U mixed oxide fuel. FBRs are compact and hence power density is high. Higher power density calls for an efficient heat removal medium and hence sodium has emerged as the preferred choice. The major design features of PFBR is tabulated in Table 1.1.

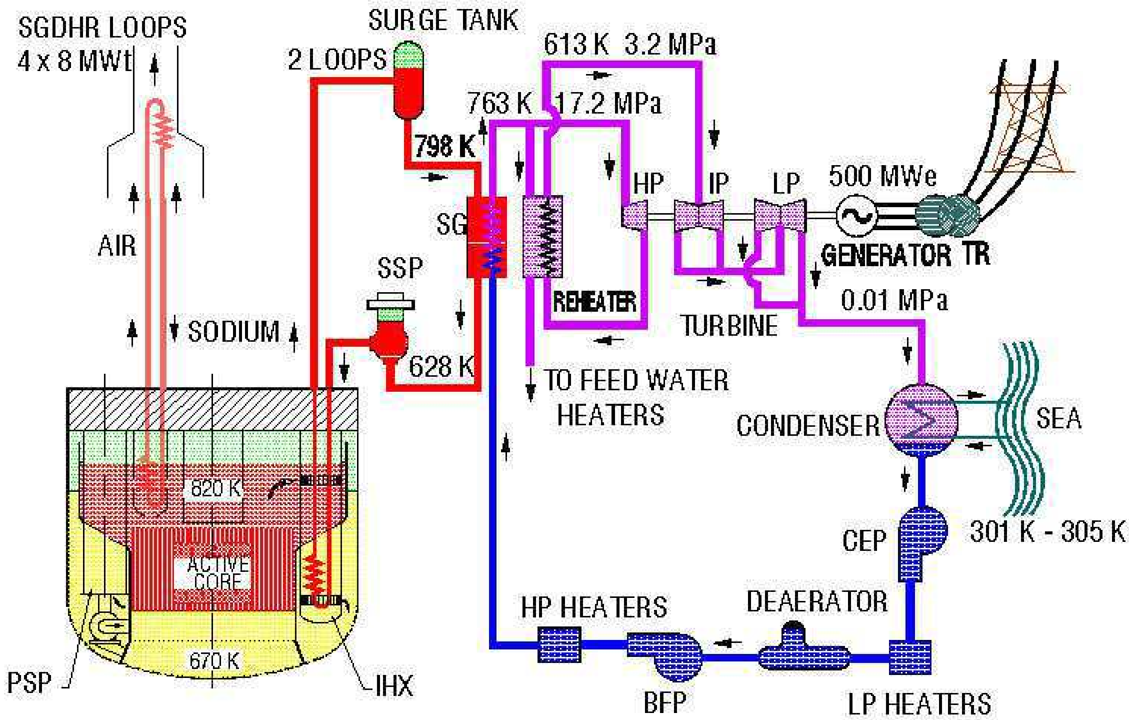

Fig. 1.1: Schematic of PFBR flow sheet

Table 1.1: Major design features of PFBR

Sl. No	Property	Value
1.	Thermal power	1250 MWt
2.	Electric output	500 MWe
3.	Diameter of main vessel	12900 mm
4.	Fuel	PuO_2-UO_2
5.	Fuel pin diameter	6.6 mm
6.	Fuel clad material	20% CW D9
7.	Primary circuit layout	Pool type
8.	Primary inlet/outlet temperature	397 / 547 ^{0}C
9.	Steam temperature	490 ^{0}C
10.	Steam pressure	16.6 MPa

1.3 Sodium as FBR coolant

Among so many other choices of coolants, sodium has emerged as the coolant for FBRs due to its better physical and neutronic properties. Sodium being a liquid metal has excellent heat transfer characteristics. Various advantages of sodium coolant in the context of FBRs are high boiling point, low neutron absorption etc. The major physical properties are listed in Table 1.2. High boiling point permits a low pressure primary system with thin walled structural components in FBRs. At room temperature sodium solidifies and allows easy transportation in the form of sodium bricks. Low melting point enables the conversion of solid sodium bricks to liquid using electrical heaters.

In spite of the above advantages of sodium as coolant, various phenomena associated with sodium pose challenges related to process and component design, structural integrity, in-service inspection and thermal hydraulics. Due to the opaque nature of sodium, under sodium inspection and diagnostics in fast reactors is quite a challenge.

Table 1.2: Physical properties of sodium

Sl. No	Property	Value
1.	Melting point	97.8 °C
2.	Boiling point	883 °C
3.	Volume change on melting	2.7 %
4.	Density	0.868 g/cc
5.	Viscosity	0.281 cps
6.	Surface tension at 100 °C	192 dynes/cm
7.	Specific heat of liquid at 100 °C	1.38 kJ/kg/°C
8.	Thermal conductivity at 300 °C	76 W/m/°C
9.	Electrical resistivity	9.67×10^{-8} Ω m

1.4 Flow path in PFBR

The main vessel of PFBR holds the primary circuit components. Primary circuit of PFBR consists of two numbers of primary sodium pumps (PSP), four numbers of intermediate heat exchangers (IHX), four numbers of decay heat exchangers (DHX), etc. immersed in the hot pool. Inside the main vessel, an inner vessel separates the hot and cold pool. The core consists of 1758 subassemblies. A control plug (CP) is in position above the core in PFBR, which consists of Absorber rod drive mechanisms (ARDMs) such as control and safety rod drive mechanisms (CSRDMs) and Diverse Safety Rod Drive Mechanism (DSRDMs), neutron detectors, thermocouples, etc. for reactor power control as well as to shut down the reactor. The flow path and major components inside a typical pool type FBR is shown in Fig. 1.2.

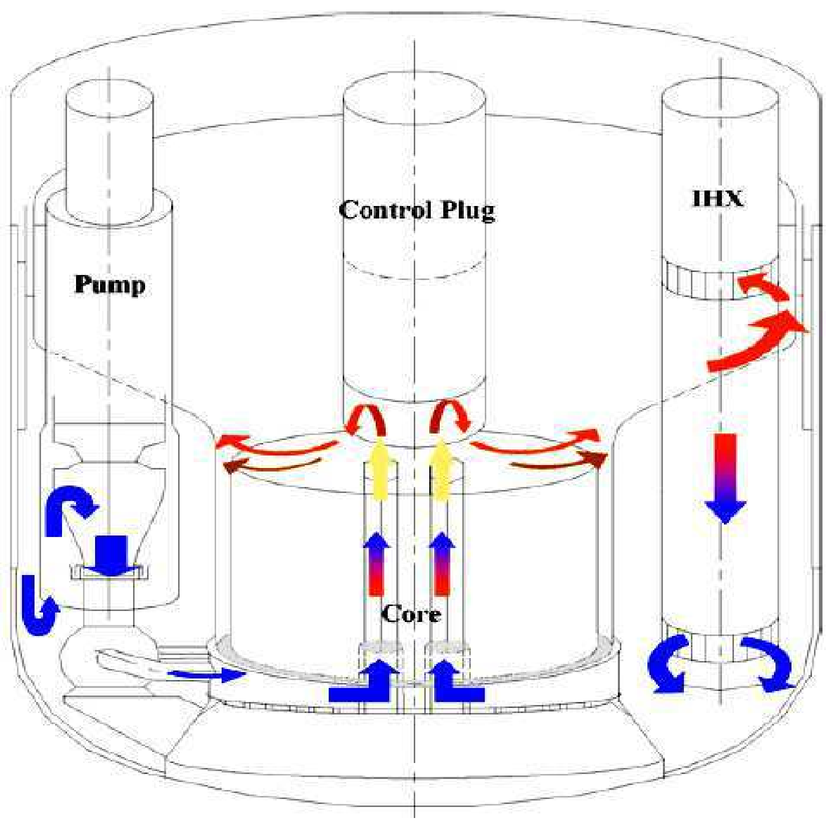

Fig. 1.2: A typical FBR primary circuit

Pool type design facilitates the compact containment of all primary radioactive components in a single chamber, on the other hand it demands development of structural components with close tolerances and also results in complex flow pattern in the primary vessel. The fission heat generated in the core is picked up by the primary sodium and is transported to the secondary circuit in the intermediate heat exchanger, which is a shell and tube type heat exchanger with primary sodium in the shell side and secondary sodium in the tube side. The primary sodium pumps in the pool provide the necessary head to drive the sodium through the core, hot pool and the intermediate heat exchangers.

1.5 Motivation for the research

NDT techniques using ultrasound waves are in common use in various industries. However, their applications related to nuclear industry for measurement under sodium are not fully developed. The limiting factors are the high temperature environment and the medium (sodium coolant) in FBRs. Not much attempts are made to use ultrasonic techniques for various applications including under sodium anomaly detection in FBRs. Economic and safety implications for conducting studies in sodium etc are the major reasons for these setbacks. However, it is required to explore the application of acoustic and ultrasonic techniques for certain challenging problems currently faced in FBRs. One such application identified for nuclear industry is the measurement of vibration of immersed components. In a pool type reactor with all the primary components immersed in a sodium pool, the complex coolant flow results in component vibration. As such no technology is available for measuring the vibration of sodium immersed components, hence it is decided to carry out an investigation oriented in this direction using ultrasonic technique.

1.6 Objectives and scope of the work

In the research work of this thesis, a challenging problem currently faced in FBR in-service inspection is addressed. The study is aimed at developing a technique as an NDT tool for vibration measurement of sodium immersed components in FBR. Towards this, following are the key areas where research work is focused on-

a) Development of ultrasonic technique for subassembly vibration measurement in FBRs
b) Development of wave guides for high temperature in-sodium vibration measurements.

1.7 Literature survey

Application of acoustic and ultrasonic techniques finds wide applications in NDT. Literature survey on ultrasonic measurement techniques has been carried out to assess and understand the current trends and attempts made world-wide in this domain. Ultrasonic technique was used in Phenix reactor to study the negative reactivity incident and to measure the core movement at low frequency [3, 4]. Au-Yang [5] demonstrated application of ultrasonics to non-intrusive vibration measurement. In his work, check valve disk flutter using non-intrusive ultrasonic technique to an amplitude as low as 0.0025 mm was measured. Development of ultrasonic waveguide sensor for under-sodium inspection was attempted by Joo. Guided waves (Lamb waves) are used for these studies.

1.8 Thesis organization

The thesis has been divided into five chapters. Chapter 1 gives a brief introduction and focuses on the motivation behind the research work, its objectives and scope of research along with a brief literature survey. Chapter 2 describes in detail the phenomenon of Flow Induced

Vibration in FBRs, its consequences and measurement methodologies. Chapter 3 dwells on the ultrasonic technique, its application for vibration measurement and preliminary experiments carried out towards the development of ultrasonic technique. Chapter 4 describes in detail the development of SONAR device for PFBR, various studies carried out, and its test results and conclusion. Chapter 5 focuses on the development of ultrasonic waveguides for high temperature applications. Chapter 6 provides the conclusions and also the directions for future research.

CHAPTER-2
FLOW INDUCED VIBRATION OF PFBR COMPONENTS

2.1 Introduction

Prototype Fast Breeder Reactor (PFBR) is liquid metal sodium cooled pool type 500MWe reactor currently under commissioning phase at Kalpakkam, India. It is a pool type reactor with all primary components such as core subassemblies (SA), pumps, and intermediate heat exchanger immersed in hot sodium at 547^{0}C [6]. The main vessel which acts as the primary containment, is supported at the top in the roof slab, takes the entire load of the primary components and primary sodium. Fig. 2.1 shows the sketch of the PFBR reactor assembly. Moreover, in PFBR primary circuit, components are basically thin walled, slender shells with diameter to thickness ratio ranging from 100 to 650 making them prone to flow induced vibrations. The PFBR core is surrounded by thin axi-symmetrical shells which separate sodium flow volumes and avoid thermal problems [7]. The shells are concentric thin walled structures (thickness–diameter ratio: t/D ~ 1/650 and height–diameter ratio: h/d ~ 1), each separated by thin annulus of liquid sodium (annulus gap–diameter ratio: w/D ~ 1/100). These geometrical arrangements with interconnected liquid columns respond to flow fluctuations which leads to vibration during reactor operation. Another special feature is the existence of free fluid surfaces which is the source of flow induced vibration.

Flow induced vibration (FIV) of components results in its premature failure, resulting in the non-availability of reactor. Vibration problems in control plug, reactor main vessel and inner vessel, steam generator failure, fuel subassembly failure etc. are experienced worldwide in several reactors. FIV of fuel subassembly can cause failure of the fuel element clad tubes from fatigue, wear and vibration induced fretting. Excessive vibration of fuel subassembly will cause reactivity noise, fatigue or rattling failure.

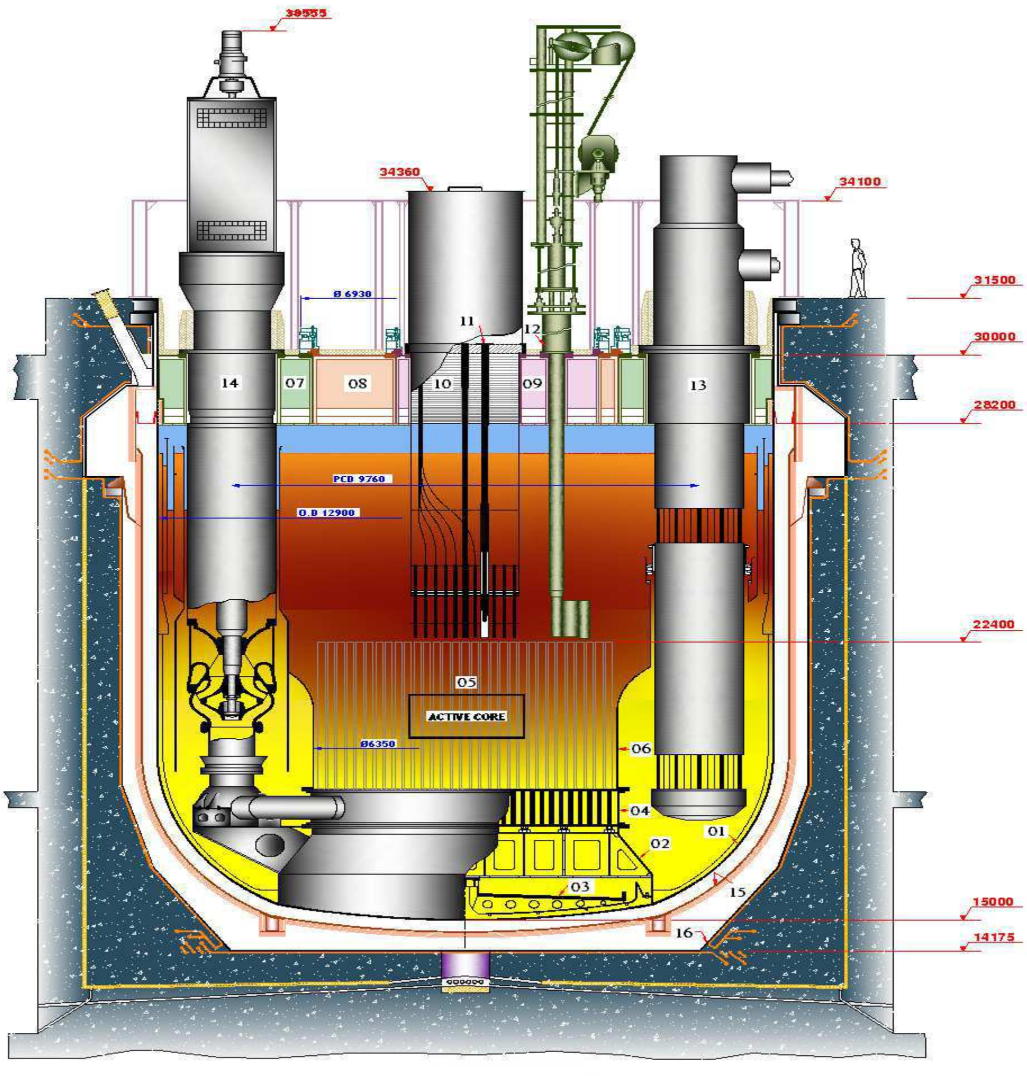

LEGEND

01. MAIN VESSEL	09. SMALL ROTATABLE PLUG
02. CORE SUPPORT STRUCURE	10. CONTROL PLUG
03. CORE CATCHER	11. CONTROL & SAFETY ROD MECHANISM
04. GRID PLATE	12. IN-VESSEL TRANSFER MACHINE
05. CORE	13. INTERMEDIATE HEAT EXCHANGER
06. INNER VESSEL	14. PRIMARY SODIUM PUMP
07. ROOF SLAB	15. SAFETY VESSEL
08. LARGE ROTATABLE PLUG	16. REACTOR VAULT

Fig. 2.1: Sketch of PFBR reactor assembly

2.2 FIV mechanisms

The flow in the primary pool is a major excitation source of vibration. The major classification of FIV mechanisms are a) Turbulence b) Vortex shedding and c) Instability.

2.2.1 Turbulence

Turbulence is the major source of vibration excitation in objects under fluid. Turbulent flow is a flow regime characterized by significant property changes. Rapid variation of pressure and flow velocity in space and time is the main characteristics of turbulent flow. The force of excitation is random in nature and excites various natural frequencies of the object. Movement of the fluid particles will be in disorder fashion in a turbulent flow. Vibration amplitude varies proportional to the square of the flow velocity.

2.2.2 Vortex shedding

Vibration due to vortex shedding occurs in cross flow. Eddies or vortices are formed wake behind the structure in cross flow and will be periodically shed from the objects with flow velocity. The collapse of eddies when it reaches high pressure region creates fluctuating pressure and flow regimes, which in turn excites the test structure. This phenomenon happens only at certain frequencies, hence chances of resonance excitation is more in vortex shedding. Hence components are designed with relatively high margins from vortex shedding frequencies. Fig. 2.2 shows the phenomenon of vortex shedding and its various stages. At low flow velocities, flow separation across the object will be slightly generated. At intermediate flow velocities, formation of vortices takes place and at higher flow velocities, vortex sheds off from the structure, generating large pressure fluctuations in the medium. Vibration of the structure is mainly in the lift direction.

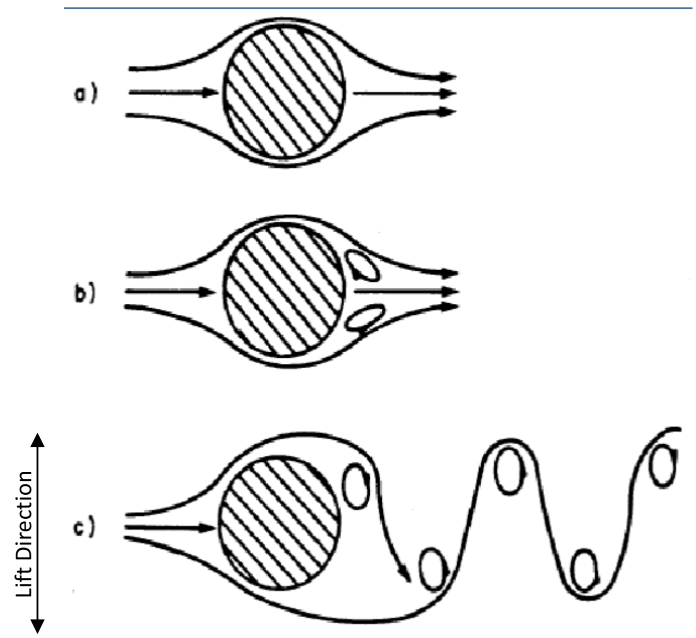

Fig. 2.2: Vortex shedding phenomenon [8]

2.2.3 Instability

Instability normally occurs in structural components, when there is an interaction between the structure and fluid. There exists always a feedback mechanism during instability phenomenon. It occurs when flow velocity exceeds the critical velocity. If the kinetic energy imparted by the liquid is greater than the energy dissipated due to structural and fluid damping, then any perturbation introduced on the structure will develop to cause instability. This phenomenon gets build up if the condition prevails, and finally results in the collapse of structures. Instability phenomenon is normally taken care at the design stage of components itself.

2.3 Vibration instrumentation

Detecting an anomaly in time and its rectification by proper planning helps in increasing the uptime of any system. Measurement of vibration signal, proper signal conditioning and its analysis helps in identifying various anomalies in running plants. Vibration instrumentation includes primary field sensors, conditioning amplifiers and signal analyzers.

2.3.1 Vibration sensors

Vibration is measured in terms of displacement, velocity and acceleration. Displacement measurement is generally used in the low frequency range, velocity measurement is used for intermediate vibration frequencies and high frequency vibration is generally expressed in terms of acceleration.

2.3.1.1 Displacement sensors

LVDT (Linear Variable Differential Transformer) and proximity sensors are generally used for vibration displacement measurement. Working principle of LVDT is similar to that of a transformer. LVDT consists of a primary winding and two secondary windings. The secondary coils are connected in series opposition and a separate cylindrical core passes through the center as shown in Fig. 2.3. The primary winding (P1) is energized with a constant amplitude A.C. supply at a suitable operating frequency of typically 1 to 10 kHz. This produces an alternating magnetic field in the centre of the transducer which induces a signal into the secondary windings (S1 and S2) depending on the position of the core. Movement of the core within this area causes the secondary signal to change. As the two secondary windings are connected in a push-pull mode, when the core is at the centre, a zero signal is obtained. Movement of the core from this point in either direction causes the signal to increase (Fig. 2.4). As the windings are wound in a particular precise manner, the signal output has a linear relationship with the actual mechanical movement of the core.

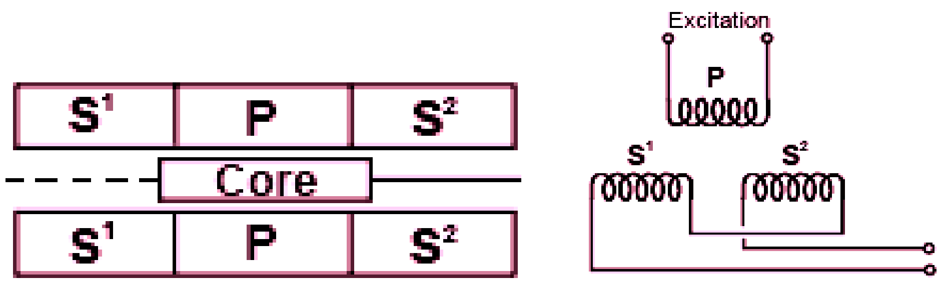

Fig. 2.3: LVDT internal arrangement

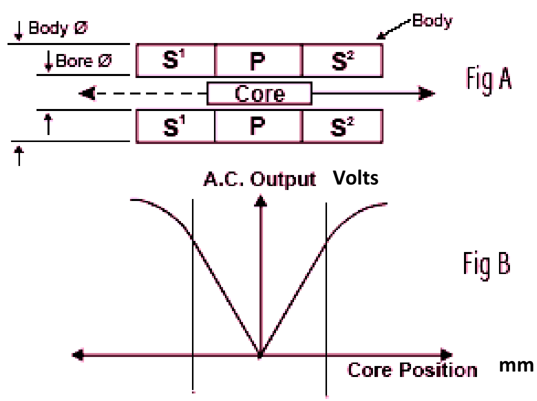

Fig. 2.4: Variation in voltage w.r.t core position [9]

The secondary output signal will be a modulated signal with the induced signal superimposed on the excitation signal. The signal is then processed by a phase-sensitive demodulator or using a lock-in amplifier circuit. The output signal thus indicates the direction as well as the amplitude of the movement in terms of dc voltage. The major advantage of LVDT is that the moving core is not in contact with other electrical components, hence offers high reliability and long life with less friction.

Proximity sensors are also used for displacement measurement and are working on the eddy current principle. Eddy-Current sensors operate with magnetic fields. A proximity sensor consists of an eddy current probe to which a high frequency RF signal is applied from a driver. This in turn creates an alternating magnetic field which induces small currents in the target material; these currents are called eddy currents. The eddy currents create an opposing magnetic field which resists the field generated by the probe (Fig. 2.5). The interaction of the magnetic fields is dependent on the distance between the probe and the target. As the distance changes, the electronics sense the change in the field interaction and produce a voltage output which is proportional to the change in distance between the probe and target. Suitable electronics are used to demodulate the signal, amplify and linearise it to provide an output proportional to the probe to target gap and/or vibration of the target.

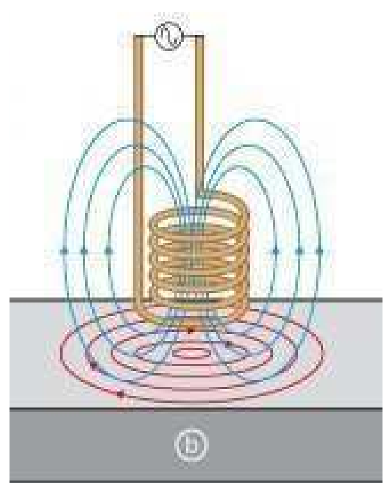

Fig. 2.5: Generation of eddy currents [10]

2.3.1.2 Velocity sensors

The velocity pickup is a very popular transducer or sensor for monitoring the vibration velocity in rotor dynamics studies. They are available in many different physical configurations and output sensitivities. When a coil of wire is moved through a magnetic field, a voltage is induced across the end wires of the coil. The induced voltage is caused by the transferring of energy from the flux field of the magnet to the wire coil. As the coil is forced through the magnetic field by vibratory motion, a voltage signal representing the vibration is produced. The velocity pickup is a self-generating sensor requiring no external devices to produce a vibration signal as shown in Fig. 2.6. This type of sensor is made up of three components: a permanent magnet, a coil of wire and a spring. The pickup is filled with an oil to dampen the spring action depending upon the application and response time requirement.

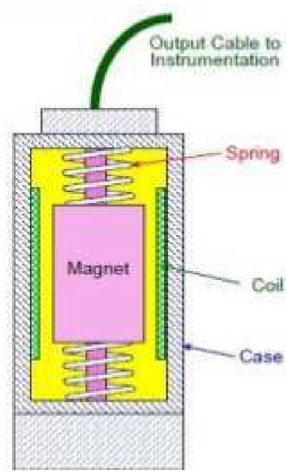

Fig. 2.6: Velocity pick-up [11]

2.3.1.3 Strain gages

In addition to the general vibration sensors, strain gages are also widely used for measuring the intensity of vibration. The main advantage of strain gages is that it directly measures the strain on the material surface, from which stress values can be directly calculated. The basic principle of strain gage is that, its material resistance changes when strain is applied to them. When a force is applied to any metallic wire its length increases due to the strain. The more is the applied force, more is the strain and more is the increase in length of the gage element. The change in resistance will be so low that special whetstone bridge amplifier is used for measuring the resistance. Earlier wire type strain gauges were used commonly, which are now being replaced by the metal foil types of gauges. The metals can be easily cut into the zigzag foils for the formation of the strain gauges. Fig. 2.7 shows a strain gage. One of the most popular materials used for the strain gauges is the copper-nickel-manganese alloy. Some semiconductor materials can also be used for making the strain gauges. The input and output relationship of the strain gauges can be expressed by the term gauge factor. Gage factor is defined as the ratio of relative change in resistance to mechanical strain. Normal strain gages have a gage factor of 2, whereas semiconductor strain gages have gauge factor greater than 100.

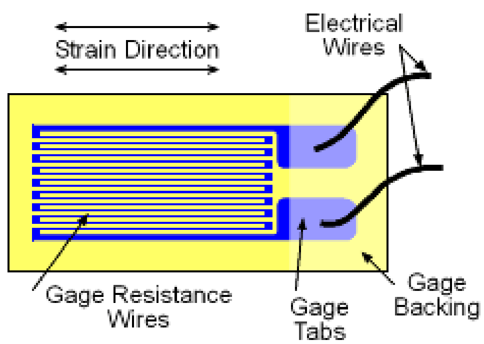

Fig. 2.7: Strain gage [12]

2.3.1.4 Acceleration sensors

For vibration measurement, accelerometers are extensively used. Accelerometers are generally miniature in size and are compact in nature. Acceleration signals can be suitably converted to velocity as well as displacement by proper integration. Hence accelerometers are widely used in industries as vibration sensors. Accelerometers are generally available in different sizes, shapes, operating temperature, frequency ranges etc. which suits to any measuring environment. Fig. 2.8 shows the photograph of a typical accelerometer [13].

Fig. 2.8: Accelerometer [13]

Table 2.1: Specifications of accelerometer

Sl. No	Property	Value
1.	Sensitivity	1 pC/g
2.	Frequency range	0.3 Hz to 15 kHz
3.	Weight	110 gm
4.	Sensing element	PZT
5.	Mounted resonance	45 kHz
6.	Case material	Titanium
7.	Operating temperature	Upto 180 ^{0}C

2.3.2 Accelerometer signal conditioners

The output of a typical piezo-electric sensor is charge with very low amplitude typically in the order of pico-coulomb. Amplifiers are used to accomplish signal amplification. A typical conditioning amplifier employs low noise operational amplifiers for charge to voltage conversion as well as for amplification of weak signals before feeding to the signal analyzers. Fig. 2.9 shows the typical schematic of a charge amplifier [14]. Capacitance feedback is used in charge amplifiers.

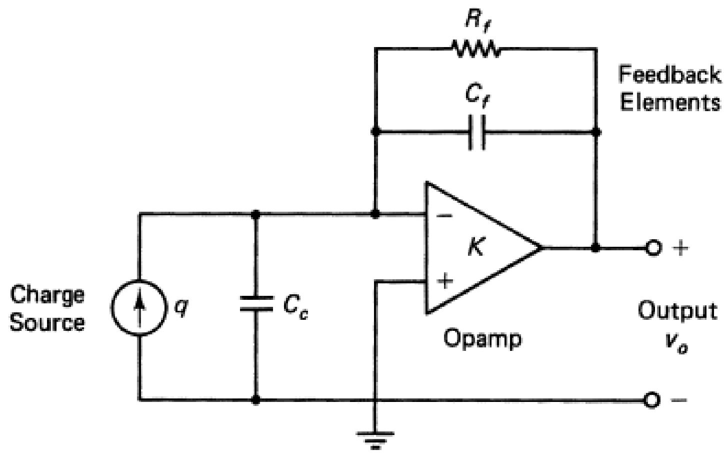

Fig. 2.9: Schematic of charge amplifier [14]

2.3.3 Signal analyzers

The conditioned output from the charge amplifier is normally recorded and analyzed using signal analyzers. Fig. 2.10 shows a typical signal analyzer. Various signal analysis techniques are incorporated in most of the analyzers.

Fig. 2.10: Vibration signal analyzer [15]

Time domain, frequency domain and amplitude domain analysis are generally used in vibration measurement to detect vibration sources, interpret the mode of vibration and to identify the FIV mechanisms. Vibration time signal is generally used to interpret resonant vibration of components, where signal is purely sinusoidal in nature. Vibration due to turbulence excitation cannot be interpreted reliably from the time signal due to multiple frequency components. Vibration spectra, which is a derivative of Fourier Transform, is used for interpreting such complex vibration signals. The sources of vibrations and contribution of each mode can be distinctly identified from vibration spectra. Amplitude domain analysis is used to interpret the FIV mechanism involved. Excitation due to turbulence is indicated in amplitude domain (Probability distribution function) as a Gaussian distribution, whereas resonance sort of excitation is indicated as a 'U' shaped curve in the amplitude domain (PDF). Advanced signal processing techniques such as correlation functions, wavelet analysis, Z-transforms etc are supported in modern signal analyzers.

2.4 FIV studies on PFBR components

FIV studies were carried out on PFBR components to qualify them for their use in reactor. Studies were carried out on critical components such as fuel subassembly, control plug and its components, weir shell, intermediate heat exchanger, steam generator etc. Even though the designed life of critical components in a reactor is 30-40 years, it is a safety requirement to test the performance of such components before its deployment in reactor [16]. Hence, studies were carried out on major critical components in water in separate test facilities. Suitable non-dimensional numbers were simulated so that the results obtained from the study can be directly transposed to reactor operating conditions.

2.4.1 FIV studies on PFBR fuel subassembly

Core of PFBR consists of 1758 subassemblies, out of which 181 nos. are fuel subassemblies. The turbulent flow through the core of PFBR can cause flow induced vibration. The coolant sodium flows from the bottom of the subassembly to top and the design of the subassembly for each flow zone is quite complex. There are 217 fuel pins in each subassembly, vertically held in the form of bundle within a hexagonal wrapper tube (hexcan). The pins are separated by spacer wires wound around the pins helically. Analytical modeling of this complex geometry of the subassembly is very difficult. So experiments were conducted extensively to get accurate evaluation of the subassembly design and for its qualification for the use in PFBR, which is designed for 40 years of operation. Flow induced vibration measurements were carried out in a water test facility on full scale dummy subassembly and the overall strain level and its resulting stress levels are checked with the design limits to qualify the subassembly design for its use in reactor.

2.4.1.1 Description of fuel subassembly

In PFBR, the entire core subassemblies are supported in the sleeves of grid plate, which acts as the main coolant header. Details of a typical fuel subassembly are shown in Fig 2.11. The total height of the subassembly is 4.5 m out of which 3.9 m is above the grid plate. The middle portion of the fuel pin accommodates the fuel pellets. On both sides of the fuel region, blanket, shielding regions, etc. are provided. The flow through a single fuel subassembly is 36 kg/s. Coolant sodium flows axially from the bottom of the subassembly to top and it is in turbulent regime. This turbulent flow can excite FIV of (a) fuel pins (b) subassembly as a whole (overall subassembly vibration). The overall subassembly vibration will be in its cantilever mode.

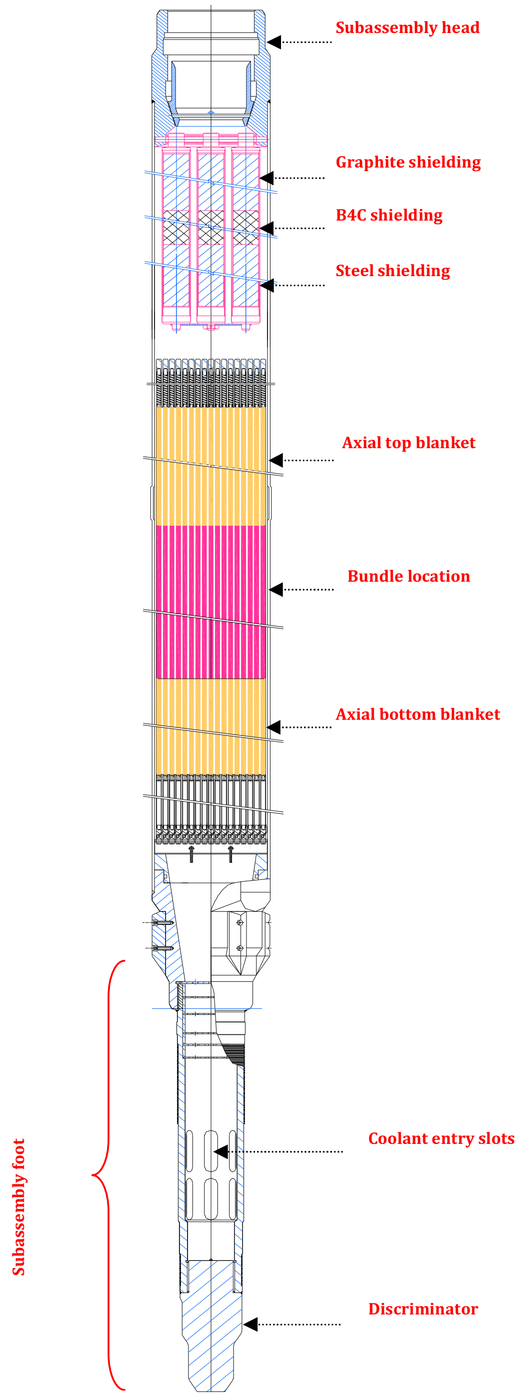

Fig. 2.11: PFBR fuel subassembly

2.4.1.2 Subassembly FIV test facility

For FIV testing, a full scale dummy fuel subassembly was used. Full scale model of grid plate sleeve was assembled with grid box for mounting the test subassembly. All the flow paths and support conditions are simulated as in reactor. Perspex embedded SS window was assembled in the test loop to view the movement of top end of subassembly during experiments. Fig. 2.12 shows the experimental facility [17].

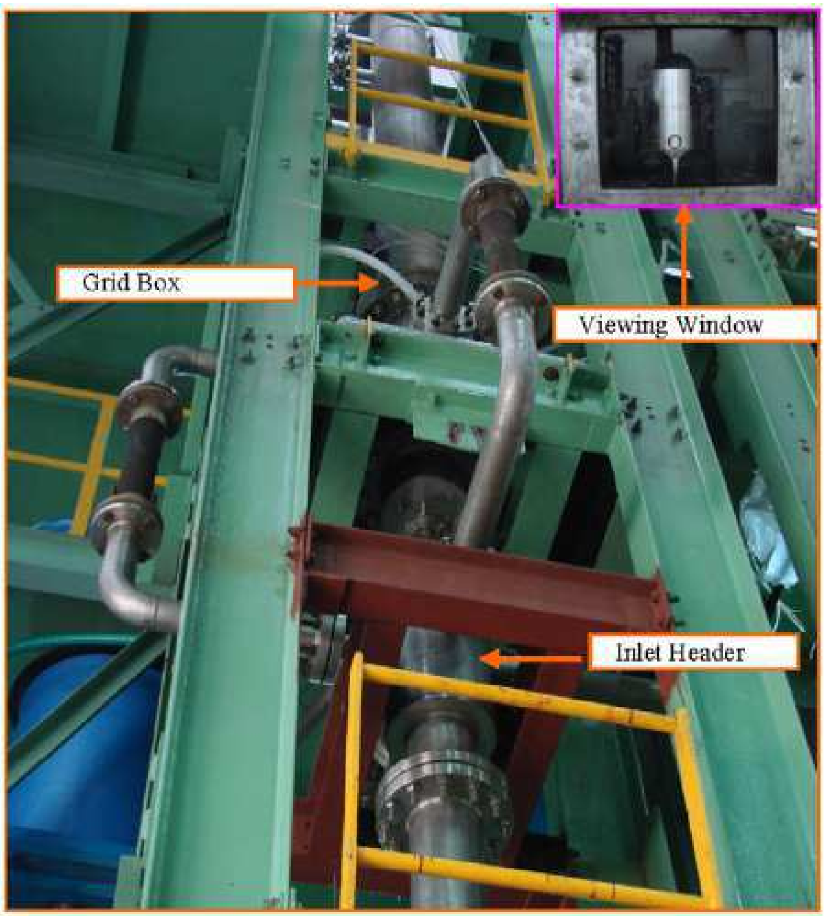

Fig. 2.12: SA FIV experimental test facility

Rubber bellows were used to isolate the test section from the machinery and other structure borne noises. To measure the amplitude and frequency of vibration, under water accelerometers were installed on top of the subassembly. Test loop schematic is shown in Fig. 2.13. To maintain the test fluid temperature a heat exchanger is introduced in the test loop and an orifice flow meter is used to measure the flow through the test section.

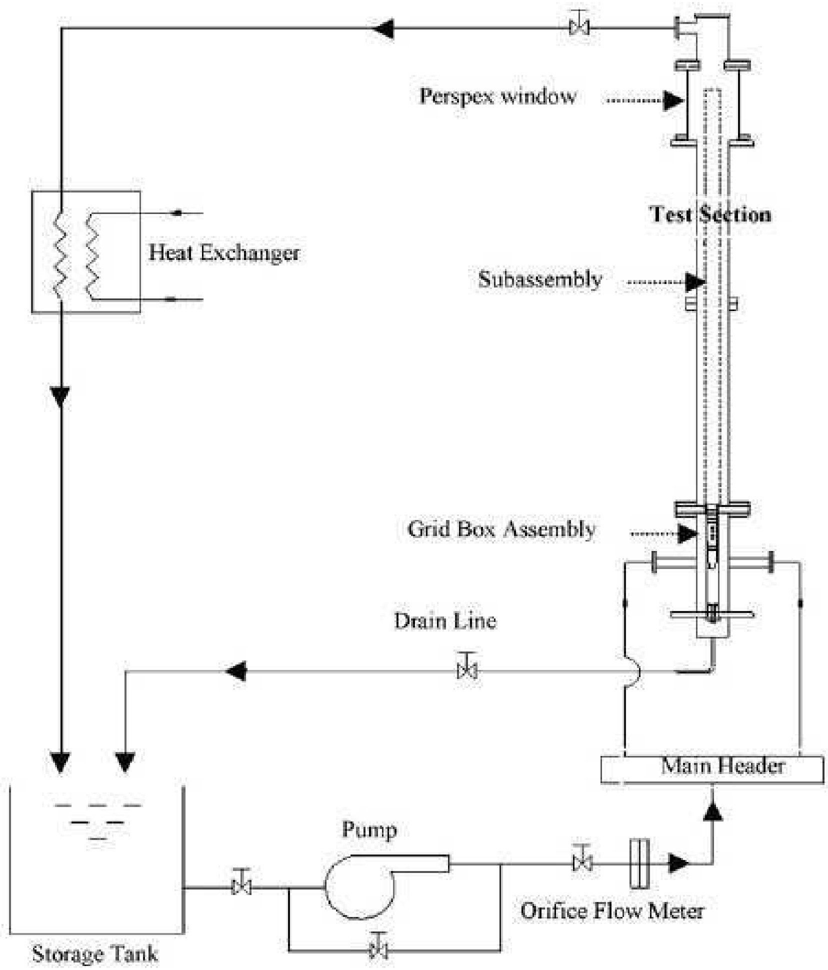

Fig. 2.13: FIV test loop schematic

2.4.1.3 Simulation criteria

The flow through the fuel subassembly is parallel flow and the main excitation mechanism is turbulence. The simulation criterion from water to sodium is established from the Burgreen correlation for the fuel subassembly vibration [18].

$$\left(\frac{\delta}{D_h}\right)^{1.3} = 0.83 \times 10^{-10} \times K \times T^{0.5} \times \Omega \qquad \text{---- (2.1)}$$

where δ is displacement of subassembly,

D_h is the hydraulic diameter,

K is the end fixity factor,

$$T = \frac{\rho \ V^2 L^4}{EI} \quad \text{and} \quad \Omega = \frac{\rho V^2}{\mu\omega}$$

where ρ is the fluid density (kg/m^3),

V is the flow velocity (m/s),

L is the span length (m),

E is the modulus of elasticity (Pa),

I is the moment of inertia (m^4),

μ = Fluid viscosity (N-s/m^2) and

$$\omega = 2\pi f_n \propto \sqrt{\frac{EI}{M}} \ . \qquad \text{---- (2.2)}$$

where f_n is the modal frequency of subassembly (Hz) and M is the mass per unit length.

The average temperature of flowing sodium in fuel subassembly is 472 °C. As per the Burgreen correlation, for the same amplitude of vibration in sodium and water, flow velocity ratio becomes,

$$\frac{V_W}{V_{Na}} = \frac{\rho_{Na}^{0.5} \times \mu_{Na}^{-0.33} \times E_{472}^{-0.33} \times M_U^{0.165}}{\rho_W^{0.5} \times \mu_W^{-0.33} \times E_t^{-0.33} \times M_{SS}^{0.165}} \quad \text{----- (2.3)}$$

Where E_t is the modulus of elasticity of Stainless Steel (SS) at the test temperature, E_{472} is the modulus of elasticity of SS at 472 °C, M_U is the mass of fuel subassembly and Mss is the mass of experimental fuel subassembly. The required test flow for FIV testing in water was calculated based on relation given in Fig. 2.14, which depicts the prototype vs model flow comparison. Testing was carried out with 65 °C water. Hence test flow is fixed using,

$$\frac{V_W}{V_{Na}} = \frac{AC}{AB} = 1.22 \quad \text{----- (2.4)}$$

The rated flow through the fuel subassembly in reactor is 154 m^3/h, therefore the test flow, Q_{Test} = 1.22 x 154 m^3/h = 188 m^3/h.

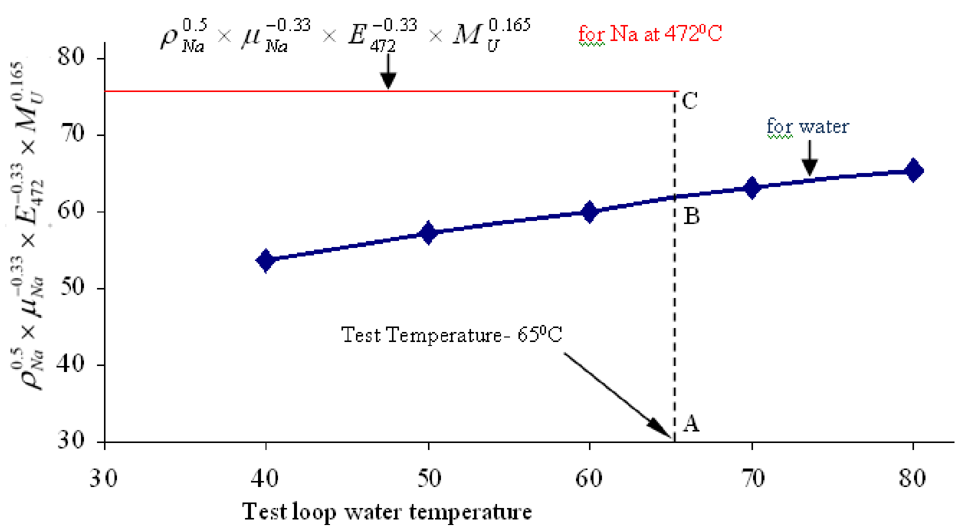

Fig. 2.14: Prototype Vs Model flow comparison.

Accelerometers were also installed at different elevation of the subassembly. The locations of the sensors are selected based on the analytically predicted mode shapes of the subassembly and the modal measurements carried out earlier.

2.4.1.4 Test results and discussion

The test section and test loop was filled with water and a centrifugal pump was used to circulate water through the test section. Flow through the test section was varied from 40% to 110% of the rated flow. For each measurement conditions, signals from the accelerometers were measured and recorded. Vibration spectra were calculated from the time signal. Fig. 2.15 shows the vibration spectra from accelerometers (0-200 Hz) for a flow rate of 188 m^3/h. It is found that the measured vibration frequencies of subassembly are 3.6 Hz, 19.2 Hz and 56.2 Hz.

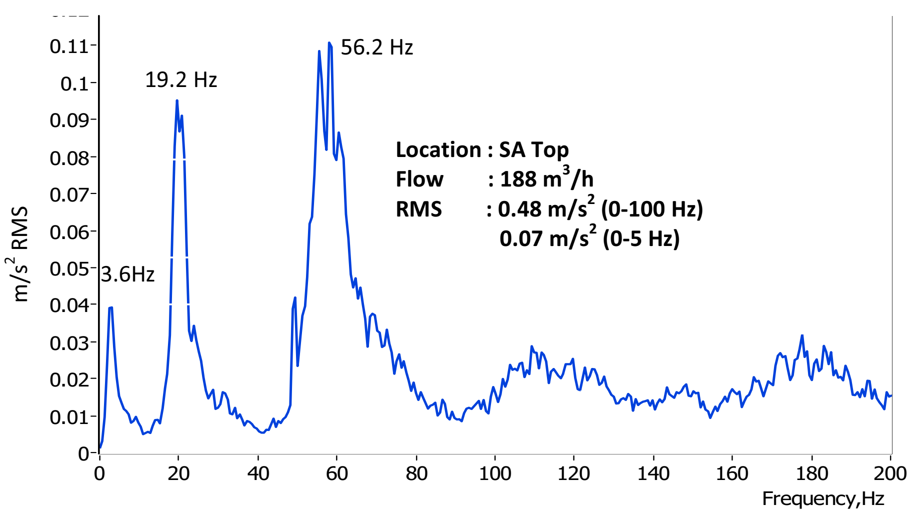

Fig. 2.15: Subassembly vibration spectra (Acceleration)

Fig. 2.16 shows the vibration displacement spectra. Subassembly being cantilever in nature, supported at the foot location, the amplitude of displacement was measured at the top of the subassembly and the strain was measured at the foot location. The overall amplitude of vibration displacement measured at the subassembly top is 0.2 mm (rms). Higher modes of subassemblies above 80 Hz are not excited. The maximum value of strain measured from the subassembly is 3.74 micro-strain, which corresponds to the stress value of 0.68 MPa, which is well within the design limit of 20 MPa from fatigue stresses by FIV [19].

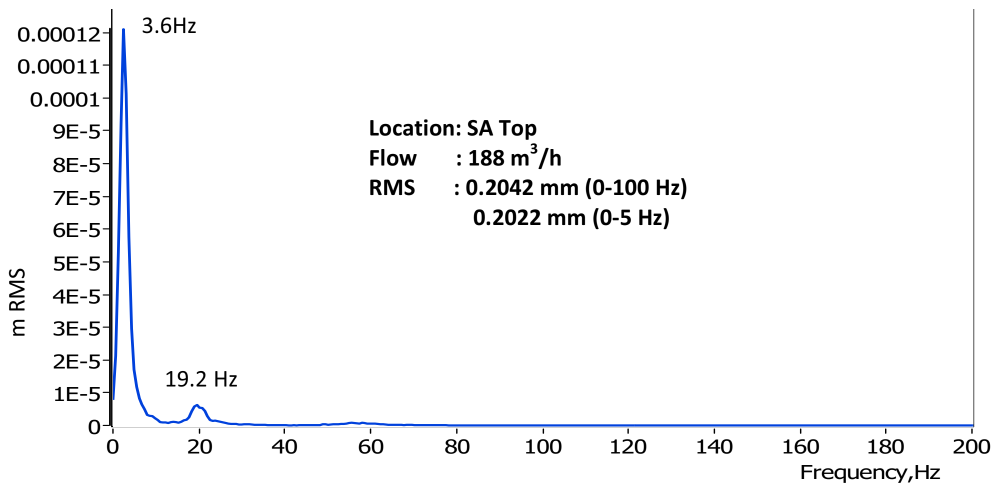

Fig. 2.16: Subassembly vibration spectra (Displacement)

This out-of-pile test has indicated that the design of subassembly is found to be safe against flow induced vibration. The test result also shows that the first natural frequency of PFBR fuel subassembly is 3.6 Hz.

2.4.2 FIV studies on PFBR control plug

Control plug is a critical component in the reactor assembly, which is located right above the core. Fig. 2.17 shows the schematic of PFBR control plug. The control plug supports control rod drive mechanisms, thermowells and thermocouple sleeve for temperature measurement, failed fuel localization module etc. The control plug is supported at the top, on the roof slab and the overall height is 7.7 m. Due to this free hanging length, control plug and its components are prone to flow induced vibrations. The existence of free liquid (sodium) surfaces, which is the source of sloshing phenomenon and the operation of primary sodium pump in the primary pool are other potential sources of vibration of reactor components. Since control plug is partially immersed in hot sodium, the reactor transients are felt by the components, hence it is very much essential to understand the vibration response of the control plug components.

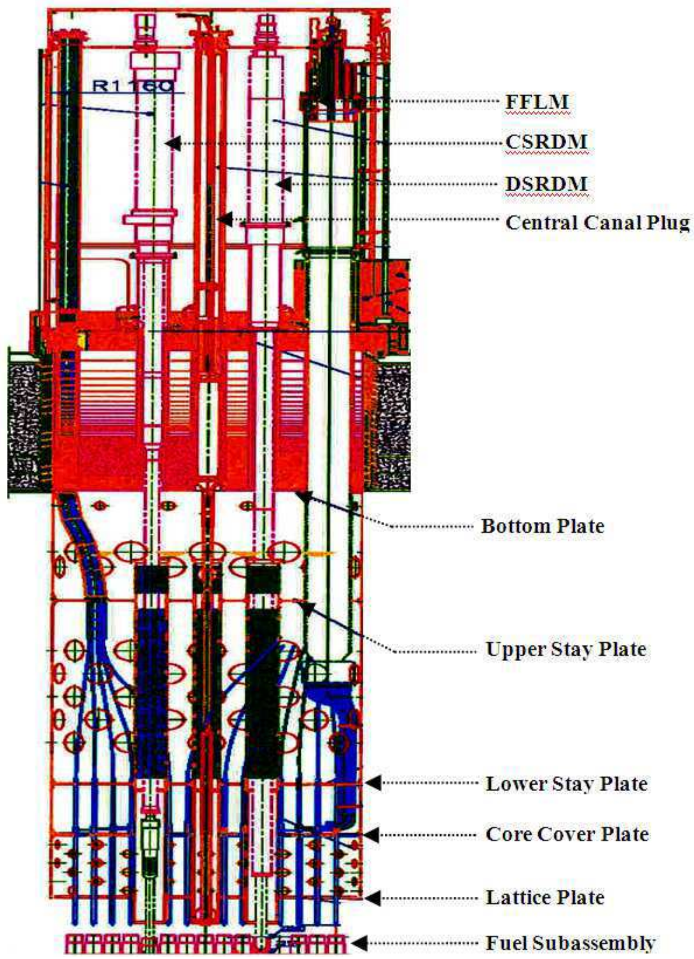

Fig. 2.17: PFBR Control plug

Control plug shell and shroud tubes have perforations to optimize the flow through the control plug. A fraction of the core flow (~10%) passes through the annular spaces between the shroud tubes in the control plug and comes out through the perforations on the shroud tubes and finally emerges out from the control plug through the control plug shell perforations.

2.4.2.1 Simulation criteria

The coolant sodium pumped by the primary sodium pump enters the subassembly through the grid plate picks up the fission heat generated in the core. Control plug is located right above the top of the core and a part of the hot sodium (10%) coming out of the core passes through the lattice plate of control plug and is deflected into the hot pool by the core cover plate. The control rod shroud tube and sampling sleeves are subjected to cross flow excitation. The central canal plug guide sleeve is not prone to FIV since the flow is axi-symmetric around it and the effect of cross flow in this location is insignificant. Vortex shedding, instability and turbulence buffeting are the main vibration excitation mechanisms in cross flow.

The natural frequency and mode shapes of each component are found out using the computer code CASTEM. Computational Fluid Dynamics (CFD) analysis was carried out and velocity profile inside the control plug was estimated. ASME Sec III Div 1 Appendix [N] procedure was followed for flow induced vibration analysis. Vortex shedding and fluid elastic instability mechanisms were considered for the analysis. These analysis results indicates that the flow velocity distribution inside the control plug internal is much lower than the critical velocity required to initiate instability mechanism. However the vibration due to vortex shedding phenomenon is relatively high and hence this excitation mechanism is considered for modeling the control plug vibrations. The experiment was carried out with velocity simulation criteria [20, 21]. The similitude requirement for vortex induced vibration scale modeling can be stated as follows.

$$\frac{S_M}{S_P} = 1 \quad \text{--- (2.5)}$$

$$\frac{Re_M}{Re_P} = 1 \quad \text{--- (2.6)}$$

Where, subscripts M and P refers to model and prototype,

S is the Strouhal number given by; $S = \frac{fD}{V}$

R_e is the Reynolds number given by; $Re = \frac{VD}{\nu}$

f is the vortex shedding frequency

D is the hydraulic diameter of the structure

V is the velocity of fluid and ν is the kinematic viscosity

Moreover, the model and prototype must be geometrically similar and the ratio of elastic moduli must be constant for all parts. From the dimensionless ratios, it can be stated that,

$$\frac{Y}{D} = \left\{\frac{f_n D}{SV}, \frac{VD}{\nu}, \frac{\rho_S}{\rho}, \delta\right\} \text{---(2.7)}$$

Where,

Y is the amplitude of vibration,

f_n is the natural frequency

V is the flow velocity

ρ is the density of the fluid and δ is the damping factor

For geometrically similar structures with the above four similitude ratios equal to unity and with equal velocity in the model and prototype, the scaling law between model and prototype can be written as shown in eqn.(4).

$$\left(\frac{Y}{D}\right)_M = \left(\frac{Y}{D}\right)_P \quad \text{---(2.8)}$$

As the control plug model used for the testing is a ¼ scaled down model, size of the components in the control plug, tubes, shell and plate dimensions are reduced to ¼ size of the

PFBR control plug. Thus the mass of the components is decreased by 64 times and the stiffness of the control plug internals is reduced by 4 times, making the natural frequencies scaled up by 4 times. The results obtained in the studies can be transposed to reactor conditions by suitable scaling factors.

As velocity simulation is maintained,

$$(V)_M = (V)_P \text{ ---(2.9)}$$

The ratio of flow in the model and prototype can be written as,

$$Q_M = A_M \times V_M \text{ and } Q_P = A_P \times V_P \text{ ---(2.10)}$$

Since scale size of the model is 1:4,

$$A_P = 16 \times A_M \text{ ---(2.11)}$$

From eqn.(5), eqn.(6) and eqn.(7),

$$Q_M = \frac{Q_P}{16} \text{ ---(2.12)}$$

The total core flow in PFBR is 28,371 m^3/h and hence from eqn. (2.12), the flow through the model is calculated and test flow is fixed as 1773 m^3/h.

2.4.2.2 Description of FIV test loop

Flow induced vibration testing was carried out in water in a test facility (Fig. 2.18) called SAMRAT (Scaled Model of Reactor Assembly for Thermal Hydraulics). The model is geometrically similar to PFBR and all major dimensions of PFBR are scaled down by a factor four [22]. Due to the large size of the model, better simulation of geometrical details is achieved. In the core region of SAMRAT model, fuel, blanket, storage and cavity zones are simulated in the model. For FIV experiments, better simulation is possible due to larger size and the results are directly transposable to the reactor.

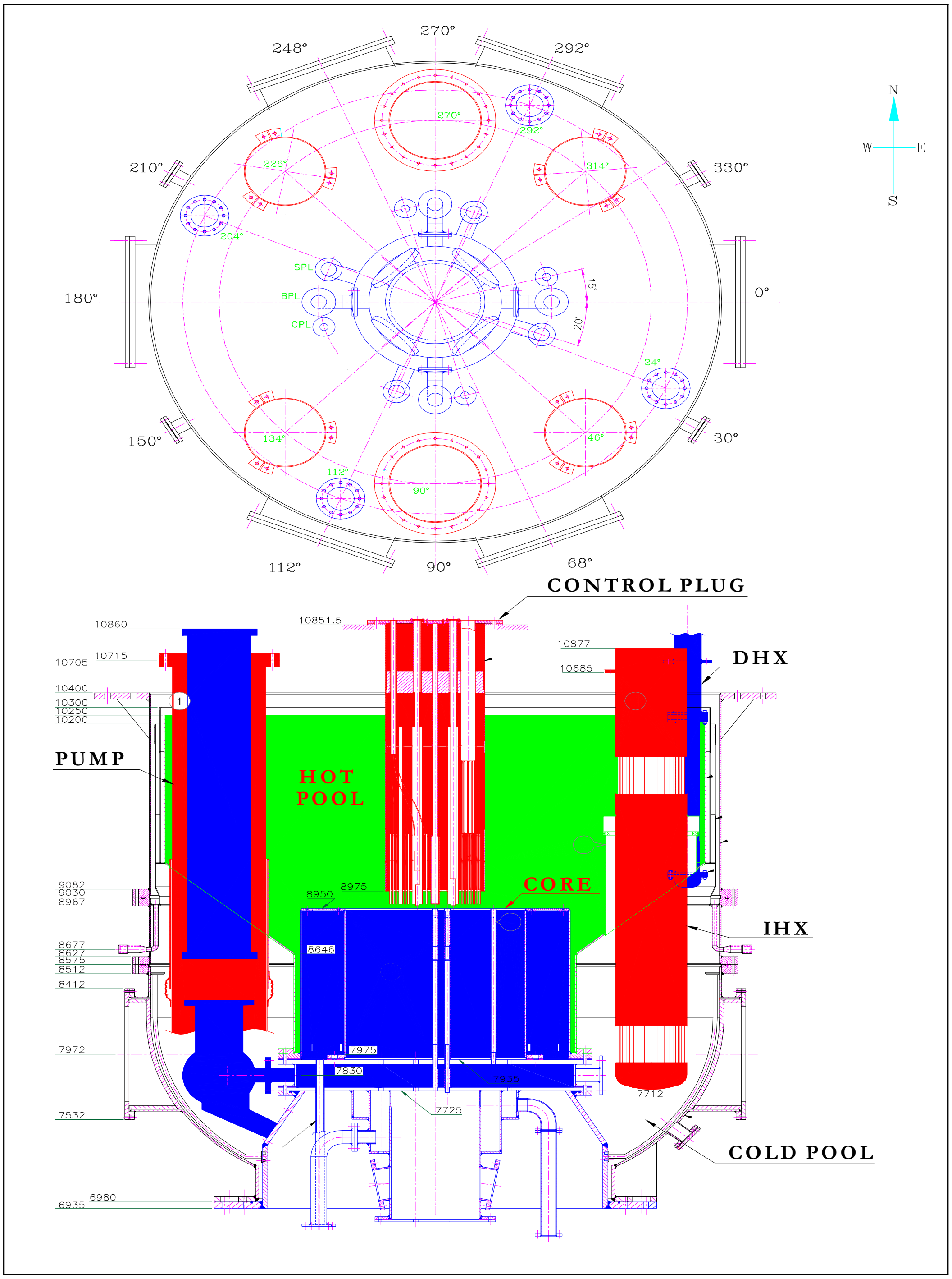

Fig. 2.18: SAMRAT model

2.4.2.3 Flow induced vibration testing

Two 500 kW pumps in the SAMRAT model with a rated flow of 1200 m^3/h were used to circulate water in the model. Accelerometers and strain gages were used as the sensors and were installed at various locations on the ¼ model control plug model. The flow rate in the loop was measured using anubar flowmeter. Studies were carried out for flows of 20 % to 110 % of maximum rated flow which corresponds to a flow rate of 354 m^3/h to 1949 m^3/h. For each flow condition, the vibration values from strain gauges and accelerometers were acquired using a multi channel FFT analyzer. The output signals from the sensors were acquired and analyzed to obtain frequency spectra and overall vibration values. The free level surface at the top in the model is maintained at 50mm below the inner vessel. Fig. 2.19 shows the cut out view of the instrumented control plug.

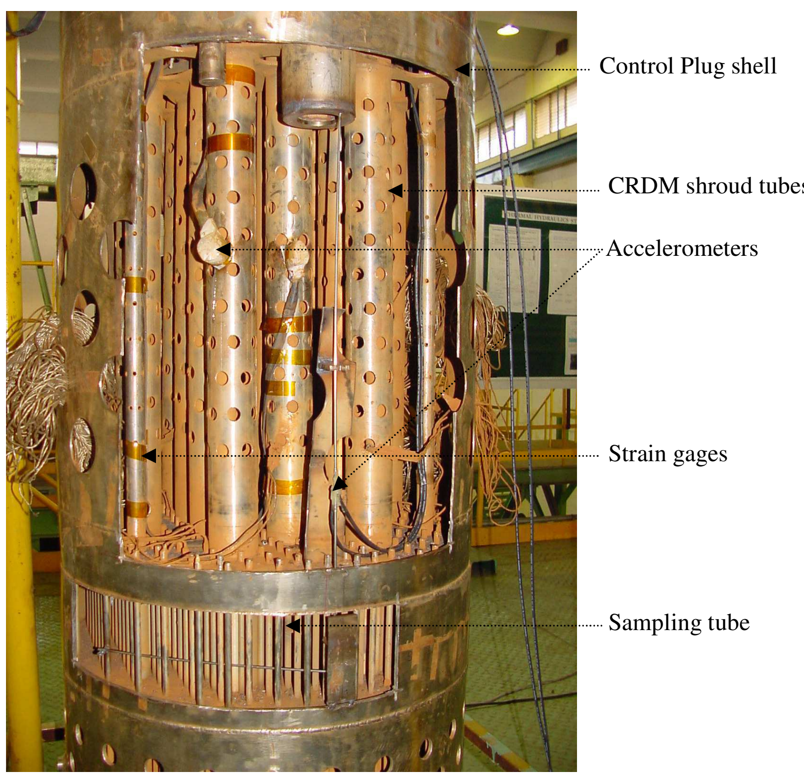

Fig. 2.19: Instrumented control plug model (cut section view)

Two thermocouples tubes, two delayed neutron detectors and two sampling tubes were instrumented with miniature accelerometers and the control plug shell was instrumented with normal general purpose accelerometer. CSRDM and DSRDM shroud tubes and thermocouple Sleeves were instrumented with strain gauges at different locations. The CP internals were instrumented with strain gages and accelerometers at locations where amplitudes were expected to be maximum based on the mode shapes obtained from modal analysis. 18 strain gages and two accelerometers were installed at various locations on the CP internals to measure vibration amplitudes and modal frequencies. The signals from these sensors were filtered and fed to the multi-channel FFT analyzer running PULSE Labshop 4.1 software for obtaining frequency power spectra.

2.4.2.4 Test results

The maximum test flow rate derived based on velocity similitude was 1773 m^3/h. Fig. 2.20 shows the frequency spectra recorded from the DSRDM shroud tube for various test flow conditions. Finite element modeling of control plug components was carried out using ANSYS software and natural frequencies for individual components are tabulated. Experimental verification of analytical prediction was performed by experimental modal analysis. Based on the results, natural frequencies of control plug components for the scaled down modal was analytically predicted [23]. Table 2.2 shows the measured natural frequencies of control plug components along with the analytical prediction and Table 2.3 shows the overall vibration amplitudes measured from control plug components for various test flow conditions. The amplitude of vibration is found to have an increasing trend with flow and is represented in Fig.

2.21 for a typical shroud tube in the control plug. Table 2.4 shows the overall strain values recorded from the control plug components.

For each component, amplitude of vibration was calculated from frequency spectra and the bending stress value was derived. The bending stress for the control plug components were in the range of 0.5 MPa to 8 MPa, which is much below the designed limit. From the experimental results, it is concluded that the control plug internals are subjected to flow induced vibration but the overall values of vibration are well within permissible limits.

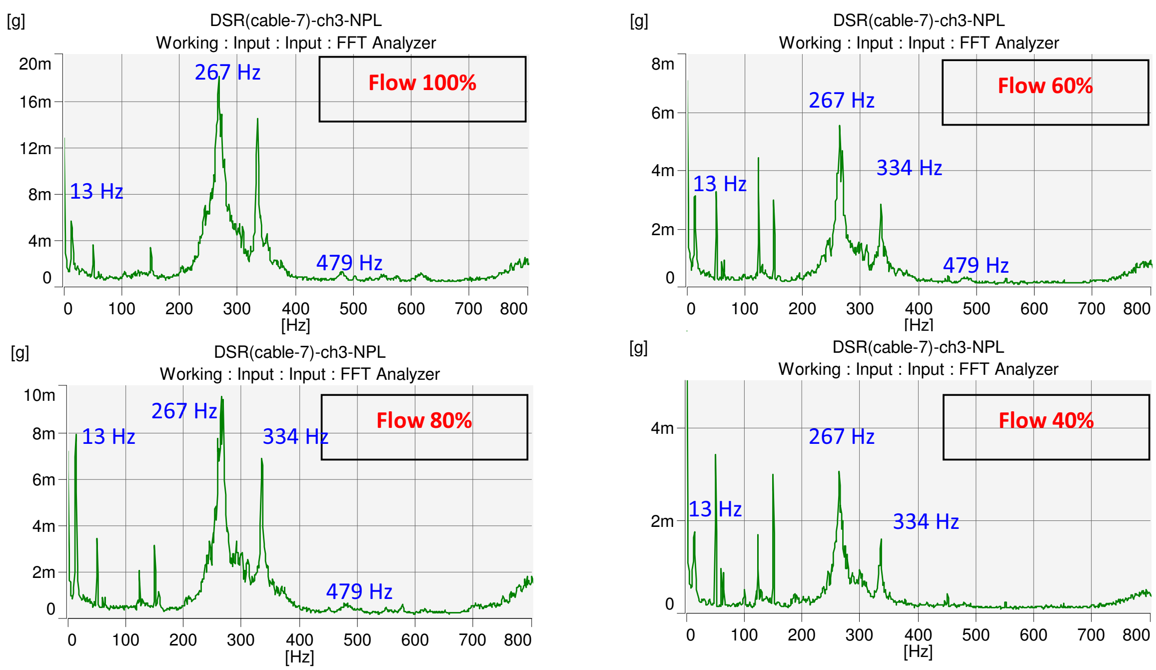

Fig. 2.20: Vibration spectra of DSRDM shroud tube

Table 2.2: Natural Frequencies of Control Plug internals

SN	Control Plug internal	Frequency (Experimental) (1:4 model)	Frequency transposed to PFBR	Frequency (Analytical) (PFBR)
1	Thermocouple tube	13 Hz	3.25 Hz	4 Hz
2	DND sampling tube	52 Hz	13 Hz	12 Hz
3	Shroud tubes	479 Hz	120 Hz	121 Hz
4	Thermocouple sleeve	267 Hz	67 Hz	74 Hz

Table 2.3: Overall vibration amplitudes

Flow (%)	Flow (m^3/h)	Overall Vibration (g rms) DND tube (g)	TC tube (g)	CSRDM shroud tube (g)	DSRDM shroud tube (g)	FFLM Sampling tube (g)
20%	354	0.0440	0.223	0.0138	0.0035	0.0086
40%	709	0.0499	0.214	0.0247	0.0116	0.0101
50%	886	0.0952	0.233	0.0298	0.0201	0.0195
60%	1064	0.1120	0.254	0.0345	0.0308	0.0211
80%	1418	0.2170	0.275	0.0624	0.0382	0.0309
100%	1773	0.3410	0.333	0.1130	0.0719	0.0429

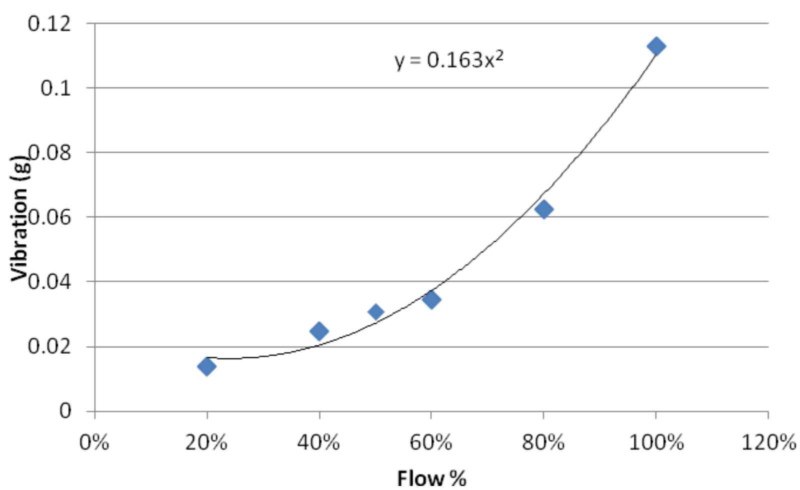

Fig. 2.21: Overall vibration Vs Flow for shroud tube in CP

Table 2.4: Overall strain amplitudes (Upto 800 Hz)

Flow (%)	Flow (m^3/h)	Overall strain (microstrain rms) DSRDM Shroud tube	Sampling sleeve	CSRDM Shroud tube
40%	709	11.9	5.5	4.3
60%	1064	30.3	17.9	6.7
80%	1418	39.0	38.3	21.1
100%	1773	43.8	57.9	47.8

2.4.3 Weir instability studies in PFBR main vessel cooling system

The main vessel of this pool type reactor carries about 2000 tonnes of weight and operates with reactor outlet temperature of 547 ^{0}C. In order to keep the main vessel temperature below creep range (<420^{0}C) and to reduce high temperature embrittlement and to ensure its healthiness for 40 years of reactor life, a small fraction of core flow (0.5 m^3/s) is sent through an annular space formed between the main vessel and a cylindrical baffle (outer baffle) to cool the vessel. A part of the reactor sodium flow (≈5%) in the grid plate leaks out at the foot of the subassemblies through specially designed labyrinths collected in a chamber below and directed to the annular space indicated above, through 24 circumferentially spaced pipes (Fig. 2.22). Sodium then overflows the top of the primary thermal baffle (weir shell of thickness 20 mm) and falls into the annular pool of sodium separated from the cold pool by the inner shell.

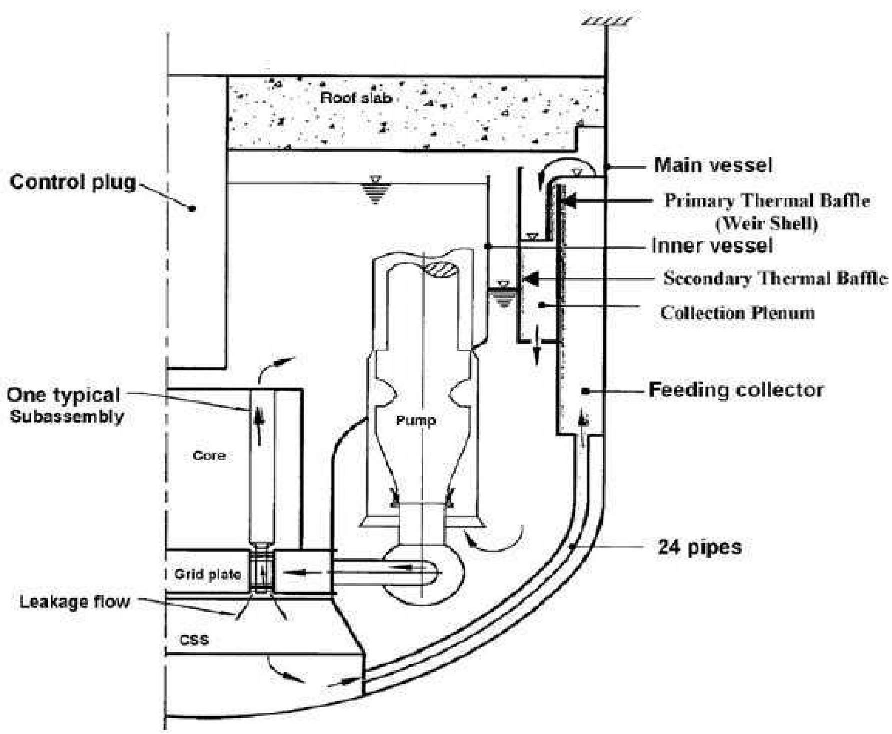

Fig. 2.22: PFBR weir shell arrangement

The weir shell, where the overflow of liquid sodium takes place, is a thin shell prone to flow induced vibrations [24] due to liquid sloshing and fluid–structure interaction (FSI). This vibration phenomenon was first observed during the commissioning of French Super-Phenix reactor [25], which has a similar main vessel cooling arrangement.

2.4.3.1 Excitation mechanisms

The two important mechanisms identified for instability of the weir cooling system is sloshing and fluid elastic instability. These mechanisms are explained below.

Sloshing (Type I)

Surface wave oscillation will be produced in a liquid filled container/tank when it is excited with an external force. In case of weir systems, the pressure pulsations due to the falling liquid over the free surface could be the source of excitation. When this exciting frequency coincides with system natural frequency, resonance like condition can occur which leads to very large surface liquid motion and vibration of the container.

Fluid elastic instability (Type II)

If the weir shell is disturbed from its equilibrium position, it naturally vibrates with a particular wave number. For the stable flow configuration, the vibration decays exponentially to zero. On the contrary, the shell vibrates with exponentially increasing amplitudes for the unstable system. If the dynamic fluid forces causing vibration are developed from the shell displacements, then the resulting unstable vibration is termed as fluid elastic instability. The fluid elastic instability which affects the weir shell is mainly due to the sloshing of the liquid free levels that is associated with the feeding and collection plenums.

If the kinetic energy imparted by the liquid falling from the weir crest on the free surface of the restitution collector (collection plenum) is greater than the energy dissipated due to structural and fluid damping, then any perturbation introduced on the shell will develop to cause instability. In the weir flow configuration this situation arises under some critical combinations of flow rate and fall height.

2.4.3.2 Modeling laws

Since there is a fluid flow with a moving free surface and vibration of a structure in a coupled mode, the forces that are dominant are gravity force, shell elastic force, fluid inertial force and the viscous force. Therefore Cauchy number (elastic/inertia), Froude number (inertia/gravity), frequency ratio and Reynolds number (inertia/viscous) need to be simulated if the results from the model are to be transposed to the reactor.

In the 1:4 scale model, the Cauchy and Froude number could be simulated by proper selection of material, baffle thickness and water as the test fluid. For simulation of Cauchy and Froude numbers, the thickness of the baffle for this model is selected as 3.2 mm, and nominal flow rate for the model is 52 m^3/h.

2.4.3.3 Experimental studies

For this experiment 34 number of strain gages were installed at various locations on the weir shell surface to measure circumferential and longitudinal strains. Apart from this an accelerometer was also mounted on the weir shell for monitoring higher order frequency spectra and vibration. The experimental study was carried out for flows starting from 13 to 66 m^3/h. For a particular flow, the fall height was varied from 0 to 40 cm in steps of 1 mm. Instability confirmed to have set in if there was a steady increase in the primary baffle vibration amplitude. For each flow, primary baffle vibrations were measured with strain gauges and accelerometer. The data was acquired in real-time and analyzed in frequency and amplitude domains employing multi-channel analyzer.

2.4.3.4 Results and discussion

It was observed that the baffle system became unstable as the fall height approached 133 mm for flow rate of 30 m^3/h. Below 30 m^3/h the instability phenomenon is not observed for any fall height in the model. For higher flow rates (more than 30 m^3/h) the instability was observed at higher fall heights. Fig. 2.23a and 2.23b shows typical real-time plots of a strain gauge for nominal flow condition during stable and unstable operation of the weir system, respectively.

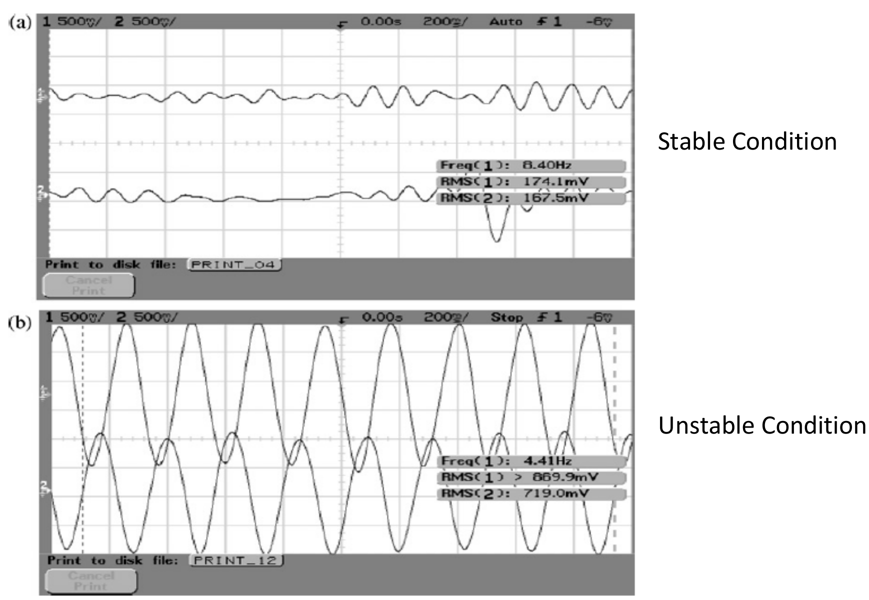

Fig. 2.23: Time signal (strain gauge) during stable and unstable weir operation

From the spectrum in Fig. 2.24a and 2.24b, it can be inferred that, compared to random vibration signature during stable operation, a single predominant frequency with much higher amplitude of vibration was observed during instability. This single frequency resonance type of vibration could be observed in time signal also.

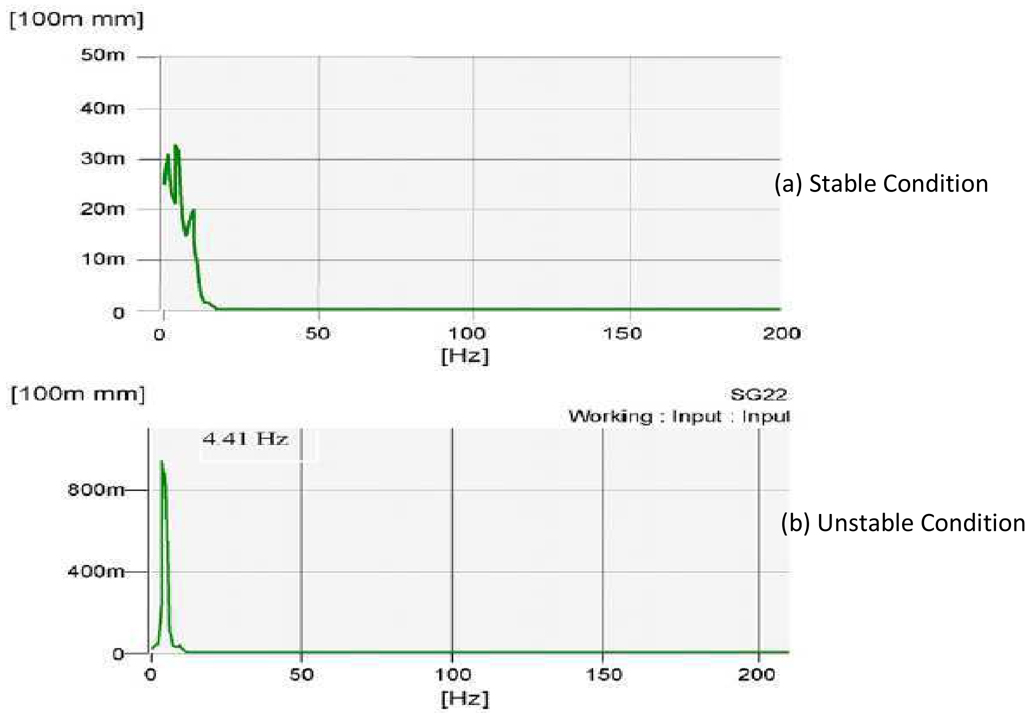

Fig. 2.24: Spectra during stable and unstable weir operation

Fig. 2.25a and 2.25b show the variation in the PDF plot during stable and unstable operation conditions. These plots clearly explain the change over from random excitation during normal operation to a predominant sinusoidal one during instability. Spectra recorded during stable and unstable operation clearly indicate an increase in amplitude level of more than 30 times compared to stable condition.

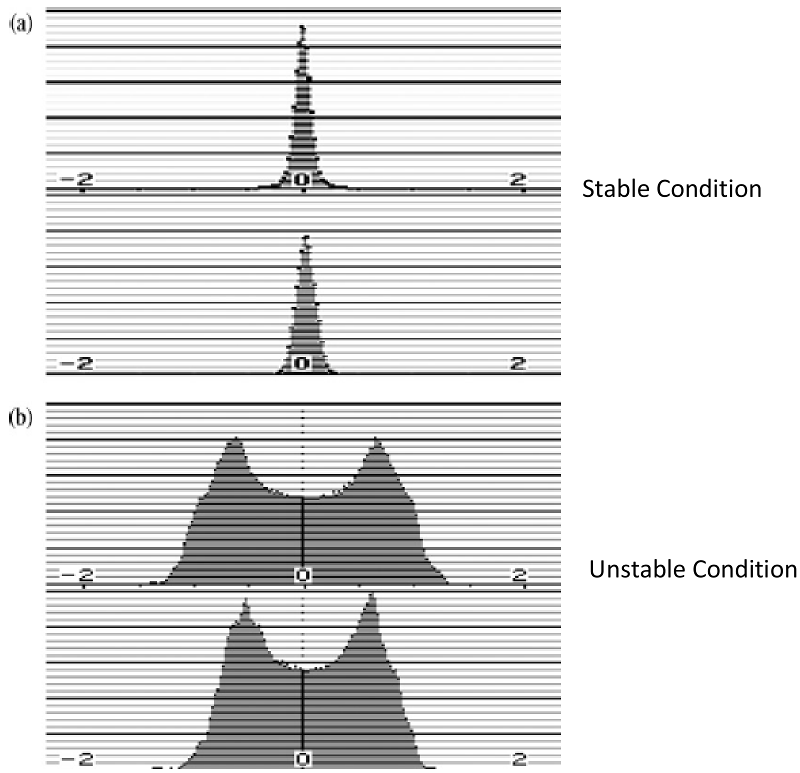

Fig. 2.25: PDF plot during stable and unstable weir operation

Fig. 2.26 shows the time plot during instability build-up at the observed resonance frequency of 4.41 Hz, for nominal flow of 52 m^3/h at a fall height of 178 mm. This instability plot (time Vs strain) shows the increase in strain level of more than 30 times compared to stable operation, which clearly demonstrates the consequences of unstable operation of the system. It was also observed that, during instability the flow over the weir was not continuous but it was interrupted type of flow and the liquid was splashing with sound above the top of the weir from the feeding and collection plenum due to the violent vibration of the thermal baffle. Based on the results obtained from the experimental investigation, the instability chart for 1:4 scale model of PFBR has been derived and is shown in Fig. 2.27.

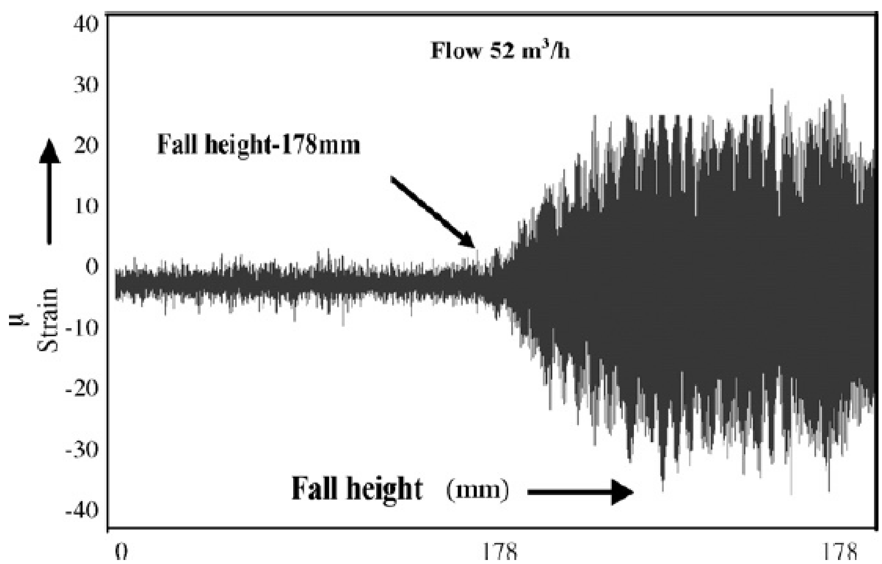

Fig. 2.26: Instability buildup

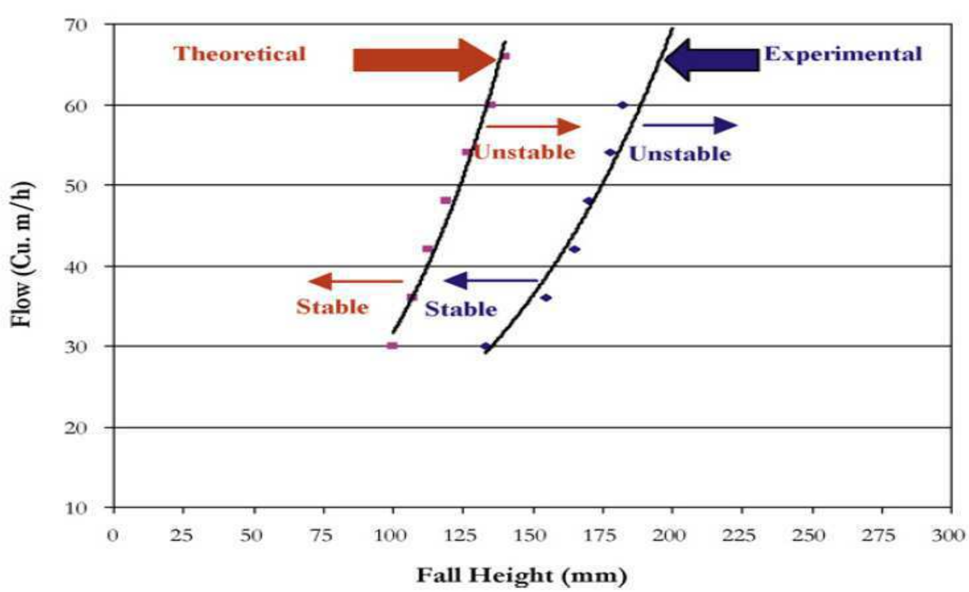

Fig. 2.27: Instability chart for 1/4 model of PFBR

Based on the experimental results, the analytical code was validated and the instability chart for PFBR weir cooling system for its selected range of flow and fall heights were analytically predicted and the weir system is found to be stable during its entire range of operation.

Even though out-of-pile testing was carried out for critical components, in many operating FBRs, real time monitoring systems are installed for assessing the performance. Many advanced methodologies are made use for in-service inspection in reactor systems. Eddy current methods and ultrasonic methods are used as in-service-inspection techniques for various anomaly detection. Since vibration is one of the major causes of failure in systems, an online vibration measurement system for FBR primary components is recommended for detecting an impending failure.

CHAPTER-3

ULTRASONIC TECHNIQUE FOR VIBRATION MEASUREMENT

3.1 Introduction

Sound waves are mechanical waves which require a medium for its propagation. Sound from a source travels in the medium as pressure fluctuations and reaches the receiver. Sound waves travel through materials by vibrating the particles that make up the material. The pitch of the sound is determined by the frequency of the wave (vibrations or cycles completed in a certain period of time). The sound wavelength is inversely proportional to its frequency ($\lambda \propto 1/f$). Sound spectra extends over a broad range of frequencies. Sound waves are classified broadly into three categories. Sound waves having frequency less than 20 Hz is known as Subsonic or infrasonic waves. Sound waves having frequency between 20 Hz to 20 kHz is known as audible or sonic waves. Sound waves with frequency greater than 20 kHz is known as ultrasonic waves.

3.2 Fundamentals of ultrasonics

The word ultrasonic combines the Latin roots ultra, meaning 'beyond' and sonic, or sound. The sound waves having frequencies above the audible range are called ultrasonic waves. Generally these waves are called as high frequency waves. The field of ultrasonics has applications for imaging, detection, navigation etc. Flaw detection, porosity detection, weld inspection, ultrasonic cleaning etc. are other major industrial applications of ultrasonic waves.

Ultrasonic waves are very similar to light waves in that they can be reflected, refracted, and focused. Reflection and refraction occurs when sound waves interact with interfaces of differing acoustic properties. In solid materials, the vibrational energy can be split into different wave modes when the wave encounters an interface at an angle other than 90 degrees. Ultrasonic reflections from the presence of discontinuities or geometric features enable detection and localization. The velocity of sound in a given material is constant and can only be altered by a change in the mode of energy transfer. Velocity of sound waves in medium in general can be expressed as the square root of the ratio of elasticity of the medium to its density. Typical velocity of sound waves in different material media is given in Table 3.1.

Table 3.1: Velocity of sound in different materials

Sl. No	Material/Medium	Velocity (m/s)
1.	Air	343
2.	Water	1480
3.	Stainless Steel	5500
4.	Sodium	2500
5.	Aluminium	6200

3.3 Wave propagation in a medium

Depending on the wave propagation methods, waves are broadly classified into four classes namely, longitudinal waves, transverse or shear waves, surface waves or Rayleigh waves and plate waves or Lamb waves.

A longitudinal wave is a compressional wave. The particle motion in the medium in the case of longitudinal wave is in the same direction as the propagation of the wave itself, whereas in the case of a shear wave, the particle motion is perpendicular to the direction of the wave propagation. The velocity of shear wave is approximately half of the longitudinal wave velocity. Surface waves have an elliptical particle motion and travel across the surface of a material. Their velocity is approximately 90% of the shear wave velocity of the material and their depth of penetration is approximately equal to one wavelength. Lamb waves have a complex vibration occurring in materials where thickness is less than the wavelength of ultrasound introduced into it. Fig. 3.1 shows the longitudinal and shear mode of wave propagation [26].

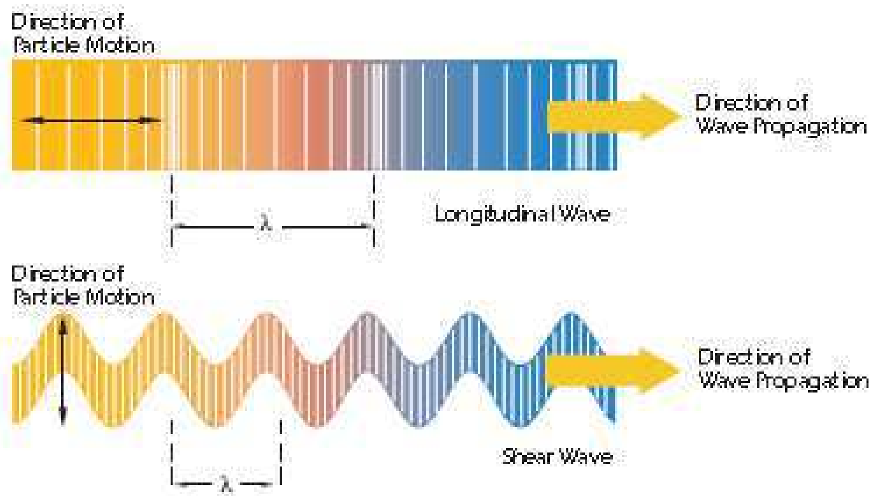

Fig. 3.1: Longitudinal and Shear mode of wave propagation [26]

3.4 Ultrasonic transducers

An ultrasonic transducer converts electrical energy to mechanical energy, in the form of sound and vice versa. Generation of ultrasonic waves in a medium can be achieved in several ways. Piezoelectric effect, magnetostrictive method, etc. are commonly used to generate ultrasonic waves. Due to ease of assembly, compactness and comparatively less circuitry requirements, piezo-electric method is commonly used in industries [27]. A piezo-electric crystal is excited using a suitable input voltage from a source, which produces mechanical waves in the medium. The commonly used piezo-electric materials are PZT (Lead Zirconate Titanate), Lithium niobate, Lithium sulphate etc. A typical ultrasonic transducer internal is shown in Fig. 3.2.

Active element is the piezo-electric crystal which vibrates at its resonance during pulse voltage excitation. An impedance matching layer is used in the transducers to transmit the energy without much loss. A special solder alloy is used for bonding the crystal to the casing. The backing material supporting the crystal has a great influence on the damping characteristics of a transducer. Using a backing material with impedance similar to that of the active element will produce the most effective damping. Such a transducer will have a wider bandwidth resulting in higher sensitivity. As the mismatch in impedance between the active element and the backing material increases, transducer sensitivity is reduced.

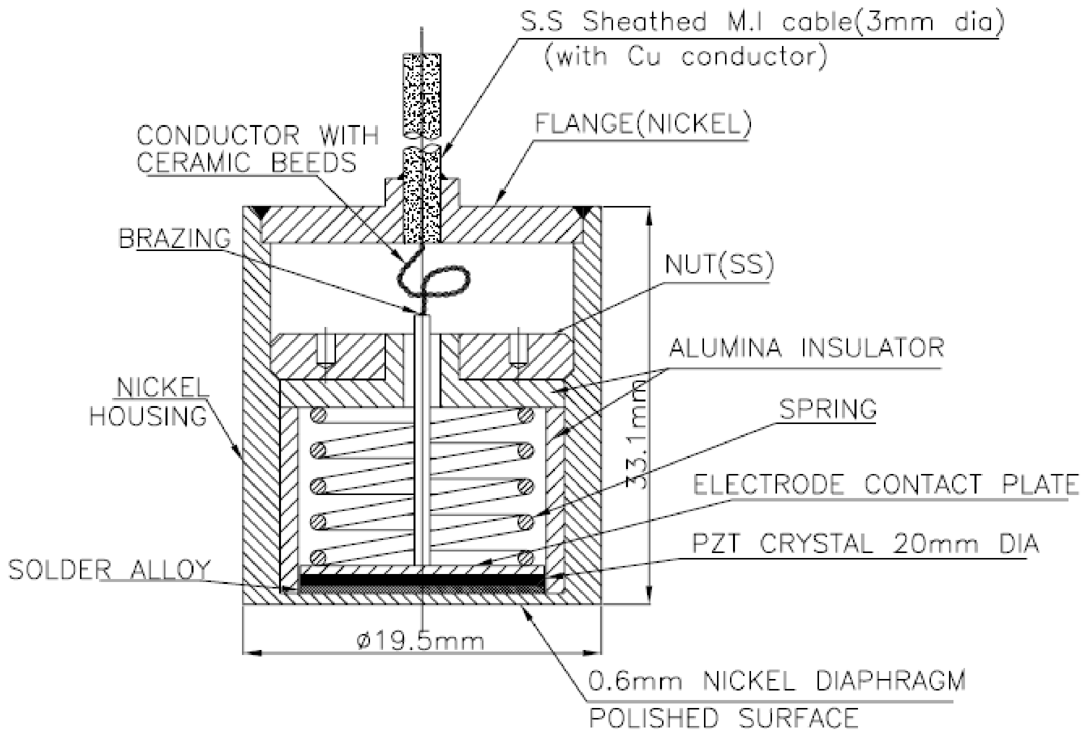

Fig. 3.2: Cut away view of a typical ultrasonic transducer

Generally, the frequency of a transducer is the central operating frequency and depends primarily on the backing material. Highly damped transducers will respond to frequencies above and below the central frequency. The broad frequency range provides a transducer with high resolving power. Less damped transducers will exhibit a narrower frequency range and poorer resolving power, but greater penetration.

3.5 Important features of ultrasonic sensors

There are some major technical parameters that should be looked into, when making measurements using ultrasonic sensors. They are briefly described in the following section.

3.5.1 Ultrasonic pressure field

Once excited the crystal with a suitable pulse, the crystal vibrates and the sound waves are generated in the medium. A typical sound field pattern is shown in Fig. 3.3. The field is divided into two zones namely, the near field and the far field. The near field is the region directly in front of the transducer where the sound intensity goes through a series of maxima and minima and ends at the last maximum, at distance N from the transducer. The far field is the area beyond near field, where the sound field pressure gradually drops to zero. Variation in amplitude of sound beam is shown in Fig. 3.4. Because of these variations, it is very difficult to accurately evaluate echo from objects within the near field. The near field distance is a function of the transducer frequency/wavelength (λ) and element diameter (D) and the relationship is given as,

$$N = D^2/4\lambda \text{ ----- } (3.1)$$

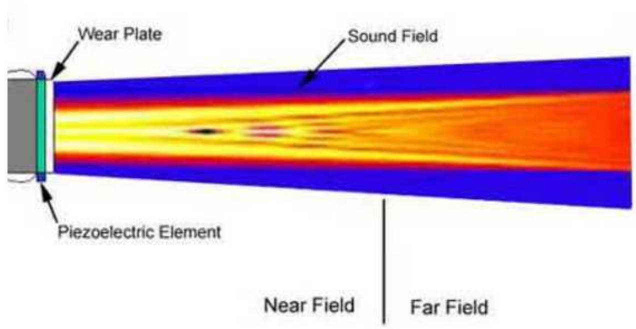

Fig. 3.3: Ultrasound pressure field [26]

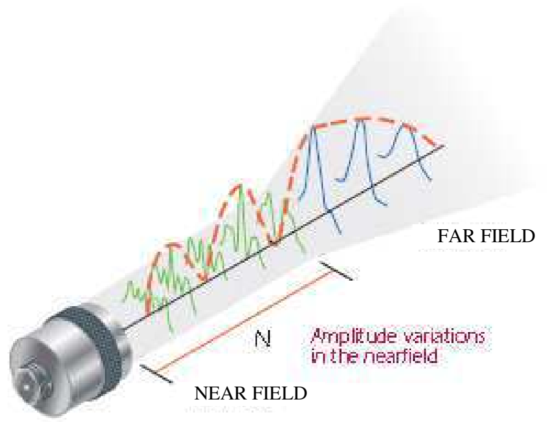

Fig. 3.4: Amplitude variations in the sound field [26]

3.5.2 Beam spread and beam divergence

Sensitivity of transducer is affected by the beam diameter at the point of interest. The beam energy doesn't follow a cylindrical path throughout, but spreads out as it propagates through the medium. The smaller the beam diameter, the greater is the amount of energy is reflected by a target object. Fig. 3.5 shows the beam spread and beam divergence of ultrasonic beam.

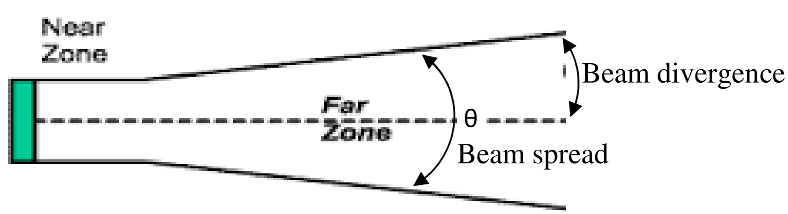

Fig. 3.5: Beam spread and beam divergence of ultrasonic waves [26]

Beam spread is always twice that of the beam divergence. Beam spread is related to the velocity (V), diameter and frequency (f) of the waves as,

$$\mathrm{Sin}(\theta) = 1.2\ V/Df \quad \text{------ (3.2)}$$

for a circular transducer of diameter D. The higher the frequency of ultrasonic waves, the lower is the beam spread.

3.5.3 Acoustic impedance of the medium

The acoustic impedance is referred to as the opposition to displacement of its particles by sound. Acoustic impedance 'Z' is given by the relation:

$$Z = \rho V \quad \text{-----} \ (3.3)$$

where, V is the velocity of sound in the material and ρ is the density of the material/medium.

Acoustic impedance plays a crucial role in determining the path of sound in different mediums. The boundary between two materials of different acoustic impedances is called acoustic interface. When sound beam enters an acoustic interface, sound intensity reflected from the interface and transmitted to the second medium solely depend on the acoustic impedances of the two mediums.

If we are considering two mediums with acoustic impedances Z_1 and Z_2 (Fig. 3.6), a sound wave travelling through Z_1 medium, when it reaches the interface it suffers both reflection and transmission. The reflection (A_R) and transmission (A_T) coefficients of sound wave intensity are given by [28]-

$$A_R = (Z_2 - Z_1)^2 / (Z_1 + Z_2)^2 \quad \text{-------} \ (3.4)$$

$$A_T = (4Z_1Z_2) / (Z_1 + Z_2)^2 \quad \text{---------} \ (3.5)$$

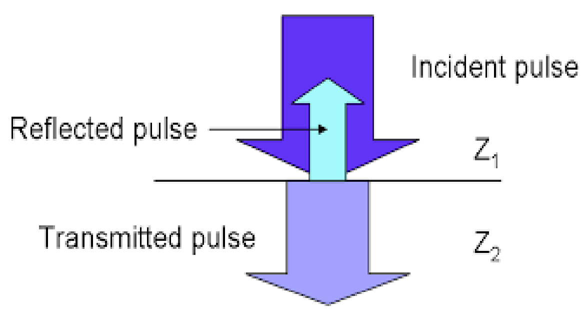

Fig. 3.6: Ultrasonic waves at an acoustic interface

Acoustic impedance is expressed in kg/m^2s or in Rayl. Acoustic impedances of important materials are tabulated in Table 3.2. Acoustic impendence of water is 1.48 x 10^6 kg/m^2s and that of steel is 46.6 x 10^6 kg/m^2s. If a sound wave traveling in water impinges on a stainless steel plate, 90% of the acoustic intensity will be reflected back and 10% will be transmitted. Hence ultrasound waves generated in water can be used for imaging or other studies when the target is stainless steel, which is the structural material in reactor circuits.

Table 3.2: Acoustic impedance value for different materials

SN.	**Material** (at room temperature unless specified)	**Acoustic impedance (kg/m^2s x 10^6)**
1.	Air (25^0C)	0.0003
2.	Concrete	9.2
3.	Aluminum	17.06
4.	Nickel	49.99
5.	Stainless Steel	46.6
6.	Water (20^0C)	1.48
7.	Sodium	2.0
8.	Copper	41.61

3.5.4 A-Scan, B-Scan and C-Scan imaging in ultrasonics

Ultrasound waves are used in various industries to gather information such as protrusions, detection of objects, imaging etc. The data obtained from the ultrasonic waves can be represented in different formats such as A-scan, B-scan and C-scan displays [29]. These methods of representation provide a different way of looking at information during ultrasonic testing especially for defect detection in materials.

3.5.4.1 A-scan representation

In A-scan presentation, the amount of ultrasonic energy received is represented as a function of time. When ultrasonic sensors are focused on a target, and triggered using a pulser receiver, we obtain a plot of Time Vs Amplitude of signal. Fig. 3.7 shows a typical A-scan representation of ultrasonic signal. In this plot the triggering of ultrasonic sensor is represented by the initial pulse followed by ringing of the crystal and the echo from the target is obtained after a period of time corresponding to the distance of the target. A-scan representation can be used to locate and estimate the distance of the target from the ultrasonic sensor. A-scan plot allows the signal to be displayed in its natural radio frequency form (RF), as a fully rectified RF signal, or as either the positive or negative half of the RF signal.

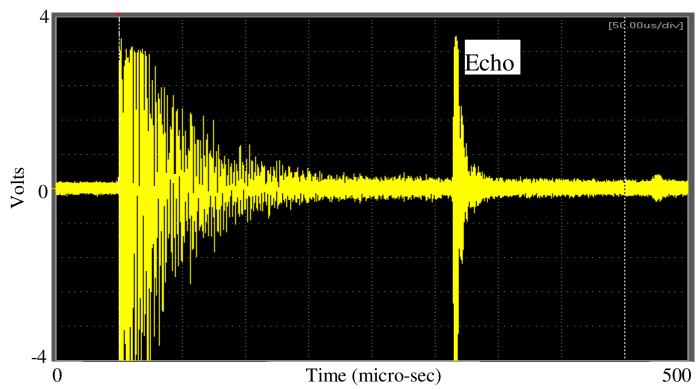

Fig. 3.7: A typical A-Scan plot

3.5.4.2 B-Scan representation

The B-scan presentation is mainly used in testing materials for defects, as it represents the cross-sectional view of the test specimen. In B-scan, the time-of-flight of the sound energy is displayed against the position of the transducer. The B-scan is typically produced by establishing a trigger gate on the A-scan echo signal. Whenever the signal amplitude crosses the gate level, a point is produced on the B-scan plot. For defect detection, when the transducer is moved on a surface, we will obtain the liner length of cracks or discontinuity in the material. A typical A-scan and B-scan representation of a specimen with defects (A, B and C) are shown in Fig. 3.8.

3.5.4.3 C-Scan representation

The C-scan presentation provides a plan-type view of the location and size of test specimen features. The plane of the image is parallel to the scan pattern of the transducer. C-scan presentations are normally produced with an automated data acquisition system, such as a computer controlled immersion scanning system. Typically, a data collection gate is established on the A-scan and the amplitude or the time-of-flight of the signal is recorded at regular intervals as the transducer is scanned over the test piece. The relative signal amplitude or the time-of-flight is displayed as a shade of gray or a color for each of the positions where data was recorded. The C-scan presentation provides an image of the features that reflect and scatter the sound within and on the surfaces of the test piece. High resolution scan can produce well defined images.

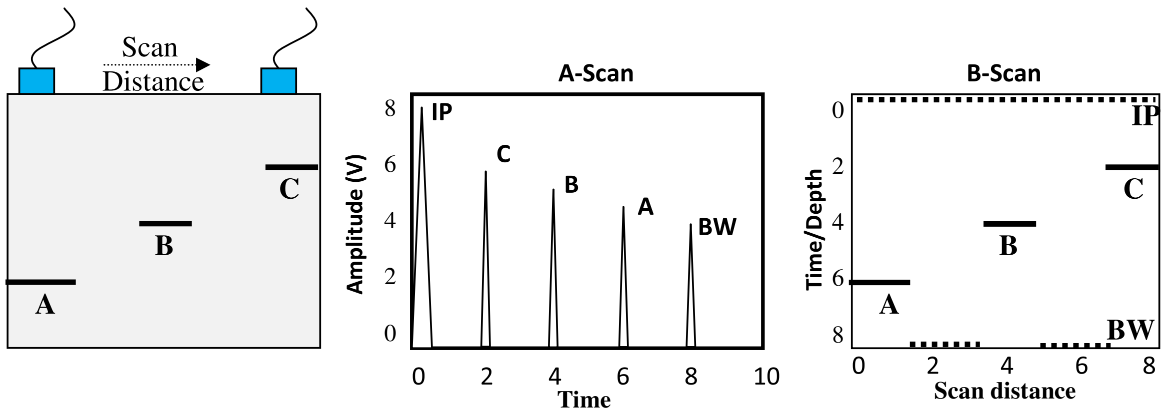

Fig. 3.8: A test specimen with defects and its corresponding A-scan and B-scan plots

3.6 Introduction to vibration measurement using ultrasound waves

In case of a pool type reactor where all the primary components are immersed in sodium measurement of vibration is quite a challenge. However, it is a safety requirement to measure the amplitude and frequency of vibration of fuel subassembly during pre-commissioning tests of PFBR. The major challenges involved were sodium environment, and high temperature (200^{0}C). Since conventional sensors like accelerometers, LVDT, strain gages etc cannot be used for under sodium applications in reactor primary system, alternate methods with non-contact type measurement technique were investigated. Due to the opacity of sodium to light, optical methods were ruled out. Due to accessibility, probe positioning issues, modification in subassembly geometrical profile etc, eddy current methods were also ruled out. The possibility of other method like ultrasonic technique was explored and feasibility studies were conducted. Non-contact measurement technique using ultrasound waves was planned to be developed and extensive experiments were carried out in various test facilities to establish the measurement technique.

3.6.1 Vibration measurement technique

A typical ultrasonic signal recorded from a target object is shown in Fig. 3.7. When the crystal is excited using a single excitation pulse initial ringing of the transducer occurs. The excitation pulse used for the study is a negative spike excitation. Fig. 3.9 shows a typical negative spike excitation. Max pulse voltage used is -360 V with a rise time of 5 ns and a pulse width of ~12 ns [30].

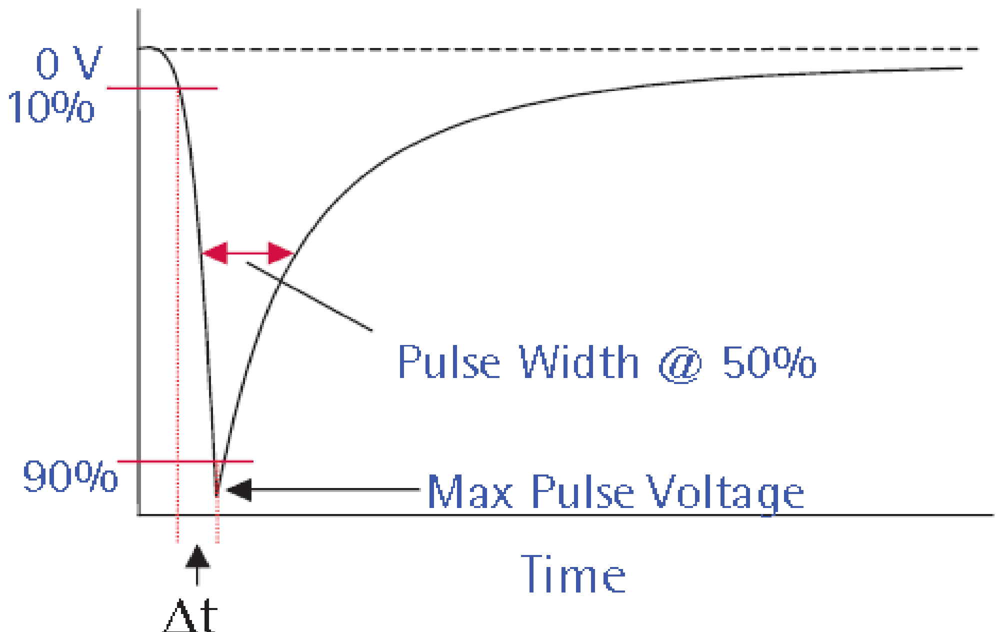

Fig. 3.9: A typical negative spike excitation [30]

The ultrasound wave travels through the medium and gets reflected from the target object. After a definite period of time, echo signal received at the sensor end will be displayed. The time difference between the initial pulse and the reflected echo represents the time taken by the sound wave to travel to and from the target object. From the time information obtained from the monitor and using the velocity of the sound wave in the medium, distance of the target from the sensor can be calculated.

Continuous periodic triggering of the sensor in pulse-echo mode fetches the same signal pattern when the target object is stationary. When the target is under motion, the distance between the sensor and the target varies, hence the time interval between the pulse and echo varies. The variation in time interval/time delay is a representation of the target vibration. By measuring the time delay exactly and multiplying with the velocity of sound, variation in distance between the sensor and the target can be calculated.

The measurement technique is illustrated in the schematic shown in Fig. 3.10a. Assume a target located in the ultrasonic beam at a distance ‘d’ from the transducer. When the transducer is triggered, ultrasonic wave is generated and it travels towards the target and get reflected from the target located at ‘A’. From the recorded A-scan signal, the time of flight is measured and multiplied using the velocity of sound in the medium to get the distance ‘d’ of the target. If the target is stationary at ‘A’, the distance ‘d’ measured will be a single point on the B-scan graph. If the transducer is repeatedly triggered, then the measurements yield a B-scan graph as shown in Fig. 3.10b.

When the target moves to position ‘B’, then time of flight increases and hence the measured distance from the transducer also increases and when the target moves to ‘C’ then time of flight decreases and hence the measured distance from the transducer also decreases. The corresponding B-scan graph is shown in Fig. 3.10c . If the target is moved forward and backward periodically, the time period from the B-scan graph will be period of motion of the target. The amplitude of movement ‘a’ of the target will be reflected as the amplitude of the extracted B-scan graph (Fig. 3.10c). Hence, from a series of ultrasonic pulses, the movement of the target can be measured. A typical ultrasonic train of pulses is shown in Fig. 3.11.

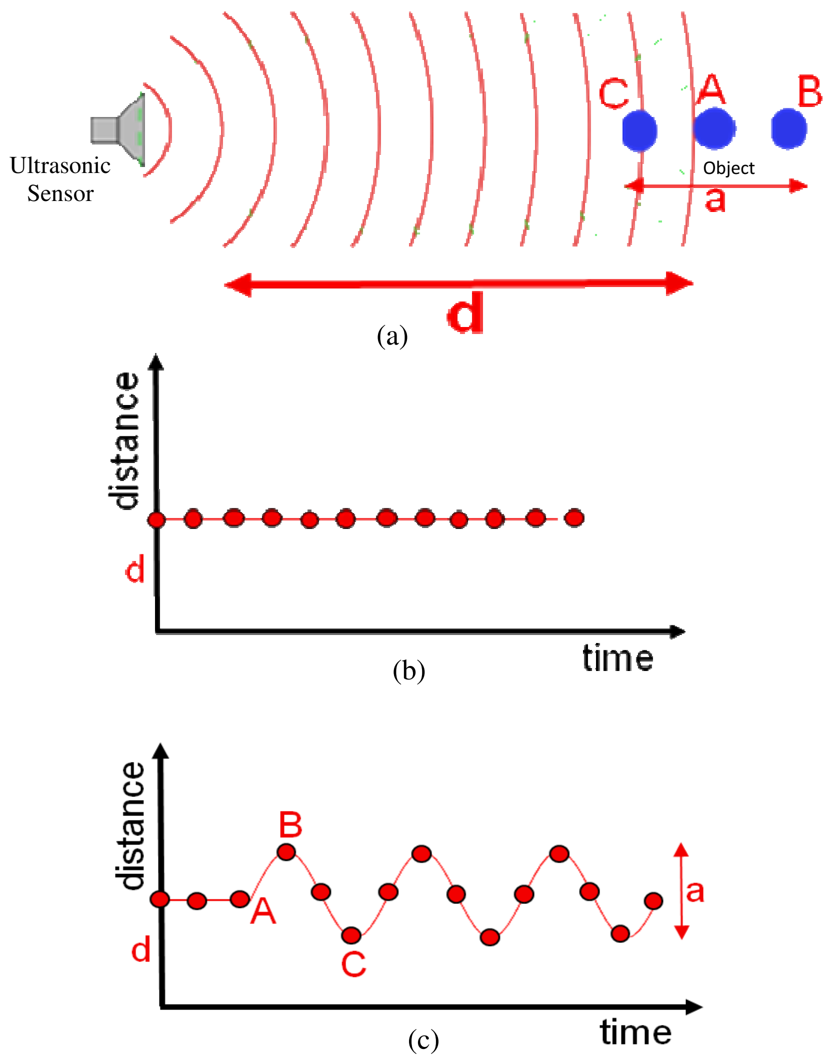

Fig. 3.10: Schematic representation of measurement of target motion

Selection of threshold point (gate level) plays a crucial role in extracting the time of flight data and should be done judiciously. To calculate the time of flight accurately the starting point of time was chosen from the initial trigger pulse from the ultrasonic pulser receiver unit. The second gate point (threshold level) is selected from the echo pulse and should be selected in such a way that the amplitude of the echo signal should not fall below the threshold level during measurement due to movement of the target.

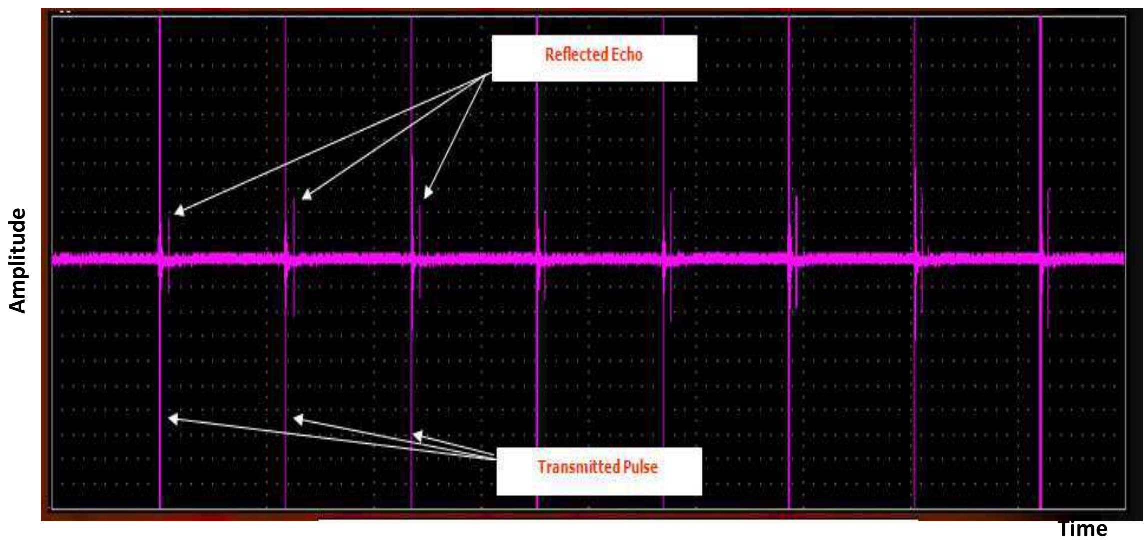

Fig. 3.11: Ultrasonic train of pulses

A typical time signal from a single excitation pulse is shown in Fig. 3.12. The zoomed view of the reflected echo is shown at the bottom. An ideal gate location is shown in the figure as 'A'. The threshold level should be selected in such a way that, it should not interfere with the immediate nearby pulses in the echo signal, which can result in error during time of flight estimation. The maximum value of the peak also should not be selected, as when the target moves away from the transducer during vibration, echo amplitude falls below the threshold value and corresponding time of flight information will not be available. Setting up of these threshold levels are done judicisously during preliminary trial measurements. The time of flight (time delay) thus measured is multiplied by the velocity of sound in the medium to estimate the target movement.

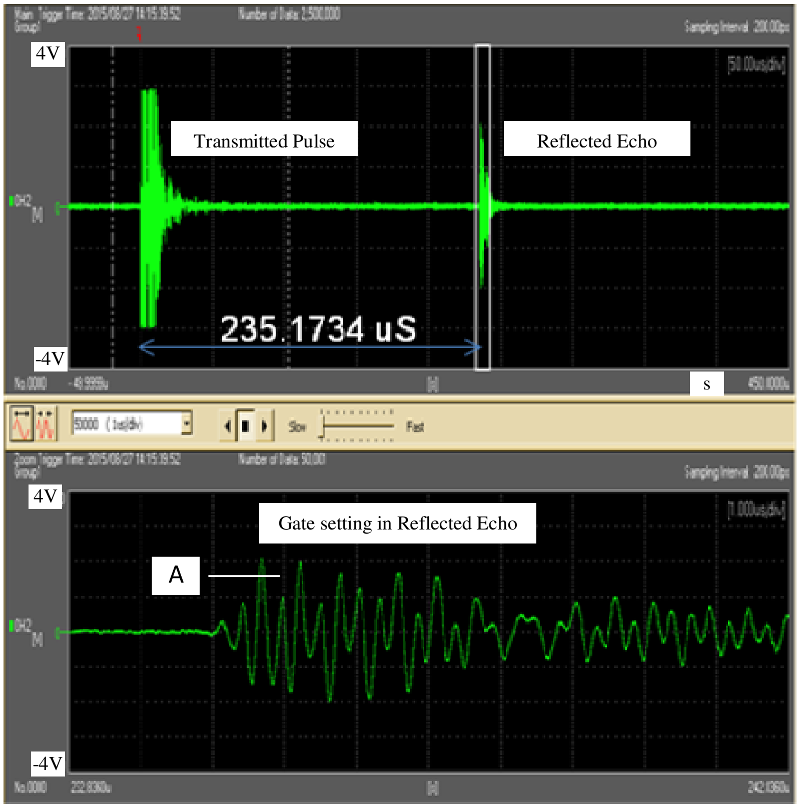

Fig. 3.12: Setting up of threshold point

Ultrasonic sensors in pulse echo mode can thus be used for the detection of target vibration. The ultrasound waves emitted by the sensors are focused on the target and measures the time delays between each emitted and echo pulses. So continuous triggering of the sensor yields the time of flight corresponding to the subassembly movement. By suitably extracting the time of flight data from the train of ultrasonic pulses, target movement/vibration is measured.

3.6.1.1 Preliminary studies

For conducting preliminary studies a water test setup was made. Test setup is shown in Fig. 3.13. A dummy subassembly was mounted in a test section in water. For imparting vibration to the subassembly, an electro-dynamic exciter was used. A signal generator and power amplifier was used to generate the parameter controlled signal to the exciter. An ultrasonic sensor was focused on top of the subassembly as shown in the figure. To measure the actual vibration of the subassembly, an LVDT is used as the reference probe for this study.

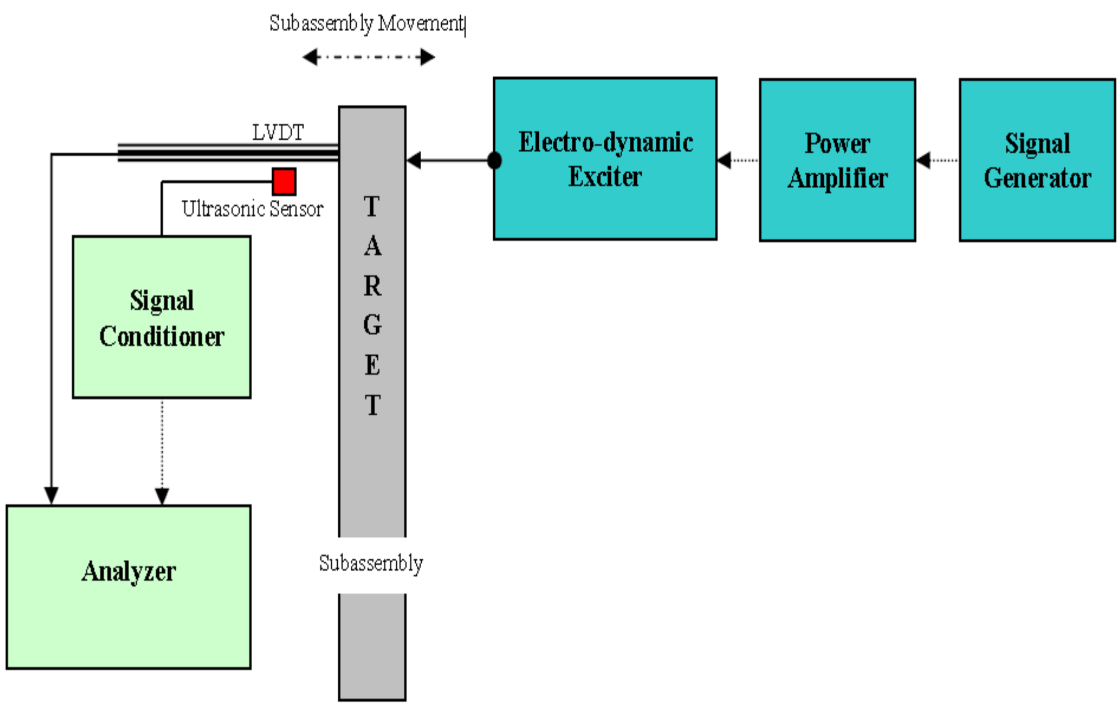

Fig. 3.13: Preliminary studies test setup

Ultrasonic probe was connected to commercially available equipment and was operated in pulse-echo mode. The signal from the sensor was recorded and analyzed. The equipment was having an in-built feature of B-scan imaging hence the B-scan images were recorded during the study. Fig. 3.14 shows the B-scan image obtained during the study, when the subassembly was excited at a frequency of 2 Hz and an amplitude of 0.4 mm. Fig. 3.15 shows the B-scan image recorded during the study, when the subassembly was excited at a frequency of 2 Hz and an amplitude 0.6 mm.

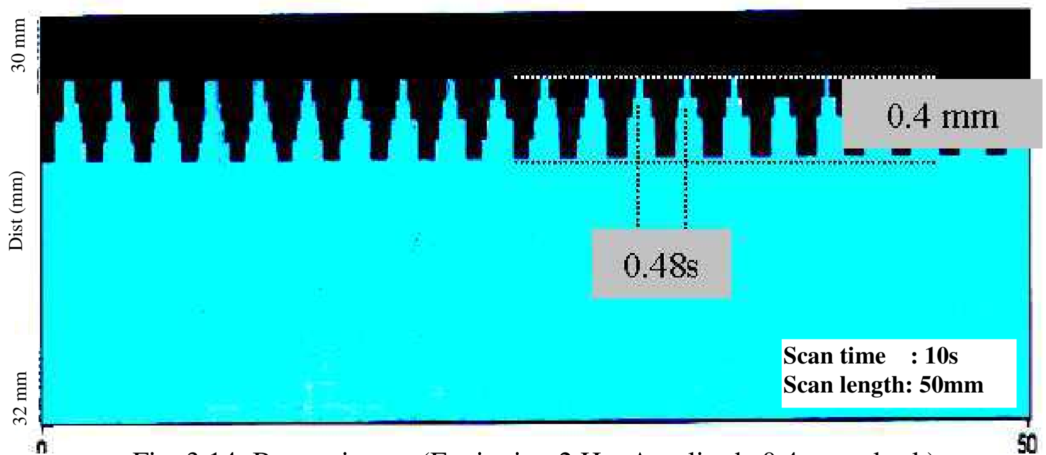

Fig. 3.14: B-scan image (Excitation 2 Hz; Amplitude 0.4 mm pk-pk)

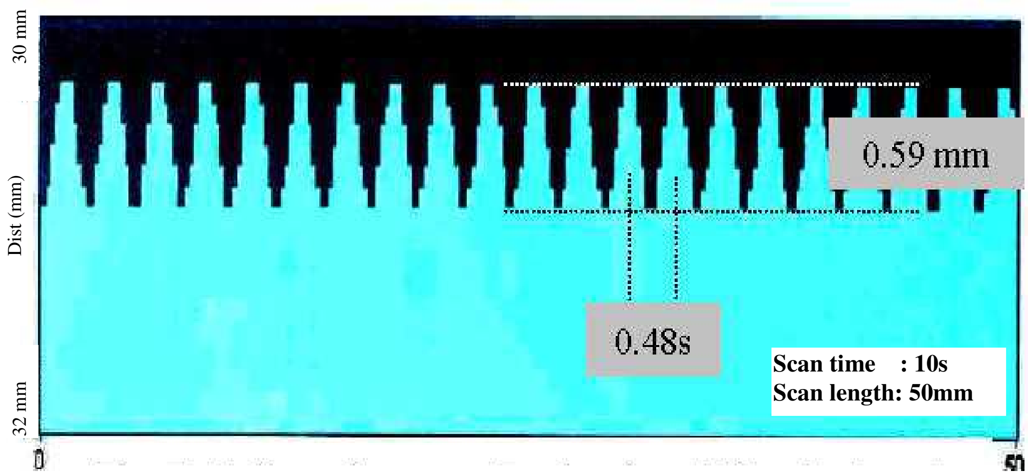

Fig. 3.15: B-scan image (Excitation 2 Hz; Amplitude 0.6 mm pk-pk)

Even though the excitation signal was sinusoidal, due to poor B-scan resolution of commercial equipment, the signal representation was not clear as expected. To exactly recover the vibration signal, the static distance between the sensor and the target needs to be removed from the signal.

The feasibility of vibration measurement from ultrasonic signal was established during this study. The need of development of suitable software, additional features, modification required in measurement techniques etc. was also studied. The preliminary test results were encouraging and the target vibration frequency and amplitude were able to be measured from the ultrasonic signal. Further experiments were carried out to have better measurement capability using improved instrumentation.

3.6.1.2 Instrumentation for vibration measurement

Ultrasonic sensor of operating frequency 5 MHz was manufactured in-house. The major details of the sensor are given in Table 3.3. Ultrasonic pulser-receiver units are used for exciting the sensor for the generation of ultrasound waves. Table 3.4 gives the major technical details of the ultrasonic pulser-receiver used for the study. The device is having provision for adjusting pulse repetition frequency, damping and energy of signal pulses. Apart from this, built-in settings for low pass and high pass filters are also available in the unit. The signal from the pulser receiver unit is connected to the sensor using mineral insulated (MI) cables. Fig. 3.16 shows the ultrasonic pulser-receiver unit.

Table 3.3: Ultrasonic sensor details

SN.	Description	Parameter
1.	Sensor Material	PZT
2.	Curie temperature of crystal	386^0C
3.	Frequency	5 MHz
4.	Diameter	30 mm
5.	Casing Material	Nickel
6.	Operation mode	Pulse echo

Fig. 3.16: Ultrasonic pulser-receiver unit

Table 3.4: Pulser-receiver specification

SN.	**Description**	**Parameter**
1.	Make	Olympus
2.	Model	5072PR
3.	Pulse type	Negative
4.	Rise time	5 nS (typ.)
5.	Pulse voltage	-360 V
6.	Bandwidth	1 kHz to 35 MHz
7.	Gain	0 to 60 dB (Adjustable)

The RF output signal from the pulser-receiver is connected to a data acquisition system using RG174 cables. The data acquisition system (DAS) is used to acquire, process, display and store the data signals. The DAS is the central processing unit and it consists of a 4-slot chassis for holding various data cards. The 1st slot is used for the controller module which controls the data acquisition, processing and storage. The 2nd and 3rd slots are used for two high frequency analog input cards. The high frequency ultrasonic signal outputs from the pulser-receivers are acquired using this card. Two numbers of cards are available in the system with two channels on each card. At a time only one card will be in use and the other card is kept as spare. The 4th slot is used for motion control card. This card is used for the controlled motion of servo motors on the drive mechanism. Fig. 3.17 shows the DAS unit and Table 3.5 gives the major technical details. The processed output from the DAS is displayed in the monitor.

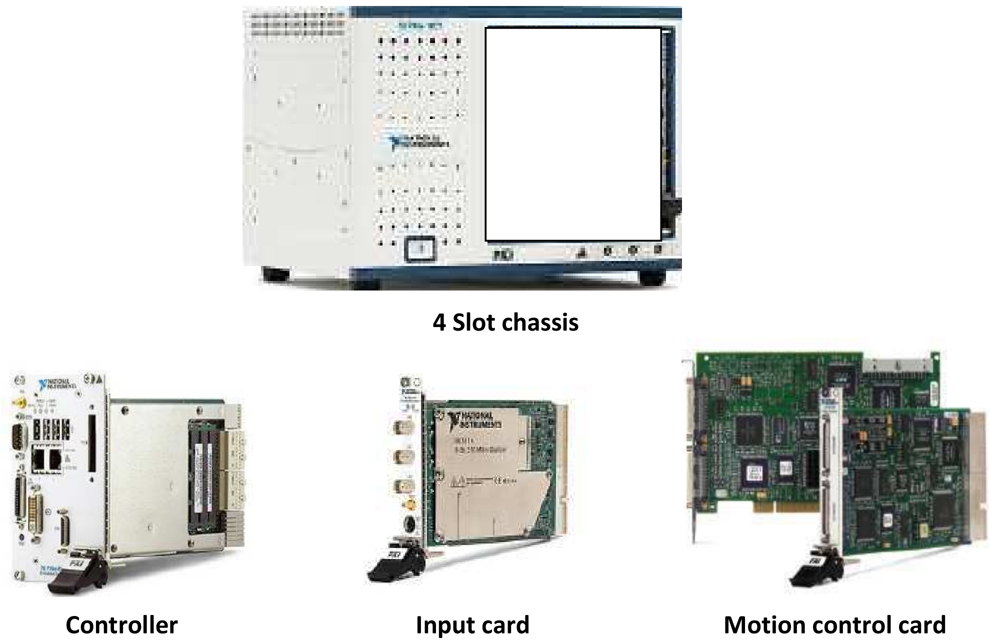

Fig. 3.17: DAS for vibration measurement

Table 3.5: Data acquisition system specification

SN.	Description	Parameter
1.	Make	National Instruments
2.	Chassis model	NI PXIe-1071
3.	Chassis type	4 slot 3U express chassis
4.	Controller model	NI PXIe-8133
5.	Controller processor	Intel Core i7 quad-core
6.	Input card model	NI PXI-5114
7.	Input frequency	125 MHz
8.	Motion controller model	NI 7342
9.	Motion axis	2 axis

3.6.2 Software development

For acquisition and display of the signal, software was written in LabVIEW platform. LabVIEW is National Instrument's (NI) unique software platform for engineering and scientific applications [31]. Its graphical programming syntax makes it simple to visualize, create, and code engineering systems. LabVIEW is unmatched in helping engineers to translate their ideas into reality by reducing test times. The software is very user friendly for its creation and deployment.

LabVIEW was used to acquire high frequency ultrasonic signal from the sensors, extraction of vibration signal and its display. Different panels are provided in the software for data handling and processing depending upon the processing requirement and ease of operation. Architecture of the software is shown in Fig 3.18. The main panel has got three subpanel namely, configuration panel, test panel and offline panel. The test panel is again subdivided into two tabs namely acquisition tab and processing tab.

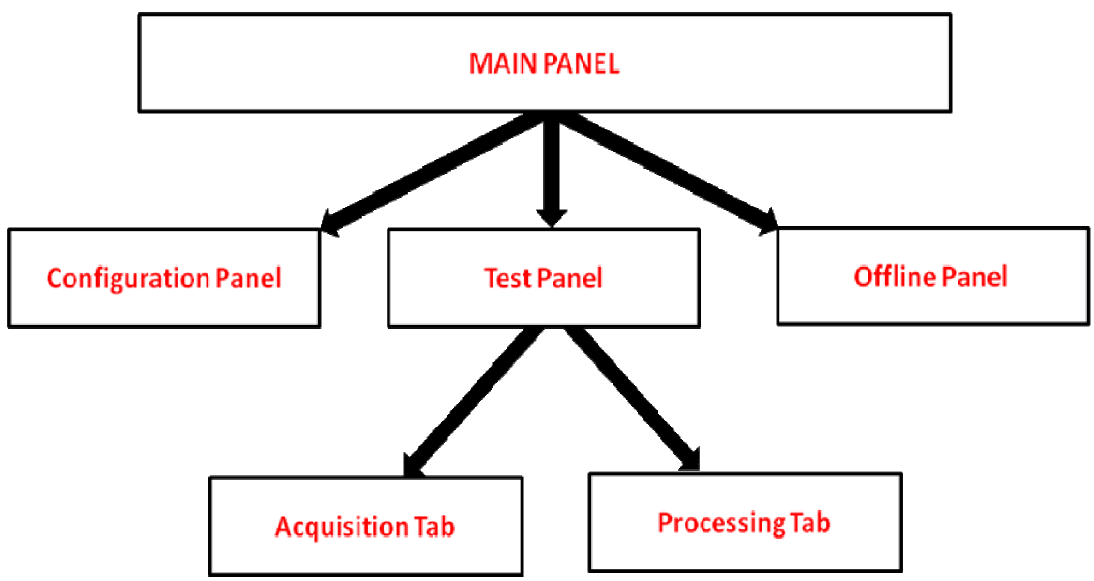

Fig. 3.18: Software architecture

3.6.2.1 Main panel:

The main open up window panel is shown in Fig. 3.19. The main panel is provided with gate ways to the three sub panels namely Configuration, Test and Offline analysis.

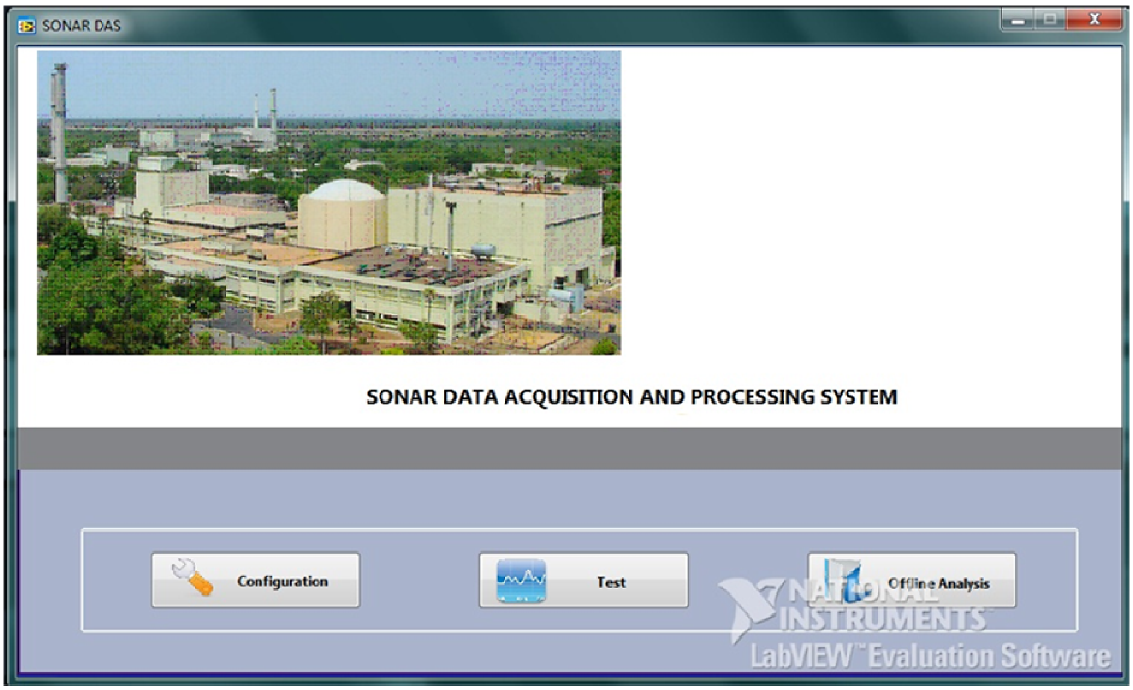

Fig. 3.19: Software main panel

3.6.2.2 Configuration panel:

The configuration panel is shown in Fig. 3.20. This panel is interfaced directly to two numbers of high frequency input cards for acquiring signal from the pulser-receiver units. Major parameters related to signal acquisition such as sampling frequency, velocity of sound in medium, pulse repetition frequency etc. are to be entered in the text boxes provided. In addition to these, parameters related to ultrasonic signal such as pulse voltage, pulse threshold, echo thresh hold, approximate distance of sensor from target etc are to be provided to configure individual channels. Selection for trigger source, trigger level and trigger slope are also provided in this panel. Switching between the two input cards and switching between the channels can be done here. Entire signal acquisition process of the DAS is controlled by the configuration setting provided in this panel.

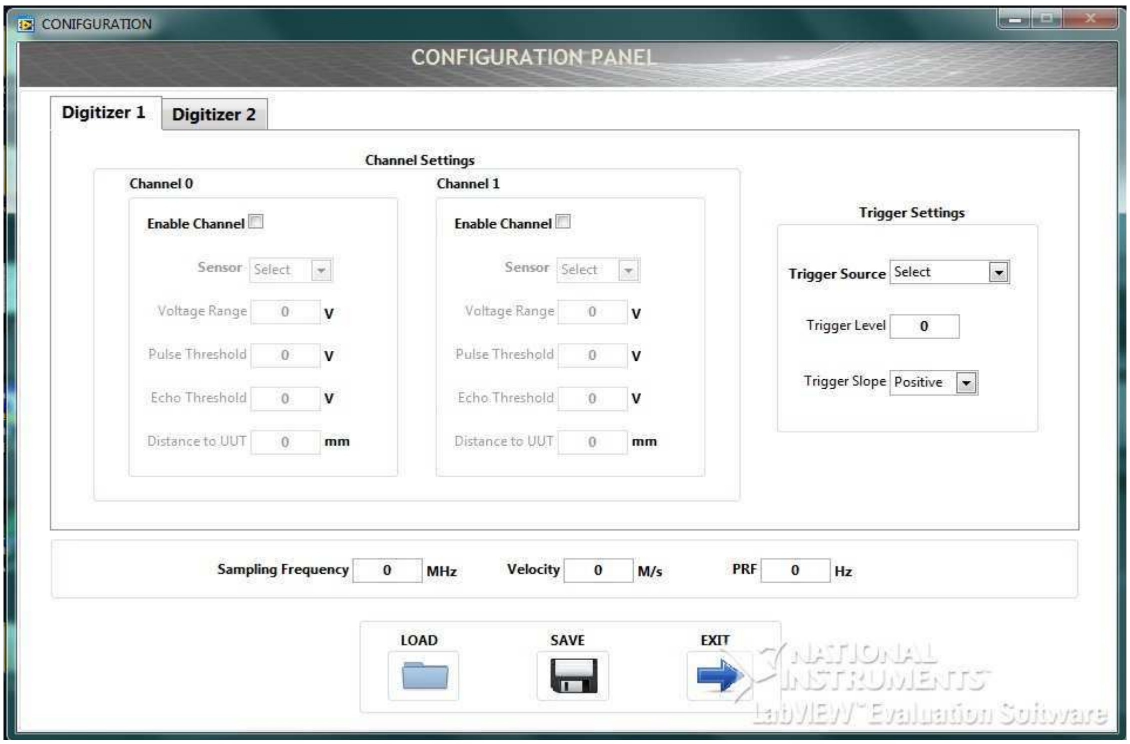

Fig. 3.20: Configuration panel

3.6.2.3 Test panel:

The test panel is equipped with two tabs namely, acquisition tab and processing tab for carrying out different operations. The entire experimental data is acquired and processed in this panel. Acquisition tab of test panel is shown in Fig. 3.21. Major measurement parameters and configuration settings can also be seen in this panel. The acquired data from the sensors, that is, the train of pulses is sliced here with pre-trigger timing so that the data packet in between the triggers is removed to reduce the data memory loading. The chopped train of pulses is made as shown in the plot (Fig. 3.21). Threshold settings for the calculation of time delay are applied to the signal after doing necessary correction in the acquisition tab. Individual pulses seen in the plot can also be zoomed to see the transmitted pulse and reflected echo (Fig. 3.22).

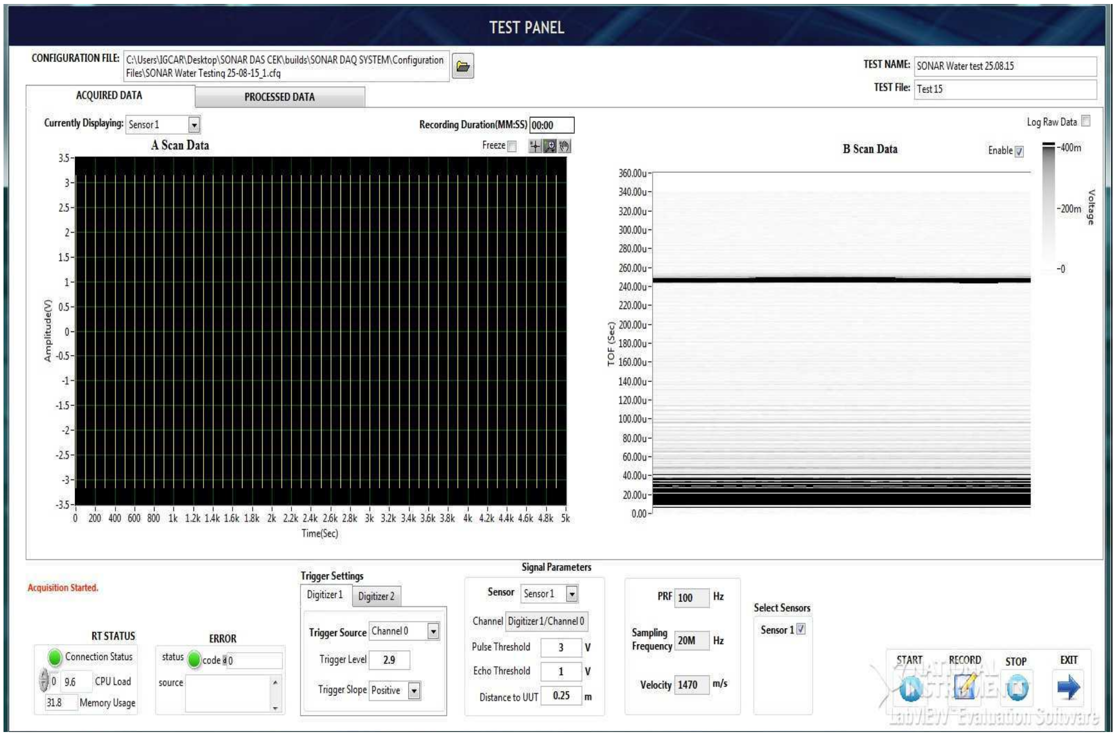

Fig. 3.21: Test panel- Acquisition tab

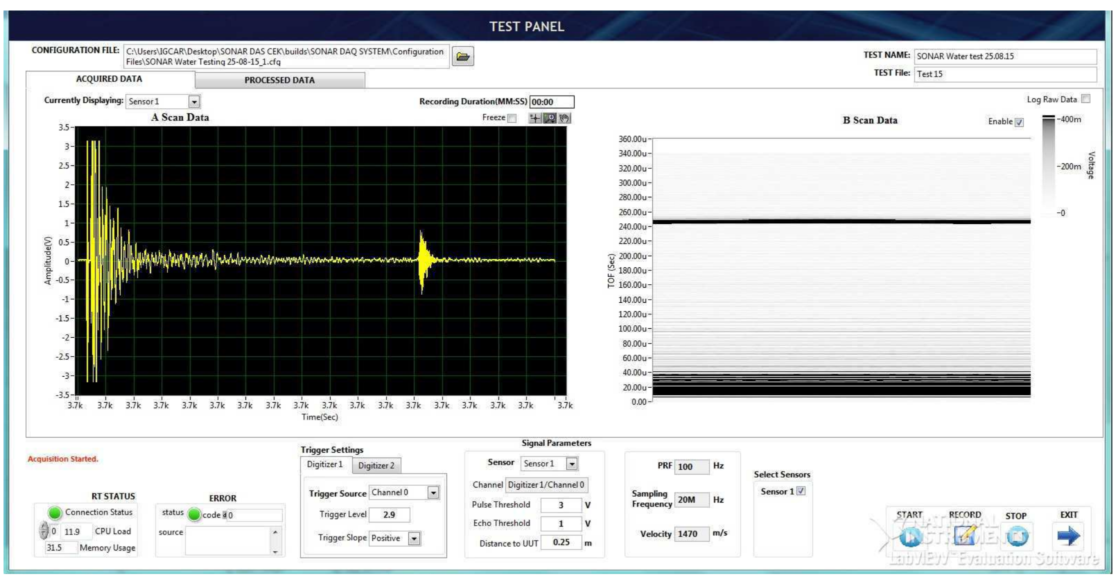

Fig. 3.22: Test panel- Acquisition tab zoomed plot

Processing tab is used to display the processed signal in time as well as in frequency. The time delay measured from the ultrasonic pulses is multiplied by the velocity to determine the target distance at each instants of time. The signal is then plotted in time scale after removing the mean, which is the constant distance between the sensor and the target. Fig. 3.23 shows the processing tab of test panel.

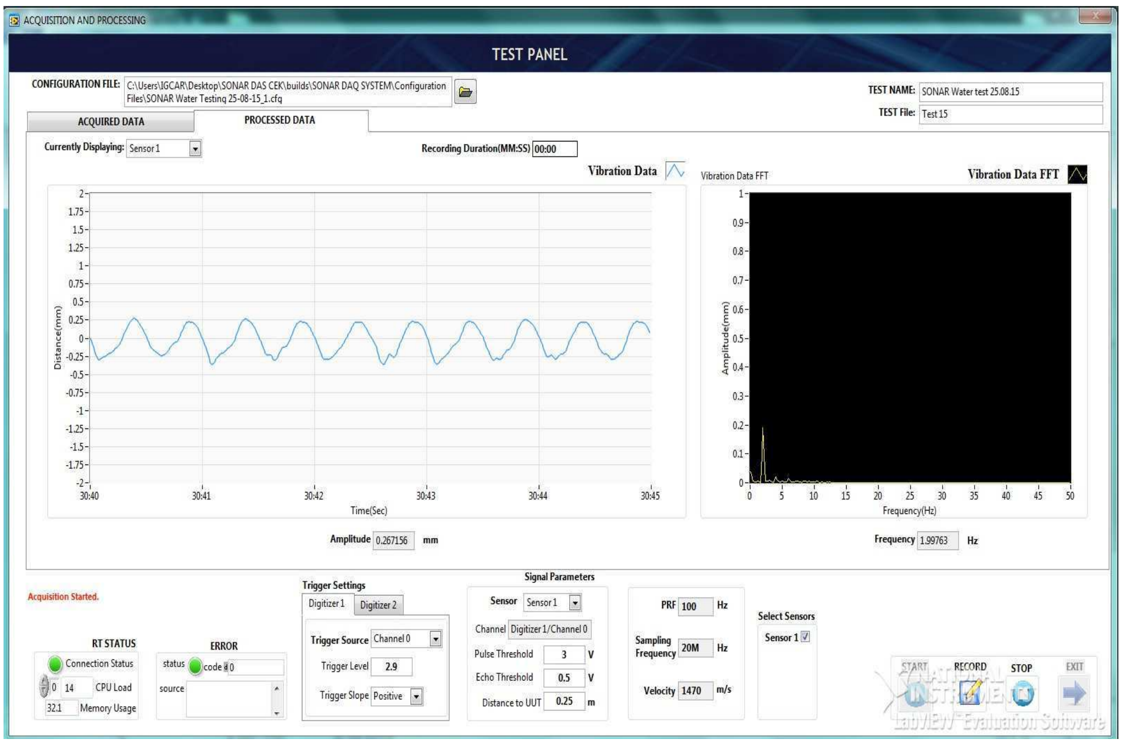

Fig. 3.23: Test panel- Processing tab

Time signal of the extracted vibration signal as well as its frequency spectrum is displayed in this tab. The measured amplitude of vibration and the predominant frequency can be directly obtained from this tab. This tab also permits the data storage with raw ultrasonic signal as well as with the processed time signal and frequency spectra with suitable test file names and folders. The data recorded are stored in the hard disk for future analysis.

3.6.2.4 Offline panel:

Fig. 3.24 shows the offline analysis panel. This panel allows the offline analysis of the experimental data. The recorded data can be retrieved in the plot area in the offline panel window. Time signal as well as frequency spectra can be recalled in the offline panel window. Provision for recalling the raw data file, i.e., the train of ultrasonic pulses is also provided in the panel window. Export of the recorded signals in ASCII format as well as image format can also be done.

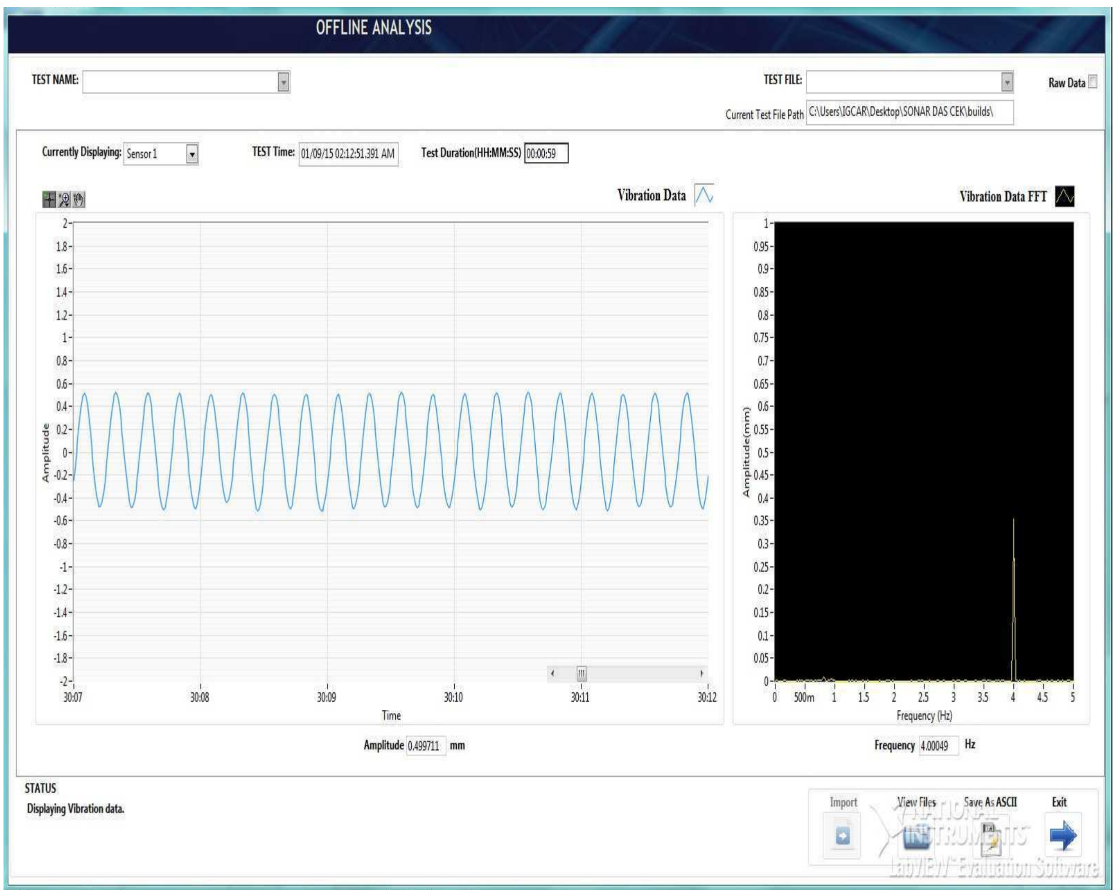

Fig. 3.24: Offline analysis panel

The developed software caters to the requirement of signal acquisition and processing for the development of vibration measurement technique. Development of an ultrasonic measurement system named SONAR for vibration measurement in PFBR is taken up and the developed software is planned to be used for signal processing.

3.7 Summary

- Fundamentals of ultrasonic techniques and features of US transducers are discussed in this chapter.
- Instrumentation system used for vibration measurement is covered in this chapter.
- Preliminary studies were conducted in water and vibration signal was extracted from Ultrasonic B-Scan image.
- Design of drive system electronics and DAS for vibration measurement was carried out.
- Software for extraction of vibration signal from ultrasonic train of pulses was designed and developed.

CHAPTER- 4
DEVELOPMENT OF SONAR DEVICE

4.1 Introduction

After establishing and demonstrating the feasibility of using ultrasonic technique for vibration measurements, design and development of a prototype model was carried out. The objective of this study was to qualify the measurement technique in water as well as in sodium.

4.2 Studies with prototype model

To have a deep insight into the technique based on the preliminary experimental results, a model mechanism was designed and manufactured. The prototype model consists of a drive mechanism and a spinner tube to hold the ultrasonic sensors in position. Ultrasonic sensors were manufactured in-house for these studies. Fig. 4.1 shows the as fabricated ultrasonic sensor used here.

Fig. 4.1: Ultrasonic Transducer

Fig. 4.2 shows the drive mechanism of the prototype SONAR device. Stepper Motor-1 (SM-1) is used for vertical movement and Stepper Motor-2 (SM-2) for spinner tube rotation. The objective of the testing was to assess the performance of the device in water and in sodium, qualification of ultrasonic sensors and testing of ultrasonic electronics and data acquisition system. The target used in the study was the crown region of the actual subassembly head.

Fig. 4.2: Prototype model drive mechanism

4.2.1 Prototype model testing in water

Prototype model was tested in water. The prototype device was installed in a test vessel filled with water. Fig. 4.3 shows the prototype model water test setup. For testing in water, configuration consisting of a target subassembly crown region welded to a SS rod was suspended from the top flange and three numbers of ultrasonic sensors were used. Sensor-1 (S1) was focused on the target subassembly crown region and Sensor-2 (S2) was focused on to a flat plate target mounted on the support rod of the target. S1 and S2 were in-house developed sensors. In order to understand the sodium wetting property, a high temperature, broad band ultrasonic sensor (S3) was also mounted on the device, focusing on a flat target plate. The positioning of the ultrasonic transducers was carried out using the drive control.

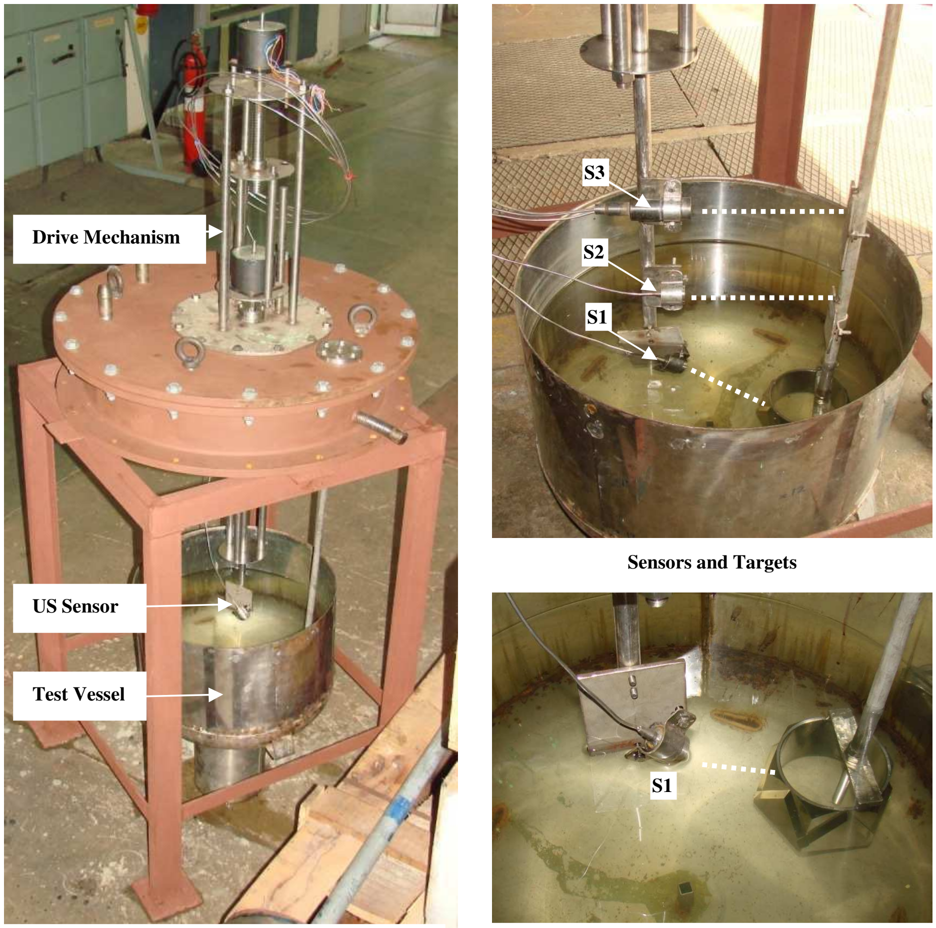

Test Setup

Sensors and Targets

S1 Focused on SA Crown region

Fig. 4.3: Prototype model water test setup

Ultrasonic waves are generated using the pulser and the received echoes were monitored and recorded. Fig. 4.4a shows a typical ultrasonic pulse before and after filling water from S1 and Fig. 4.4b shows the signals from S2. And also it is seen that signal is damped effectively in water medium than in air. Since S3 is a broad band, highly damped sensor, the amplitude of signal was very small and was used only to compare the wetting property of sensors.

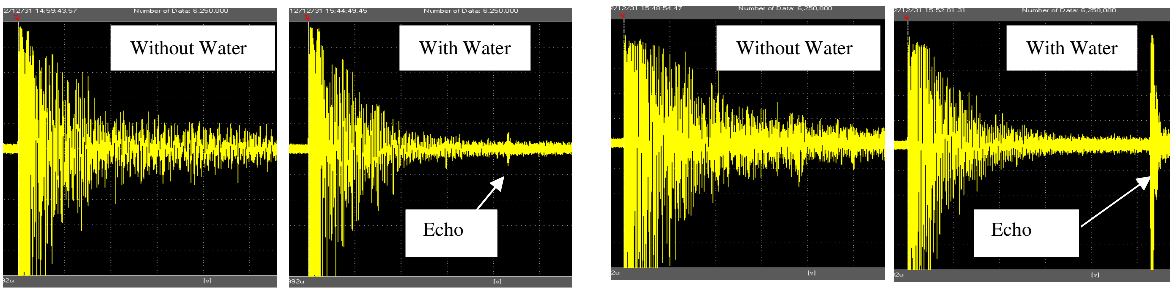

a) S1 Signal **b) S2 Signal**

Fig. 4.4: Ultrasonic signal variation in water

A typical water test result during preliminary testing of prototype model is shown in Fig. 4.5. The target was excited with 2 Hz and the ultrasonic signal was recorded and analyzed. The vibration signal extracted using this technique clearly indicated the target vibration frequency.

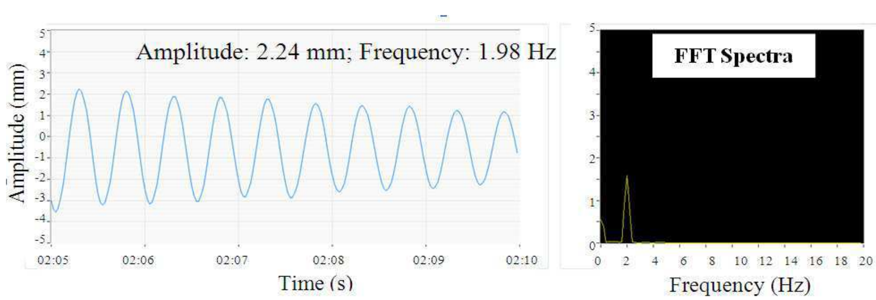

Fig. 4.5: Extracted vibration signal and spectra in water (Frequency 2Hz).

4.2.2 Prototype model testing in sodium

Testing of the device in sodium was carried out in a sodium test pot (TP-1). Outer diameter of TP-1 is ~900mm and its height is ~2.5m. The vessel is provided with all the necessary instrumentation such as thermocouples, level probes and leak detectors. The top flange of TP-1 is modified and extended by 200 mm to accommodate the device and to provide excitation to the target assembly from outside. Fig. 4.6 shows the test setup. Leakage of cover gas through the space between the support flange and the ring flange of the vessel is prevented by the O-rings. The movement of the transducer inside the vessel was done using the central spinner tube. The argon leak tightness through the clearance between the spinner tube and the top flange penetration was achieved using oil seals.

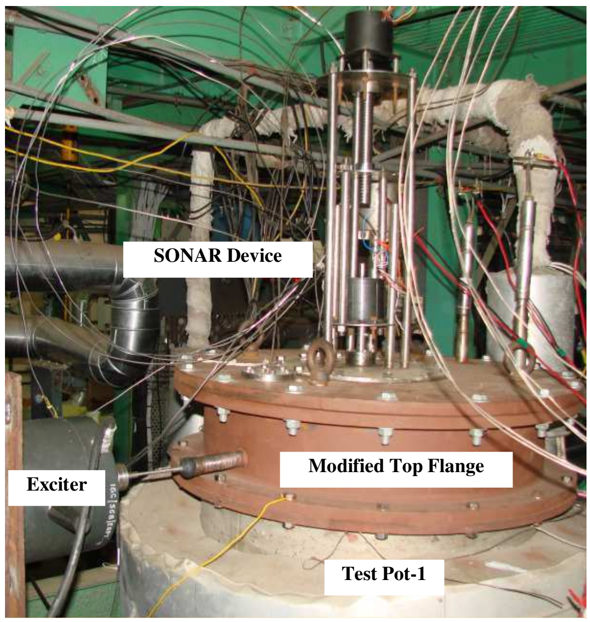

Fig. 4.6: Test setup for sodium testing

All the sensors on the device are kept below the sodium operation low-level in the test vessel. Fig. 4.7a shows the ultrasonic transmitted pulse before and after filling sodium for sensor-2 and Fig. 4.7b shows the signal from sensor-1. It is observed that the sodium medium offers damping to the ultrasonic signal. Fuel subassembly crown region is used for simulating the target subassembly suspended from the top flange and the excitation of the target is done using an electro-dynamic exciter. Stinger rod of the electro-dynamic exciter is introduced in the argon space through the penetration provided on the extended part of top flange. Suitable metallic bellow seal arrangement is provided externally to the test vessel to achieve leak tightness. Fig. 4.8 shows the test setup with electro-dynamic exciter installed on the test setup. Measurements were carried out in sodium at 200^0C with a cover gas pressure of 0.4 kg/m^2. Target was excited with different frequencies and the ultrasonic signals were recorded and the vibration signal was extracted.

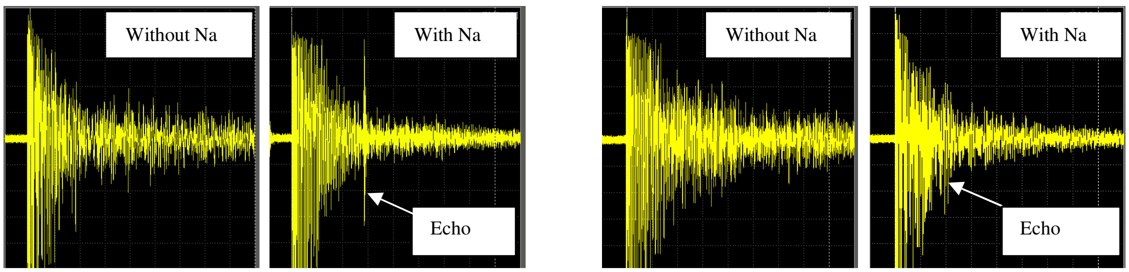

a) Sensor-2 Signal **b) Sensor-1 Signal**

Fig. 4.7: Signal variation in sodium

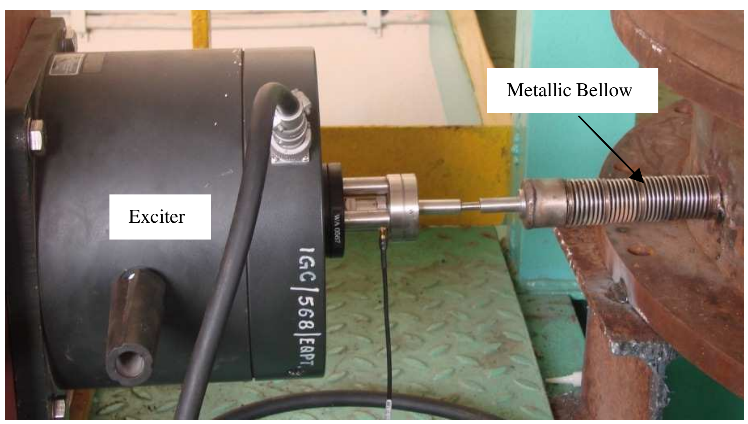

Fig. 4.8: Electro-dynamic exciter setup

During the measurements, the target was excited for different input frequencies and the ultrasonic train of pulses were measured and analyzed. From the recorded signal, vibration signal was extracted using the developed software. Fig. 4.9 shows the typical test results obtained from the sodium testing. It was observed that the input vibration time signal is reliably recovered from the train of ultrasonic pulses. This study gave a clear indication of the possibility of using this measurement technology in sodium for reactor applications. Moreover performance of the sensors was also established during this study.

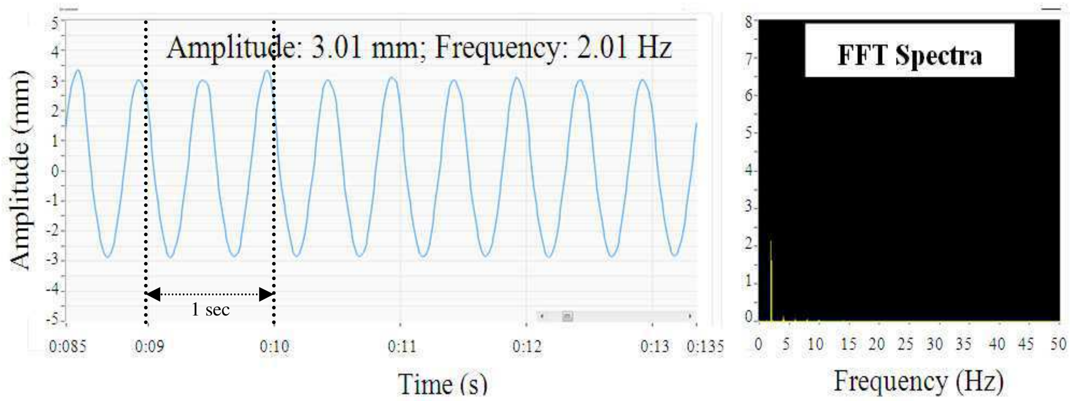

Fig. 4.9: Extracted vibration signal and spectra in sodium (Frequency 2 Hz)

4.3 Optimization of measurement parameters

During the studies using prototype model, various measurement and acquisition parameters were optimized. The parameters involved in the development of ultrasonic technique for vibration measurement, which can highly influence the accuracy of measurements are:-

a) Ultrasonic sensor operating frequency

b) Pulse repetition frequency (PRF) of ultrasonic pulser

c) Target vibration frequency, which is to be measured and

d) Ultrasonic signal acquisition frequency

From the flow induced vibration studies carried out on PFBR fuel subassembly in water, the natural frequency of subassembly was measured to be 3.5 Hz to 4 Hz. Since the target vibration frequency is ~ 4 Hz, PRF was chosen as 100 Hz. Moreover 100 Hz PRF which is 25 times the measurement frequency is a reasonably good approximation for the faithful recovery of the signal with good accuracy. Moreover during the measurement of subassembly vibration, the sensor will be approximately at a distance of 180 to 250 mm from the subassembly, hence the time taken by the reflected echo from the subassembly will be 200 μS (for 2 times distance travel). Subsequent pulse is to be triggered only after the echo, hence selection of PRF as 100 Hz is adequate for the study.

The sensor to the target distance is between 180 to 250 mm during measurement. Since the distance is comparatively less a higher frequency of sensor (5 MHz) is selected for better resolution. Operating the sensor above 5 MHz may result in large attenuation/scattering in the medium and also demands higher sampling rate processing system and higher data handling rates, which may result in less-efficient/slower processing of the signal. Since the sensor operating frequency was fixed at 5 MHz, the processing system with front end high frequency digitizer was selected with a sampling rate of 125 MHz (maximum) per channel.

The sensor used for the measurement was developed in-house using special grade PZT-crystal with an operating temperature of 230^0C [32, 33, 34]. The casing material of the ultrasonic sensor was made up of Nickel so as to have better wetting in sodium compared to stainless steel casing [35, 36, 37]. Sensors were also tested in sodium for the rated temperature after its manufacturing. A typical ultrasonic sensor is shown in Fig. 4.10.

Fig. 4.10: Ultrasonic sensor

4.4 Development of SONAR device for PFBR

4.4.1 Introduction

With the confidence obtained from the testing, a device named SONAR was designed and manufactured for FBR applications (Fig. 4.11). SONAR device is composed of an upper part, which includes the drive mechanism (Fig. 4.12) and other instrumentation devices and a lower part which includes the cover pipe, spinner tube and the transducer holder (Fig. 4.13).

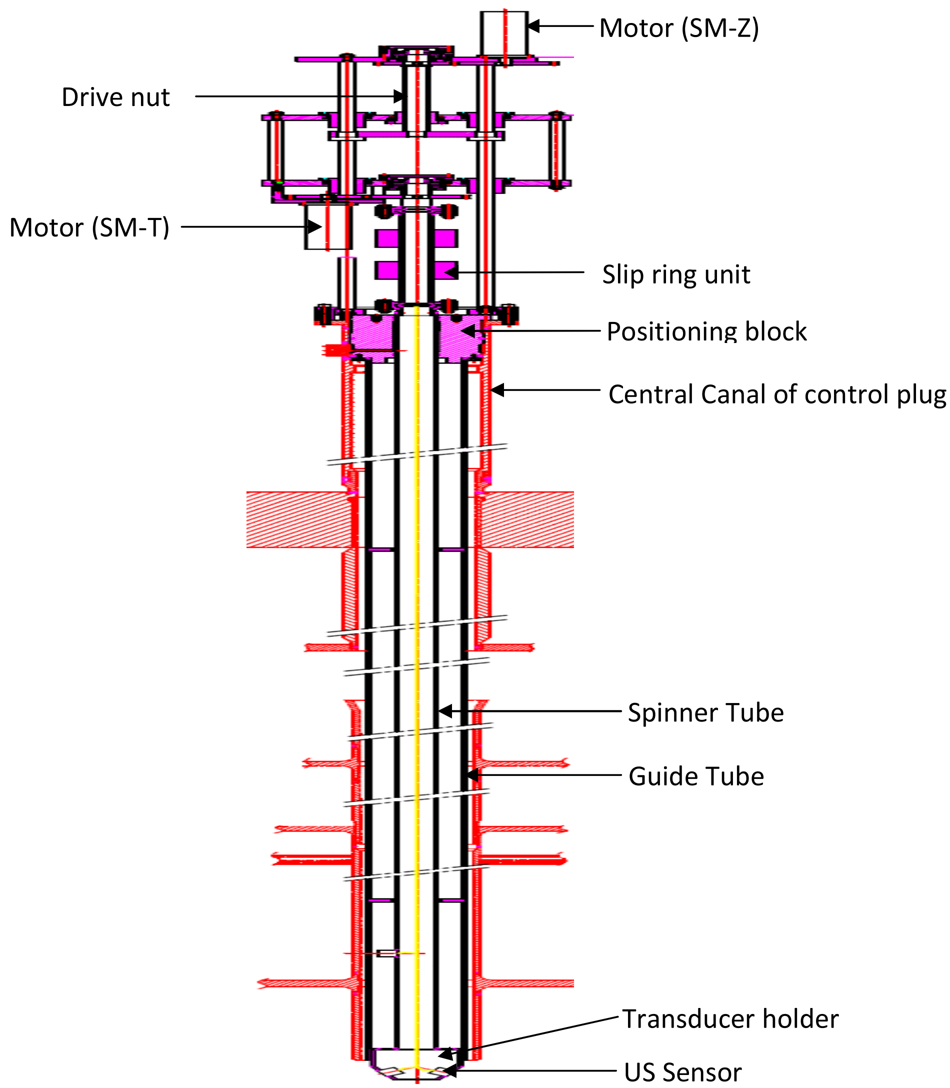

Fig. 4.11: PFBR SONAR Device

Lower part of the device will be in contact with liquid sodium up to a temperature of 200^0C and argon cover gas atmosphere. Upper part of the mechanism will operate in reactor containment building atmosphere. Since measurements are planned during the commissioning trials with dummy subassemblies in the core, no radiation shielding is provided in the device. After measurements the device will be dismantled and will be removed from the central canal. The major challenges involved in this measurement is the development of device with proper leak tightness, mounting in the central canal of PFBR, focusing the target inside sodium, self vibration of sonar device itself in sodium flow etc.

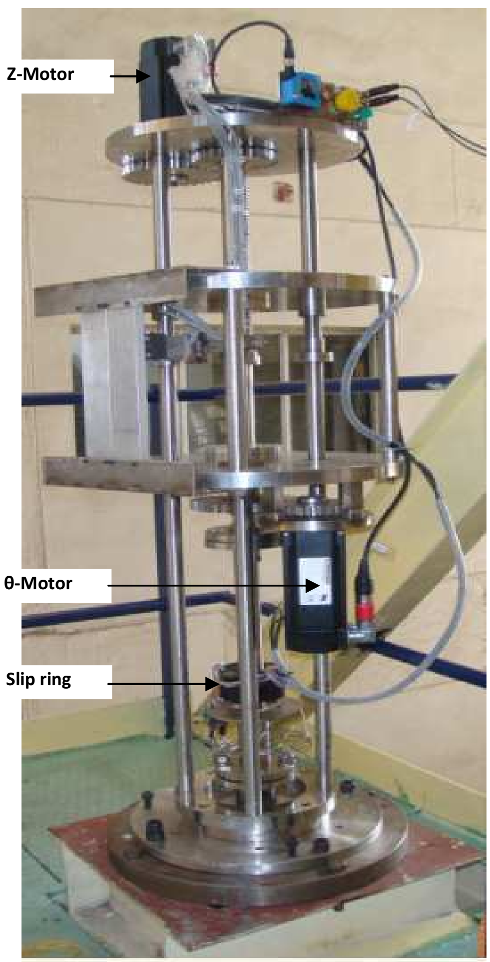

Fig. 4.12: SONAR device drive mechanism


Fig. 4.13: SONAR device lower part

4.4.2 Motion control software for SONAR device

To position the ultrasonic transducers for focusing on the target, drive mechanism is used. The ultrasonic transducers attached to the spinner tube of sonar device can be moved in Z-axis (for raising and lowering) and in Theta axis (for rotation). Software was designed in LabVIEW platform for achieving the required movement of the transducers. The main panel window is shown in Fig. 4.14.

Fig. 4.14: Main panel window for motion control

Two entry keys are provided for calibrating the drive system (Motion Calibration) and for positioning the transducers (Motion Control). Motion calibration mode is mainly used for calibrating the servo motors SM-T and SM-Z for setting various parameters. Fig. 4.15 shows the window for motion calibration. Calibration to the required initial 'Home position' of SM-T and SM-Z motors can be made in this mode. The parameters like target position, motor acceleration and motor velocity are set in this mode. The home position of SM-T motor is 0^0 or 360^0 with respect to the Large Rotatable Plug and the home position of SM-Z is ~ 200 mm above core. Indications for movement in forward direction, reverse direction, movement of motor, completion of movement etc. are provided.

Fig. 4.15: Motion calibration window

Once the home position is fixed, motion control mode can be used for the Z-direction and Theta-direction motion of the device. Fig. 4.16 shows the Motion control window. The accurate movement of servo motors SM-T and SM-Z for Theta and Z axis is controlled using this operation mode. The home position set in the previous mode will be taken as the reference position for any motion in Theta and Z axis in this mode. The required angle and elevation needs to be mentioned here w.r.t the home position. After setting up the parameters, START button is pressed and movement to the required target position can be monitored on the visual display meter. The selection for forward and reverse movement of the theta motor and Z- motor is permitted in this window.

.

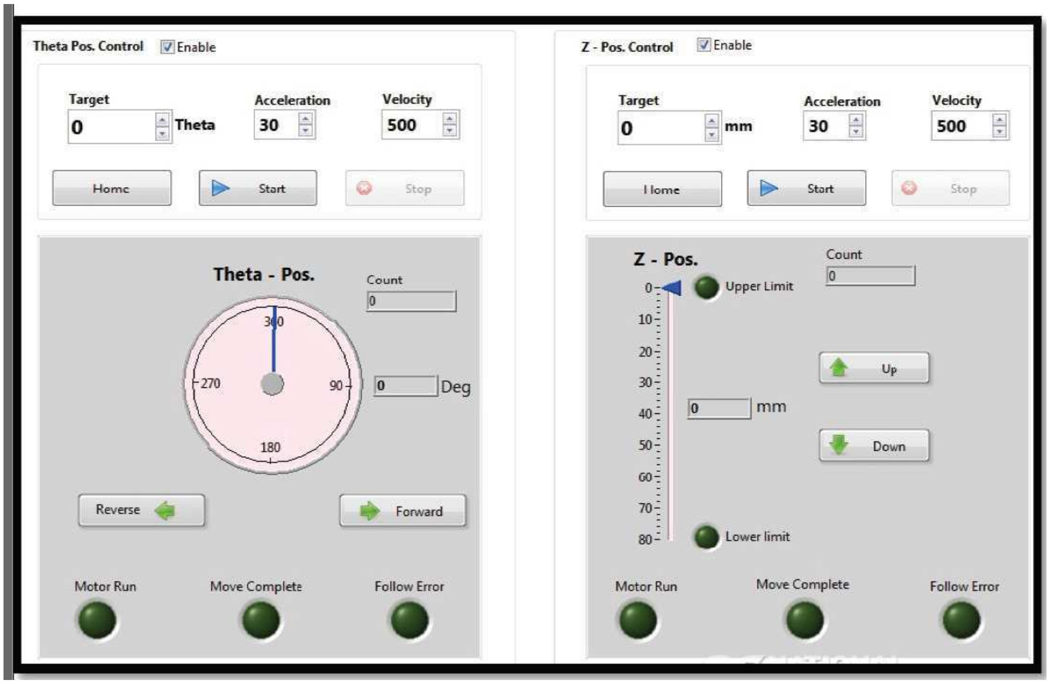

Fig. 4.16: Motion control window

4.4.3 Control panel for SONAR device

The block diagram of the developed control panel is shown in Fig. 4.17. The components on the control panel are-

1. Cabinet.
2. Switch for AC mains 230 V supply.
3. Lamp indication of AC mains 230 V supply.
4. Ultrasonic sensor (S1) position indication in Z and Theta axis.
5. Data Acquisition System (DAS).
6. Operating buttons for servo motors SM-T and SM-Z.
7. Upper limit and lower limit switch indication in Z-axis.
8. Auxiliary power supply units for servo drives.
9. Display monitor.

10. Keyboard with mouse.

11. Two numbers of ultrasonic pulser-receiver units.

12. Industrial computer.

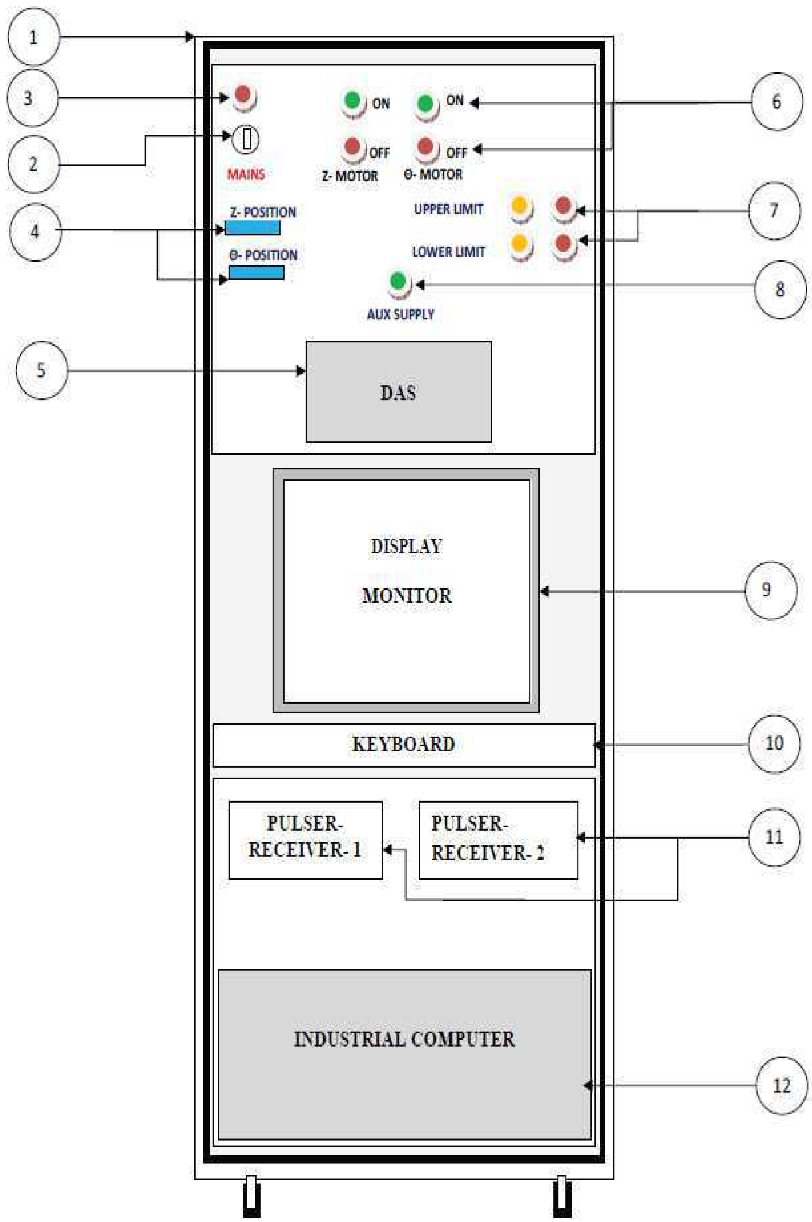

Fig. 4.17: Control panel block diagram

4.4.4 Access zone of SONAR device

SONAR device is located in the central canal of control plug. Control plug is located in the small rotatable plug (SRP), which is positioned in the large rotatable plug (LRP). By suitable combinations of rotation of SRP and LRP, SONAR device can be positioned on top of the subassemblies. Fig. 4.18 shows the access zone of SONAR device. Ultrasonic sensors are mounted on the transducer holder, which is attached to the spinner tube. For focusing the ultrasound waves on the subassembly crown region, rotation of spinner tube is required. Even though the rotational movement is discontinuous for proper focusing, the maximum rpm considered in the design is 50 rpm and the movement is restricted to 0 to 360^0.

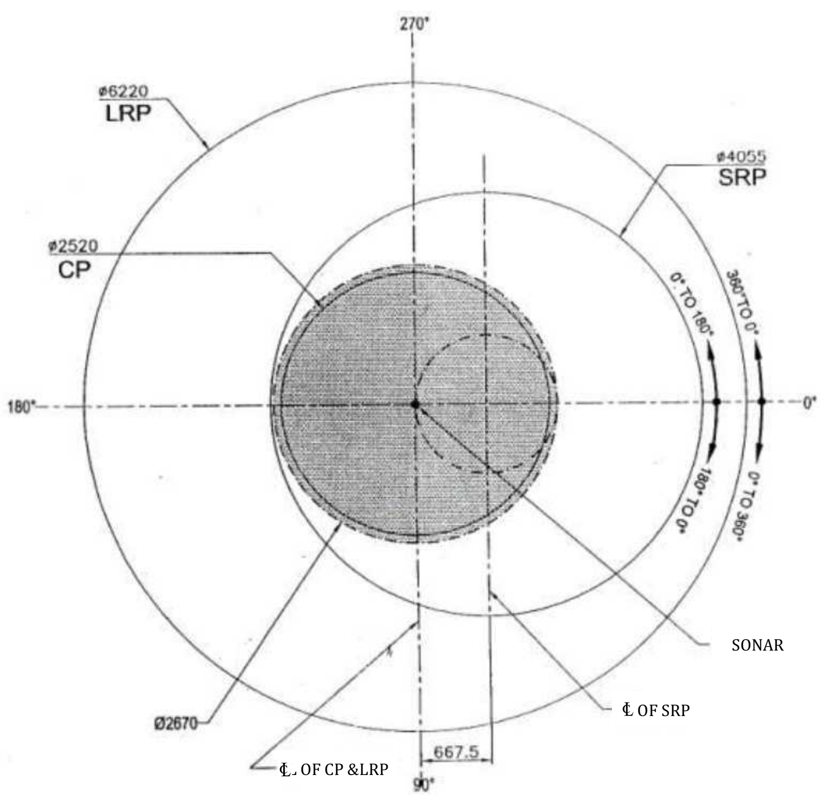

Note:

1. Chain dotted line indicates path of movement of SONAR device
2. Shaded zone is accessible

Fig. 4.18: Access Zone of SONAR device

4.4.5 Description of SONAR device

Translation motion of spinner tube is provided for proper focusing of the ultrasonic waves. During normal condition, the spinner tube will be positioned inside the cover pipe, which is the home position. During measurements it can travel up to 150 mm downward from the home position. At the bottom most position, the spinner tube will be 50 mm above the core subassemblies. During the rotation of plugs for positioning the SONAR device, spinner tube will be positioned in the home position to avoid any chances of interference/contact with the subassembly. As the mechanism penetrates into the reactor, necessary leak tightness is provided. Leak tightness between the moving part of the mechanism, i.e. spinner tube and cover pipe is achieved by means of ‘O’ ring seals. Limit switches and laser position sensors in the drive mechanism are used for the position indication of SONAR device. Limit switches are provided to indicate the home position of the spinner tube and the bottom most elevation of the spinner tube, i.e. 150 mm down from the home position. Apart from this laser position sensor is provided for the continuous position indication of the spinner tube. SONAR device is designed for easy dismantling after measurement. Since the device is made as lower part and upper part, it can be removed at site without affecting the leak tightness of the reactor by using shielding flask.

The lower part of the sonar device is equipped with three numbers of ultrasonic sensors namely, S1, S2 and S3 (4.19). Sensor S1 and Sensor S2 are mounted at an angle of 60^0 so as to focus on the crown region (Fig. 4.20) of the subassembly, where as Sensor S3 is used to measure the self vibration of the sonar device itself. The device is capable of movement in two axis, Theta-axis/rotational motion and Z-axis/vertical movement. The control panel of the sonar device is equipped with ultrasonic pulser-receivers to excite the sensors, a high frequency data acquisition system for capturing the signals from the sensors and application software to process the acquired signal and to extract the vibration signal.

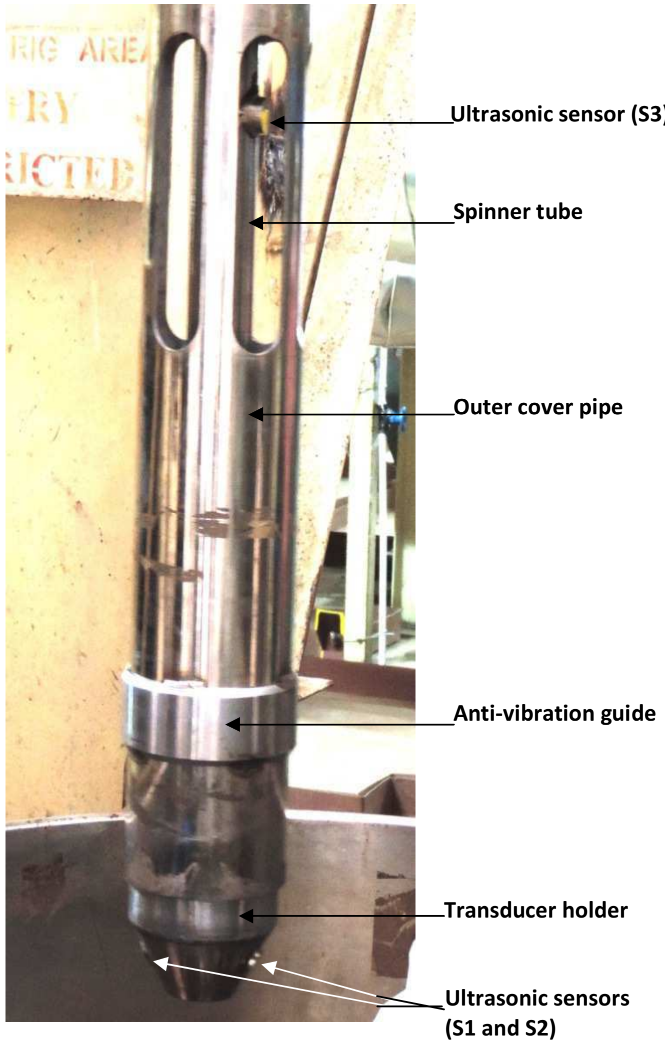

Fig. 4.19: Bottom part of SONAR device

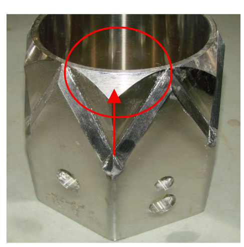

Fig. 4.20: Subassembly crown

4.4.6 Positioning of SONAR device

'Servo motor' (ZM) supported on the 'top fixed plate' is used for the 'Z' motion of the 'spinner tube' (Fig. 4.21). When 'ZM' rotates, the rotary motion is transmitted to the 'drive screw' through the 'gear' and 'pinion'. The 'drive screw' is supported on the 'top fixed plate' using a double row deep groove ball bearing. The rotary motion of the 'drive screw' is converted into translation motion using the 'drive nut' which is fixed on the 'top moving plate'. 'Top moving plate' is fixed to the 'bottom moving plate' using 'fixed rods'. The translation motion of the 'top moving plate' and 'bottom moving plates' is guided using the 'guide rods' and 'sliding bushes'. 'Spinner tube' of the SONAR device is supported on the 'bottom moving plate' through 'slip ring assembly' and 'spinner rod', hence movement of 'bottom moving plate' results in the 'Z' motion of the 'spinner tube'.

The material of construction of 'drive screw' is SS304 and that of 'drive nut' is Aluminium bronze. The gears are fitted to the motor shaft through a bush fitted to the motor shaft. The machined bush is interference fitted to the motor shaft and is also screwed. Parallel keys are used for the motor-gear assembly. Provision for manual operation (Z-motion) using a handle wheel is also provided for the rotation of 'drive screw' from the 'top bearing cover'.

'Servo motor' (TM) is used for the 'Theta' motion/rotation of the 'spinner tube'. 'TM' is coupled to 'spinner rod' through 'gear' and 'pinion'. As 'TM' rotates, 'spinner rod', which is supported on the 'bottom moving plate', also rotates, which in turn rotates the 'spinner tube' connected through the 'slip ring assembly'. The 'slip ring assembly' connects the 'spinner tube' to the spinner rod. Signal cables from the ultrasonic sensors at the lower part of SONAR device are terminated at the bottom end of the slip ring and output connections are taken from the top end. This arrangement of slip ring allows the free rotation of the spinner tube, without any crossing over of sensor cables.

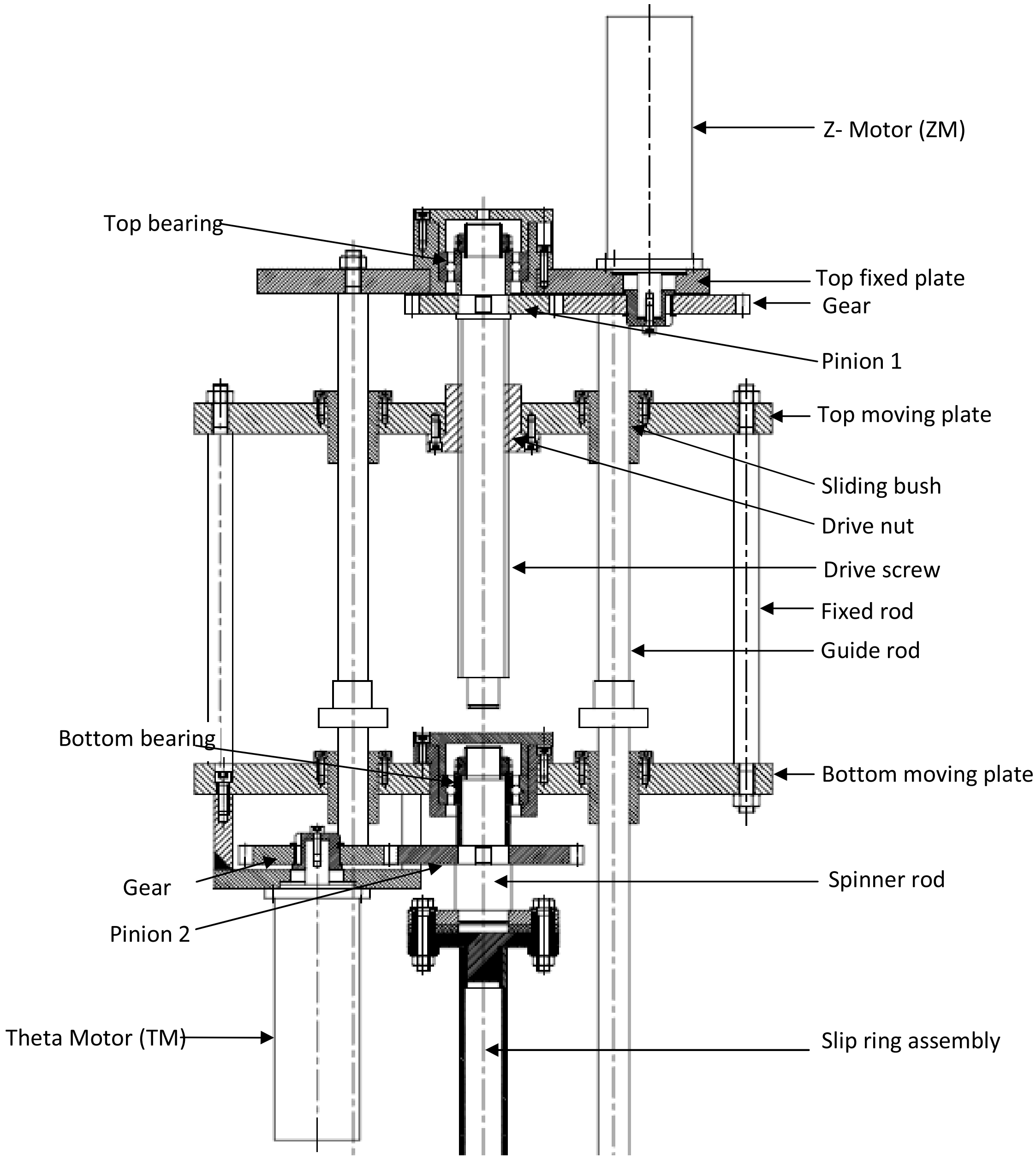

Fig. 4.21: Upper part of SONAR device

4.4.7 Testing of ultrasonic sensors

Three numbers of ultrasonic sensors are used in SONAR device. Axial and cross sectional beam profiling of the ultrasonic sensors were carried out by immersion technique using a standard pinducer from Valpey Fisher (USA) in an automated ultrasonic beam profiling system TraCSS from Dhvani Research and Development Solutions (India). Fig. 4.22, Fig. 4.23 and Fig. 4.24 show the axial beam profile pattern depicting the intensity distribution in the axial plane of the sensors S1, S2 and S3 respectively. Profiling was carried up to a distance of 250 mm from the face of the transducer to study the symmetry of wave intensity distribution. Effect of beam spread was also observed to be less in the measurement range [38].

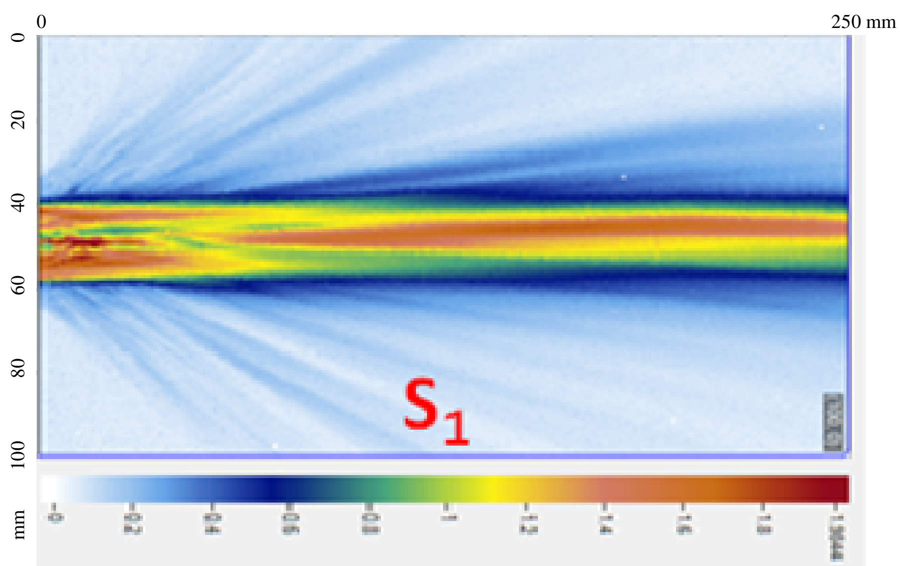

Fig. 4.22: Intensity distribution in the axial plane of the sensor- S1

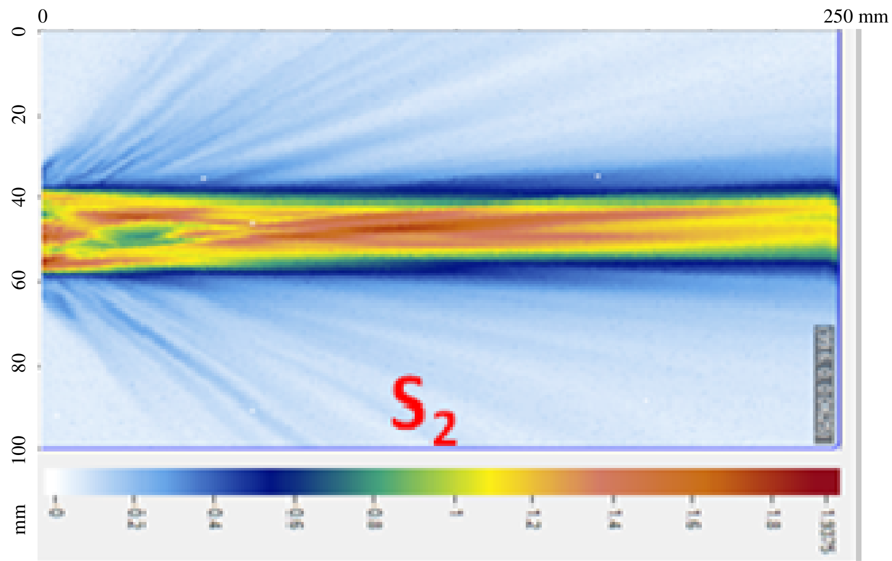

Fig. 4.23: Intensity distribution in the axial plane of the sensor- S2

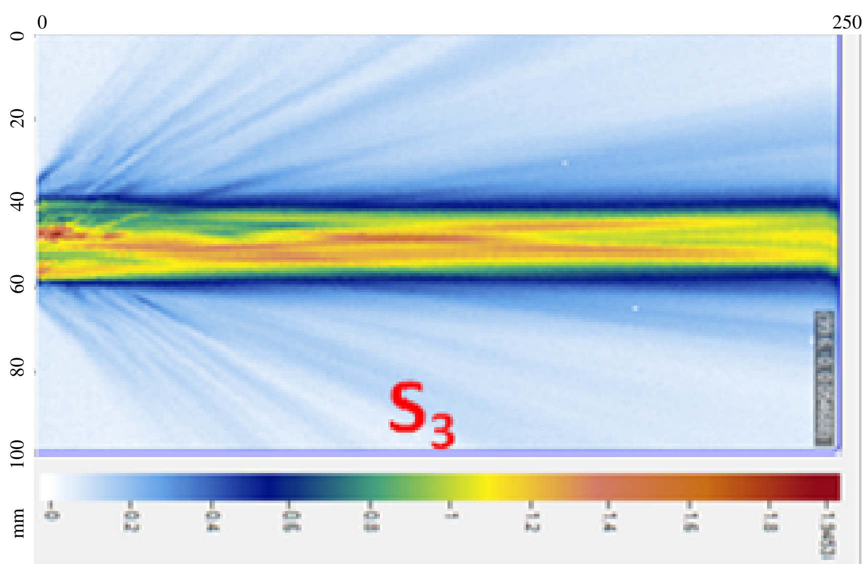

Fig. 4.24: Intensity distribution in the axial plane of the sensor- S3

Fig. 4.25, Fig. 4.26 and Fig. 4.27 show the cross sectional beam profile pattern depicting the intensity distribution in the cross-sectional plane at a distance of 200 mm from the transducer face for S1, S2 and S3 respectively. A fairly good bonding of the crystal to the sensor casing is observed in the intensity plots.

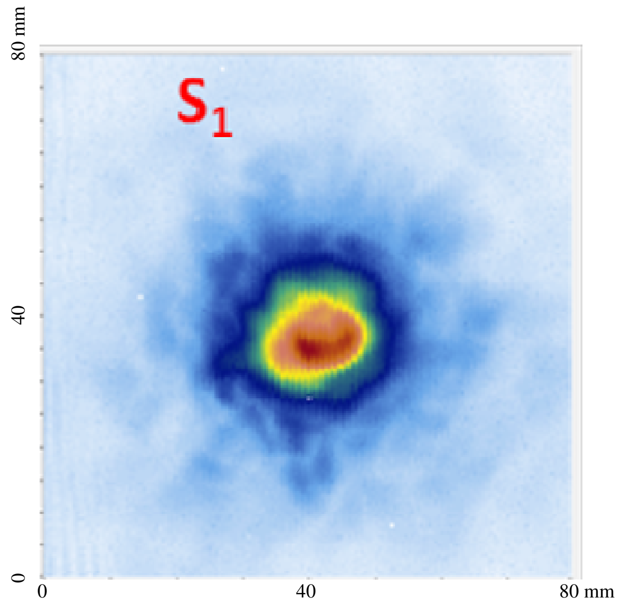

Fig. 4.25: Intensity distribution in the cross-sectional plane of the sensor- S1

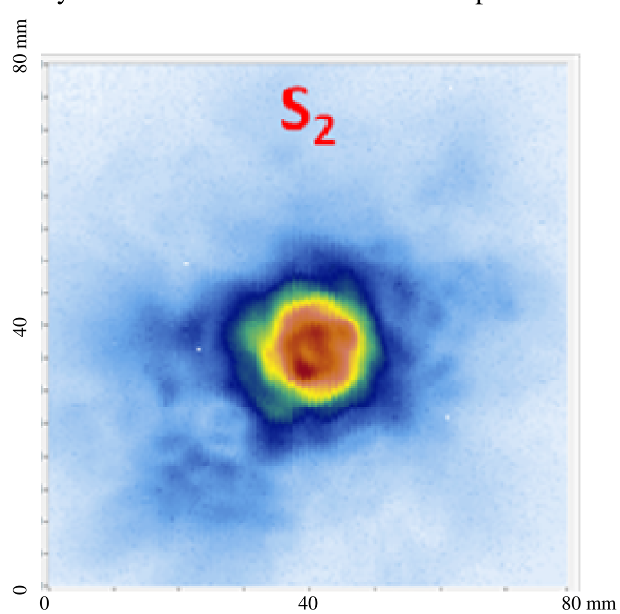

Fig. 4.26: Intensity distribution in the cross-sectional plane of the sensor- S2

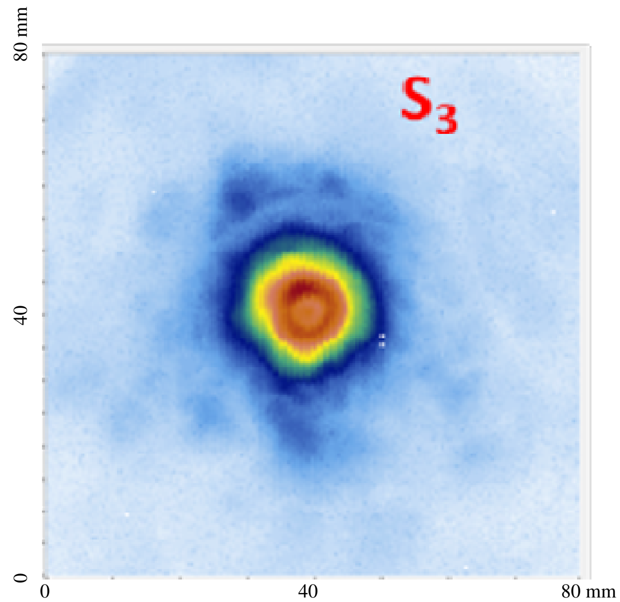

Fig. 4.27: Intensity distribution in the cross-sectional plane of the sensor- S3

4.5 Testing of SONAR device

4.5.1 Details of test setup

After assembling the device in a test vessel, focusing trials were carried out by rotating the spinner tube (Theta movement) and moving it up and down (Z-movement). Subassembly heads were arranged in the vessel so as to simulate the reactor core top. Fig. 4.28 shows the experimental setup used for the testing. Two numbers of electro-dynamic exciters were used for the testing. The first exciter was connected directly to the sonar device, to study the characteristics during the vibration of sonar device. The second exciter was connected to the target subassembly crown region. Subassembly head (crown region) was suspended from the top and was connected to the stinger rod of the exciter to facilitate its required movement. Both the exciters were controlled separately to induce vibration through the shaker control system. Two numbers of reference LVDTs are connected to the target subassembly crown region as well as to the sonar device to measure the actual movement. The output from these sensors are taken as the reference for comparing the output from the sonar device.

4.5.2 First phase of testing and test results

The first phase of studies were conducted by exciting the target with known frequencies. The ultrasonic sensor S1 was excited using the pulser receiver and signal from the sensor S1 was recorded. Using the developed software, vibration signal was extracted and compared with that of reference LVDT mounted on the target. Experiments were repeated with frequencies 2 Hz, 3 Hz, 4 Hz, 5 Hz, 10 Hz and random signal. Fig. 4.29 shows typical results representing the time signal as well as its frequency spectra.

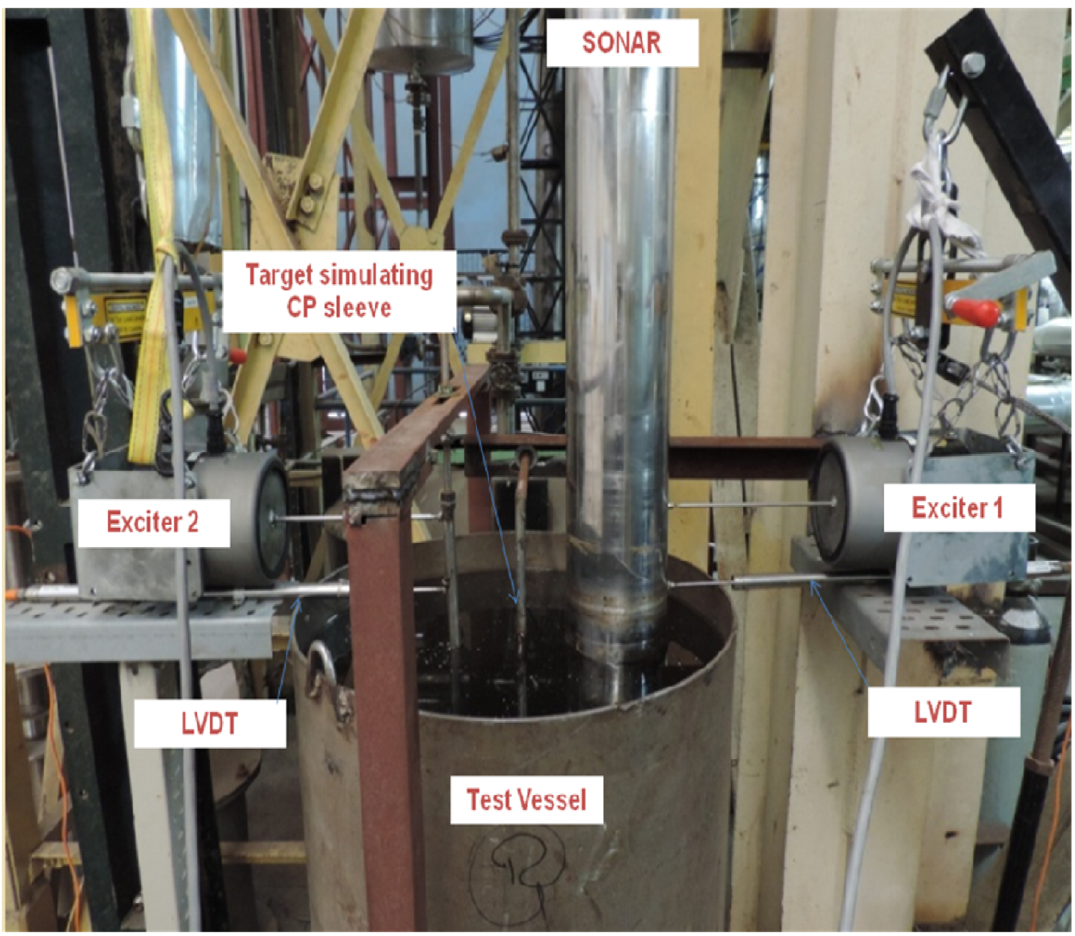

Fig. 4.28: Water test setup for sonar device

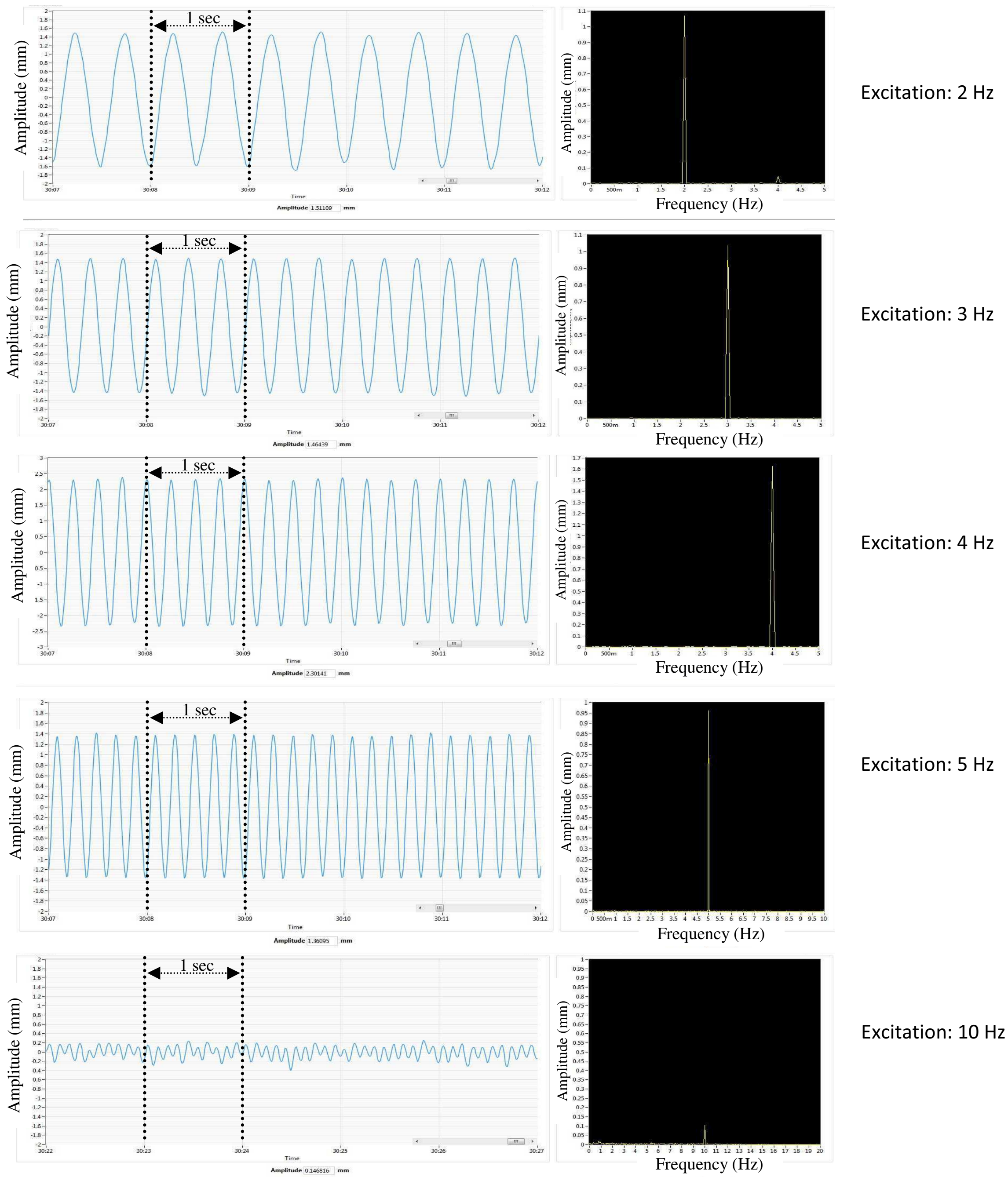

Fig. 4.29: Test results plots (Extracted time signal and frequency spectra)

It was observed from the test results that the developed algorithm reliably recovered the vibration signal. The time signal and frequency spectra were analyzed and were compared with the reference LVDT reading and were found to be matching well.

To study the performance of the developed system, measurements were also taken with frequencies 3.0 Hz, 3.1 Hz and 3.5 Hz. The target was vibrated using the exciter and signals were recorded and analyzed. The developed technique and the software could distinguish clearly the target vibration frequencies. Fig. 4.30 shows the test results. In all the studies, it was observed that the vibration of target was accurately recovered from the ultrasonic signal (Table 4.1).

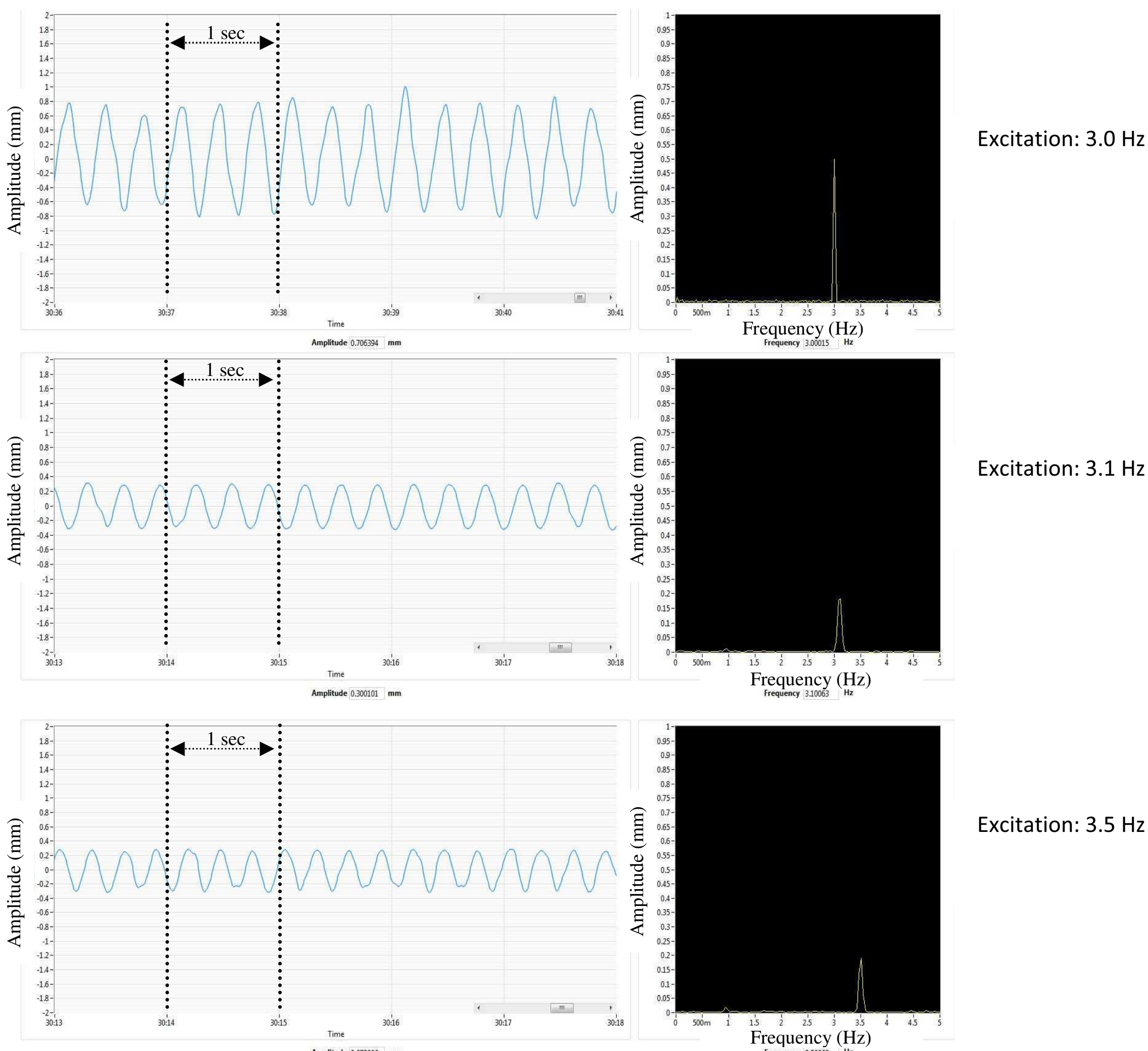

Fig. 4.30: Extracted vibration signals for excitation frequency 3, 3.1 and 3.5 Hz

4.5.3 Studies on phase of echo signal

During vibration measurement, ultrasonic signal travels through the medium to the target and is reflected back to the sensor. The intensity and phase of the reflected signal depends on the acoustic impedances of the medium and the target object. To study the variation in phase, signals were recorded using a high frequency oscilloscope. Fig. 4.31 show the time signal recorded from the target at two instants of its movement.

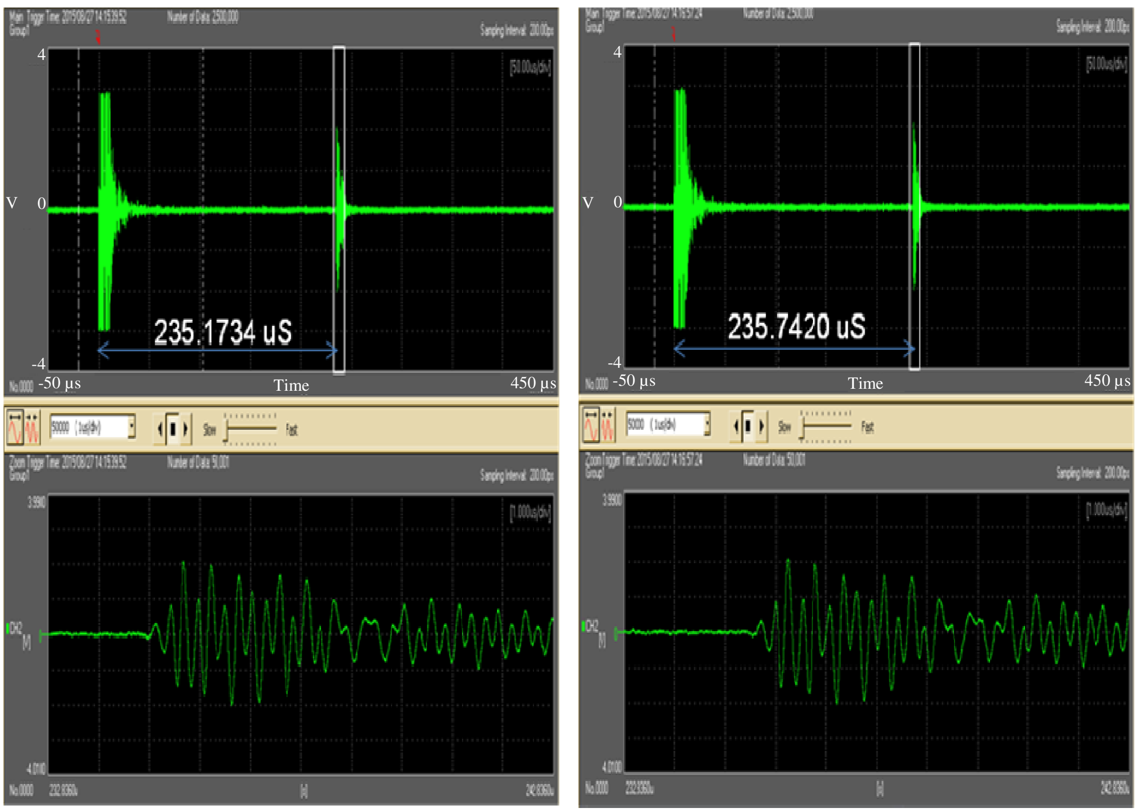

Fig. 4.31: Phase of reflected echoes during vibration

The displacement was calculated from the time plot from the two instants of time as (235.7420 µS – 235.1734 µS) x 1.470 mm/µS = 0.84 mm. No measurable phase shift was observed in the signal.

4.5.4 Second phase of testing and test results

In the second phase of experiments, target was made stationary and sonar device was excited using electro-dynamic exciter. The experiment was conducted for various excitation frequencies ranging from 2 Hz to 5 Hz and the signal from the side viewing sensor S3 was recorded and analyzed. Analysis of the data from Sensor S3 clearly indicated the movement of sonar device and the measured vibration data was matching with the reference LVDT mounted on the sonar device. This study was conducted to assess the performance of sensor S3, which in case of reactor, is focused on the shroud tube of the central canal which is the stationary reference target for vibration measurement. During vibration measurements inside the primary pool of a FBR, there can be random movement of the sonar device in the turbulent coolant flow, hence this study was conducted towards developing the vibration compensation technique. Fig. 4.32 shows a typical signal recorded from the sensor S3 for excitation frequencies of 2 Hz and 3 Hz (Table 4.1).

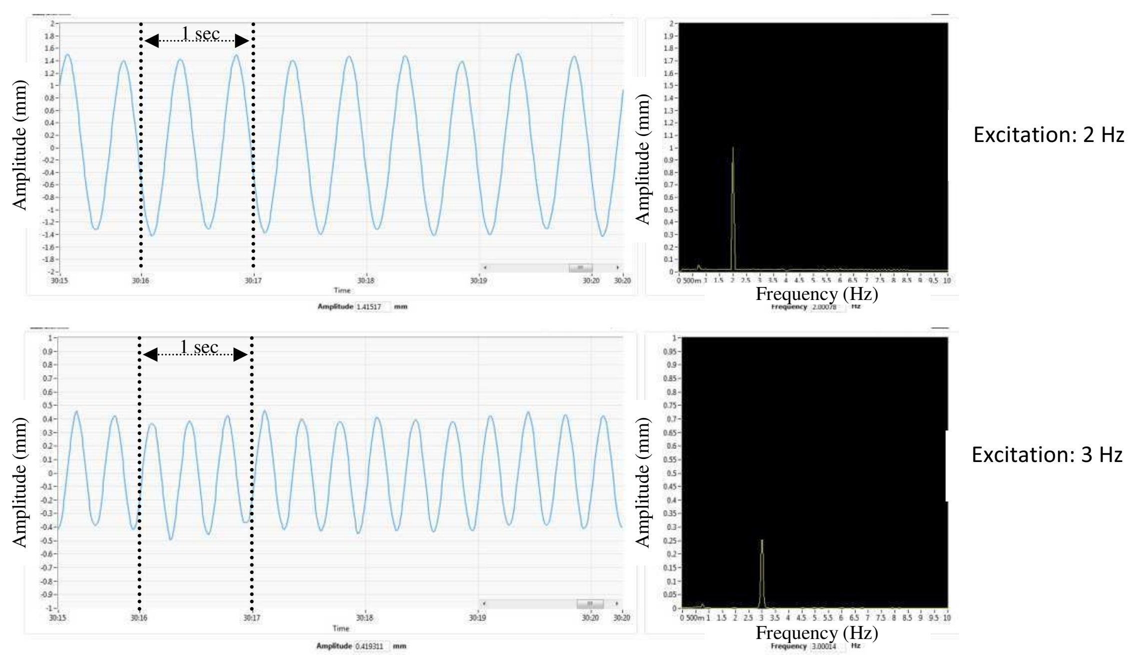

Fig. 4.32: Vibration time signal and frequency spectra from Sensor S3

4.5.5 Third phase of testing and test results

In the third phase of measurements, both the target subassembly head and the sonar device was excited using electro-dynamic exciter and simultaneous measurements were carried out using sensor S1 and S3. Signals from the sensors S1 and S3 were recorded and analyzed. Sensor S1 measured the vibration of the target whereas sensor S3 measured the vibration of the sonar device. Studies were carried out with various excitation frequency combinations. Fig. 4.33 shows typical time plots and frequency spectra, when target subassembly is excited at 4 Hz and sonar device at 3 Hz. Since, sonar moving at 3 Hz is measuring the vibration of the target, which is at 4 Hz, both the frequency components can be seen in the frequency spectra and in the time signal of signal from S1. Whereas S3, which is focused to the fixed reference measures the self vibration (frequency 3 Hz) of sonar device. When the excitation of sonar is stopped, S1 signal represents purely the target vibration which is at 4 Hz.

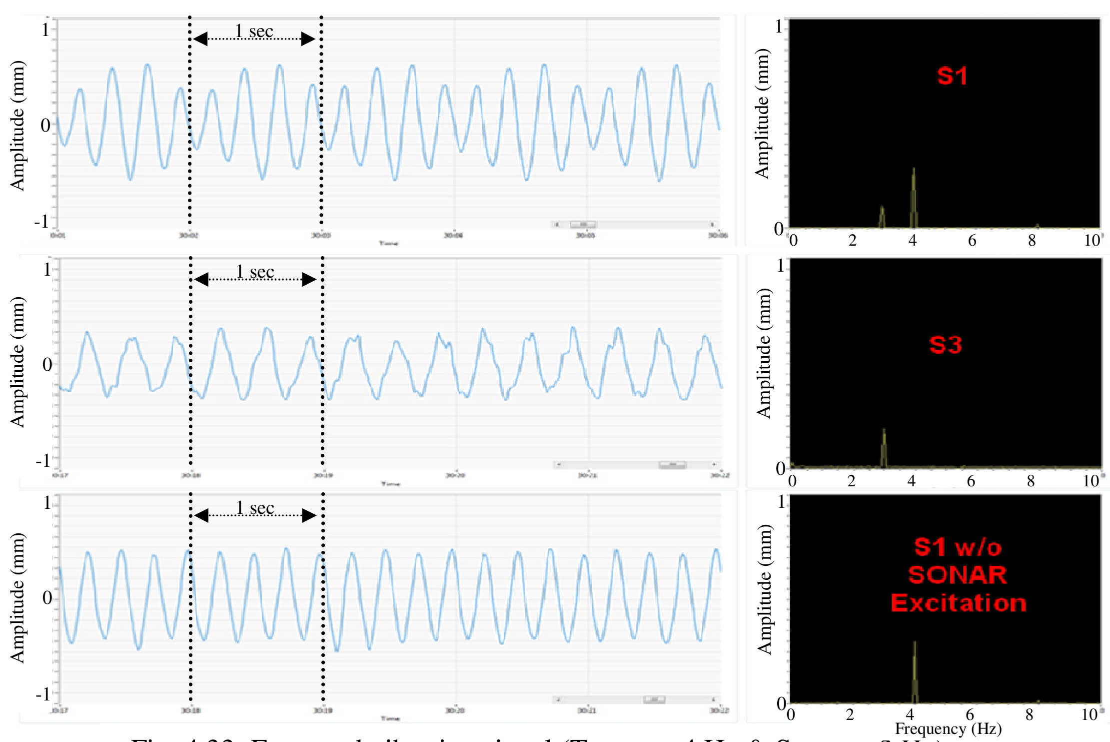

Fig. 4.33: Extracted vibration signal (Target at 4 Hz & Sonar at 3 Hz)

Fig. 4.34 and Fig. 4.35 represent the vibration signals extracted during the excitation of target at 4 Hz and sonar at 2 Hz and target at 3 Hz and sonar at 2 Hz respectively.

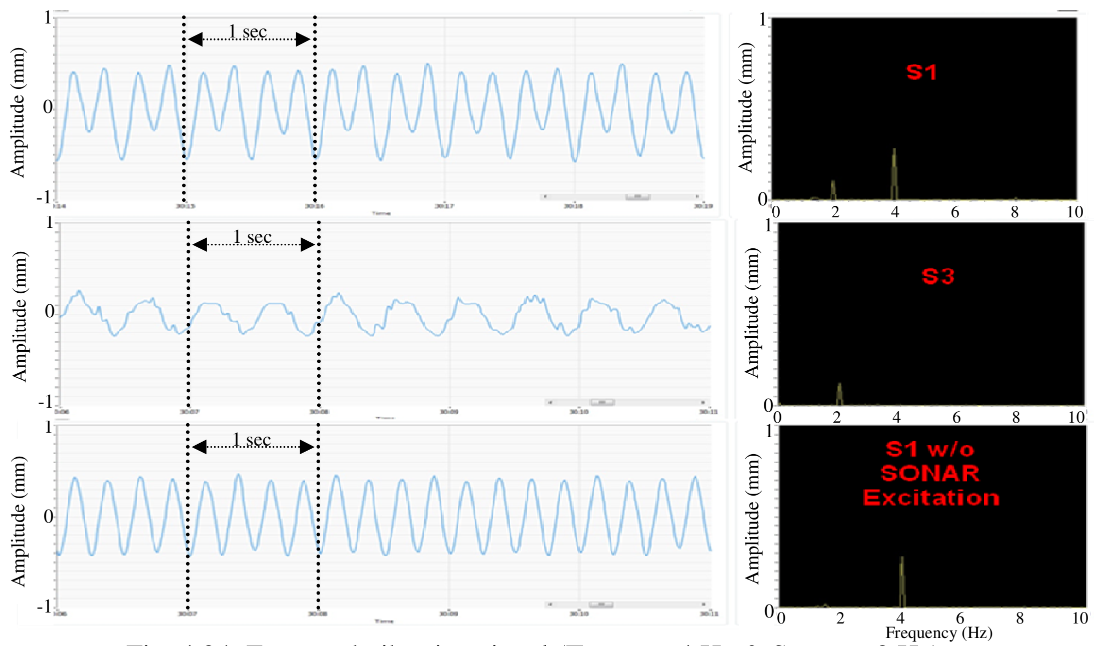

Fig. 4.34: Extracted vibration signal (Target at 4 Hz & Sonar at 2 Hz)

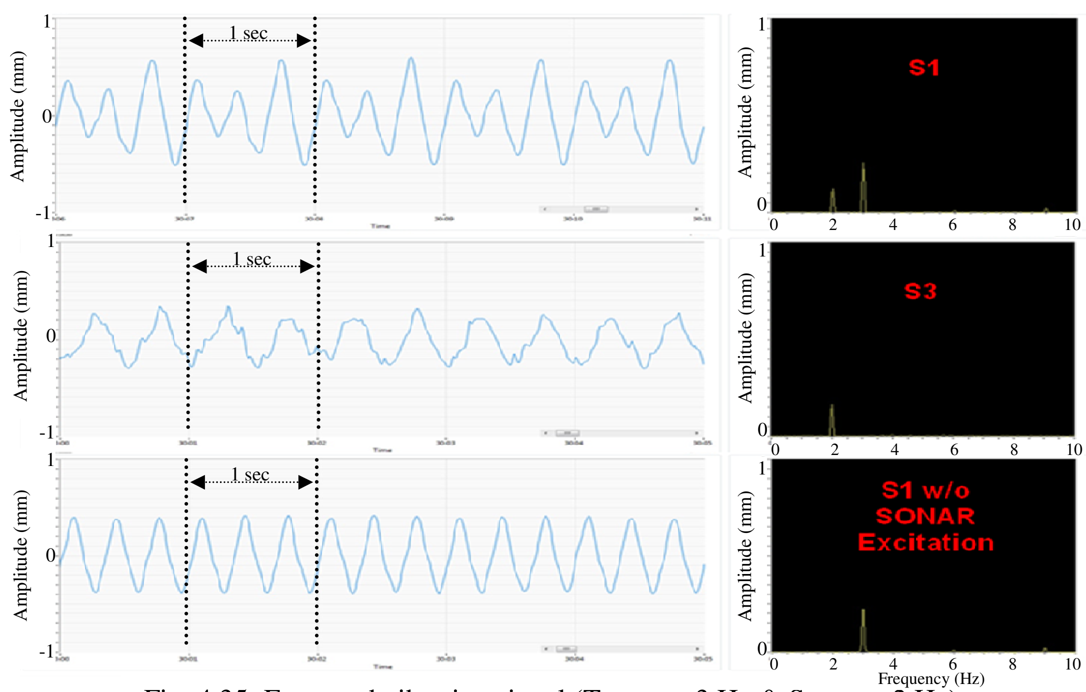

Fig. 4.35: Extracted vibration signal (Target at 3 Hz & Sonar at 2 Hz)

In all the measurement campaigns the device was able to reliably measure the vibration of the target as well as the sonar device (Table 4.1).

4.6 Vibration compensation technique

After measuring both the amplitudes of vibration, vibration compensation was done by applying the correction factor. Fig. 4.36 shows the correction factor calculation for vibration compensation. Sensor S1 measures the amplitude of vibration of target with respect to the sonar device at an angle of 30^0 with the horizontal, whereas S3, which is at 0^0 to the horizontal, measures the amplitude of vibration of sonar device. S3 is located at an elevation of 688 mm above sensor S1. The sensors S1 and S3 are installed in the same vertical plane. In order to measure the vibration of the target, sonar device vibration needs to be corrected. The correction is applied for obtaining the vibration compensation for the sonar device.

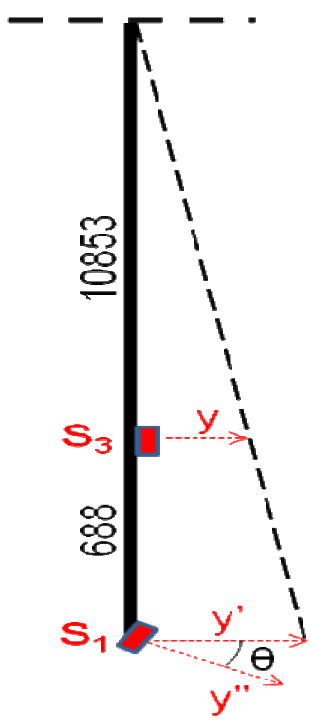

Fig. 4.36: Vibration compensation

Vibration compensated amplitude = Amplitude of S1- (C_f x Amplitude S3) --- (4.1)

Vibration of Sonar device is measured using S3 sensor signal. Assuming the Sonar device as a cantilever, the corresponding amplitude at sensor location S1 is calculated using the following method,

$$\frac{\text{Vibration amplitude } y' \text{ at S1}}{10853 + 688} = \frac{\text{Vibration amplitude } y \text{ at S3}}{10853}$$

$$y' = y \times \frac{(10853 + 688)}{10853}$$

$$y' = y \times 1.063$$

Hence, Correction factor C_f is given by,

$$C_f = 1.063 \times \cos\theta \text{ ----- } (4.2)$$

$$C_f = 1.063 \times 0.866 = 0.921 \text{ ---- } (4.3)$$

The test results from the studies after applying the correction factor are tabulated in Table 4.1.

It was also observed that the technique used for vibration compensation for Sonar device is effective and can be followed for extracting the actual vibration frequency and amplitude (displacement) of target in a turbulent primary pool of reactor where the measurement device itself is subjected to flow disturbance/vibration. Using this developed technique it is planned to measure the vibration of fuel subassemblies in PFBR, which is in the final stage of commissioning. Measurements are planned during the isothermal run of the reactor at 200^0C with dummy subassemblies in the core.

Table 4.1: Calculated amplitude of vibration after applying correction factor

SN	Target Exc Freq	SONAR Exc Freq	S1 $(rms)^2$	S3 $(rms)^2$	$(S1\text{-}C_f^2xS3)^{0.5}$ (mm)	Reference sensor (mm)	Error (mm)	Error (%)
1	2 Hz	2 Hz	1.034	0.040	1.000	0.991	0.009	0.91
2		3 Hz	0.824	0.019	0.899	0.887	0.012	1.35
3		4 Hz	0.855	0.135	0.861	0.869	-0.008	0.92
4	3 Hz	2 Hz	0.121	0.044	0.289	0.283	0.006	2.12
5		3 Hz	0.085	0.045	0.216	0.222	-0.006	2.70
6		4 Hz	0.101	0.041	0.257	0.273	-0.016	5.86
7	4 Hz	2 Hz	0.140	0.025	0.345	0.349	-0.004	1.15
8		3 Hz	0.144	0.059	0.307	0.291	0.016	5.49
9		4 Hz	0.111	0.038	0.281	0.292	-0.011	3.77
10	Random	Random	0.244	0.005	0.490	0.481	0.009	1.87

4.7 Discussion of limiting factors in measurement

Even though the developed technique reliably measured the target vibration, there are some limiting factors, which influence the measurement results. These limiting factors are discussed in this section.

Under turbulence induced vibration, the predominant frequency of vibration is the first modal frequency of the subassembly (f_n). For accurately measuring the vibration frequency, proper sampling should be done and hence PRF should be at least 10 times greater than f_n.

$$PRF > 10 \text{ x } f_n \qquad \text{------ (4.4)}$$

In all the current testing and measurements, a PRF of 100 Hz is used in the pulser receiver units, hence errors are expected when the target vibration exceeds 10 Hz. In the case of subassembly vibration measurement, the natural frequency of subassembly ~ 4 Hz, hence the selected PRF of 100Hz is 25 times the measurement frequency, which is a reasonably good approximation for the reliable recovery of the signal with good accuracy.

During subassembly vibration measurement using SONAR device the time taken by the ultrasonic signal for its to-and-fro travel from the sensor to the target and back to the sensor is ~ 0.2 mS. Since PRF is selected as 100 Hz, subsequent triggering of the sensor will be made only after 10 mS. Hence error in time overlapping is well addressed by selection of measurement parameters such as PRF and sensor distance. By varying the PRF, measurement frequency range can be increased.

For better accuracy in measured amplitude and shape of ultrasonic signal, the sampling frequency of the DAS (f_s) should be at least 10 times that of ultrasonic transducer (f_{US}). Hence the relation is,

$$f_s > 10 \times f_{US} \qquad \text{------ (4.5)}$$

Since the ultrasonic sensor is operated at 5 MHz, a minimum sampling frequency of 50 MHz is required. However a DAS having acquisition rate upto 125 MHz was used for SONAR device.

4.8 Error in measurement

Table 4.1 shows the measured vibration values and the readings from the reference sensor during the testing of SONAR device in water. The percentage of error is also shown in the table. The maximum error observed during the measurement is 5.8 %, which corresponds to a value of 16 micron.

4.9 Measurement scheme in PFBR

The developed sonar device is planned to be deployed in the central canal of PFBR control plug. The gap between the control plug bottom and the top of the subassembly is only 100-150 mm. To measure the vibration of a subassembly (say no. 8), the position of sonar device should be as shown in Fig. 4.37.

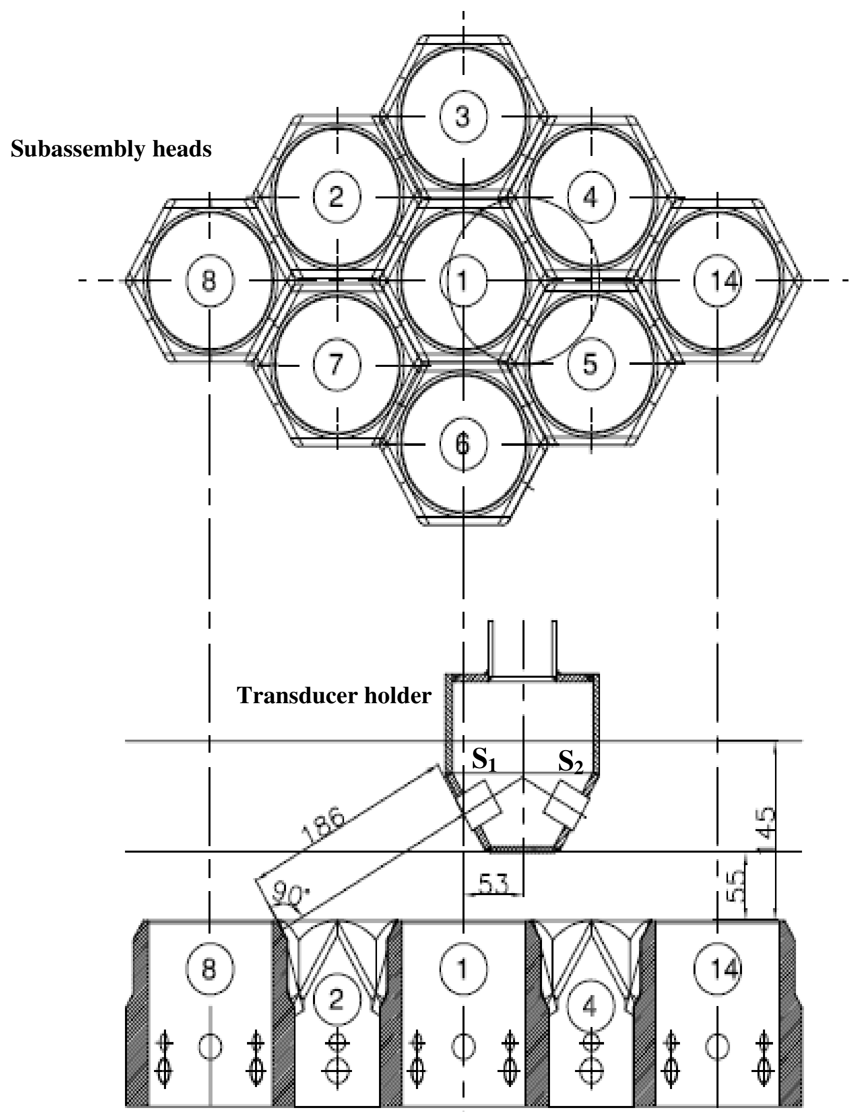

Fig. 4.37: Measurement scheme in PFBR

Five number of core subassemblies were identified for measurement in PFBR during commissioning. The identified subassemblies are shown in Fig. 4.38. For each subassemblies, measurements will be taken at two different directions and the resultant will be calculated.

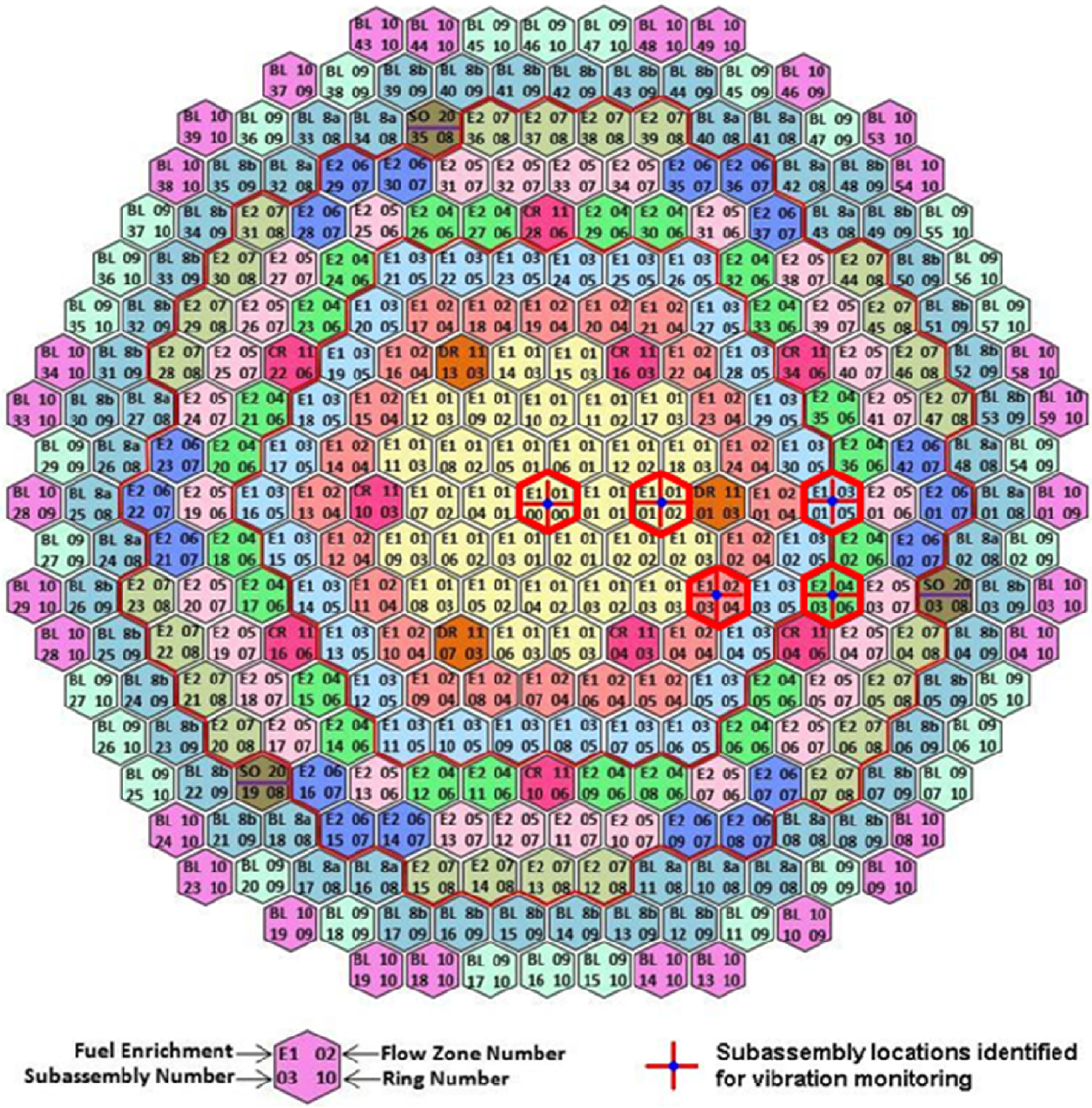

Fig. 4.38: Measurement subassemblies in PFBR

4.10 Summary

- A prototype model of SONAR device was assembled and performance testing completed in water and sodium. The device measured the vibration of target accurately.
- Measurement parameters such as ultrasonic operating frequency, PRF, ultrasonic signal acquisition frequency, etc. were optimised.
- Development of SONAR device for PFBR was carried out with 3 ultrasonic sensors.
- Axial and cross sectional beam profiling of ultrasonic sensors were plotted by immersion technique to study the beam divergence.
- Beam diveregence was very minimal in the measurement range of 250 mm and cross sectional intensity plot is circular. The energy distribution is uniform at a distance of 200 mm.
- Testing of drive system of SONAR device was carried out and qualified for reactor application.
- No measurable phase shift was observed in the reflected echo compared to the transmitted pulse.
- Vibration compensation technique was demonstrated and correction factor was estimated and applied to the measured target vibration to calculate the true vibration of the target.
- Testing of SONAR device was carried out by exciting both target subassembly and SONAR device using electro-dynamic exciters and the maximum error observed in the measurement in comparison with reference LVDT reading was found to be 5.8% which corresponds to 16 microns.

- Five numbers of core subassemblies in different flow zones were identified for vibration measurement in PFBR.

CHAPTER-5
DEVELOPMENT OF ULTRASONIC WAVEGUIDES

5.1 Introduction

Ultrasonic techniques for under sodium imaging, core protrusion detection, core mapping, etc. are well matured for low temperature applications whereas measurements at still higher temperatures is yet to be demonstrated [39, 40, 41]. High temperature ultrasonic sensors for reactor applications are commercially not available, hence development of suitable waveguides as an alternative is very important for various measurement techniques. Waveguides are generally defined as conduits for acoustic/ultrasonic waves and can be utilized for transfer of information/signal from inaccessible and hostile locations to a more accessible location.

Vibration measurement technique developed for FBR primary pool applications can not be extended as such for high temperature applications (550^0C) due to limitations in high temperature sensor availability. In order to facilitate vibration measurements under operating conditions (rated flow and high temperature 550^0C), development of waveguide (SS316 plate) based measurement system was carried out. Hence the ultrasonic signal is generated outside the hostile environment and transmitted to and from within the reactor core using the waveguide. The principal advantage of this arrangement is that the source of the ultrasound wave is located in a low temperature environment at one end of the waveguide [42, 43, 44]. Hence, conventional low temperature ultrasonic sensors/piezoelectric crystals can be used to generate ultrasonic pulse. Even though, waveguides provides the flexibility of signal transfer from even remote and hostile environment, its design to suit the in-process requirements and handle the surrounding environment are equally important. Hence, theoretical modeling of the ultrasonic wave propagation in waveguide is needed for the actual design and development of the waveguides.

5.2 Design of waveguides

In the last few decades, Rayleigh/Lamb and other guided waves have been used increasingly in ultrasonic NDT application to detect small cracks located near an interface or narrow cracks that run normal to an interface or free surface. Lamb waves are guided waves which are characterized by their inherent ability to travel long distances without much loss in their energy content and to follow the contour of the boundaries between which they are propagating. Lamb waves propagates in plates, as a superposition of various modes possible at that particular combination of frequency and thickness. Numerical methods can predict the modes existing at any frequency-thickness product as dispersion curves.

Development of waveguides for underwater or under-sodium applications demands the propagation of ultrasonic waves through the waveguide (metal) and then through the liquid medium. To achieve a single pulse as a result of a single excitation the guide must be operated such that only a single mode may exist [45]. Analytical studies were carried out using DISPERSE software. DISPERSE software is used in NDT technique to generate dispersion curves for a wide range of test specimens. Dispersion curves for different material medium helps us to obtain a better understanding of guided wave propagation in the medium [46]. Disperse software is capable of modeling several geometries and types of material. Dispersion curves can be obtained for various models with multiple layers, free or leaky systems, elastic or visco elastic isotropic materials etc. The process of generating dispersion curves includes, selection of material, selection of geometry, external boundary conditions, velocity in the material etc. After choosing the required parameters, tracing of the dispersion curves will be done and the output can be obtained in the following forms such as phase velocity plots, group velocity plots, attenuation characteristics etc.

In generating the dispersion curves analytically, we end up with possible wave propagation possibilities or wave resonances that occur in the structure. Wave propagation possibilities come from points on the dispersion curve. The modes or the curves are labeled as ‘S_0’, 'S_1’, 'S_2’ etc. for symmetric modes and ‘A_0’, ‘A_1’,‘A_2’ etc. for asymmetric modes. The vibrational character of the structure is responsible for the mode naming. The symmetric modes have associated with them a compression/rarefaction expansion of the structure in which the wave propagates and asymmetric nature is associated with flexural mode propagation.

Dispersion curves were plotted for SS plate (1.6 mm) using DISPERSE software to understand the different wave modes that could actually propagate in the plate waveguide [47, 48, 49]. Fig. 5.1 and Fig. 5.2 show the phase and group velocity dispersion curves for a traction-free Stainless steel 316 (SS 316) plate generated using the DISPERSE software.. Symmetric modes (‘S_0’, 'S_1’) and anti-symmetric modes (‘A_0’, ‘A_1’) along with the higher order modes are shown in the dispersion curves.

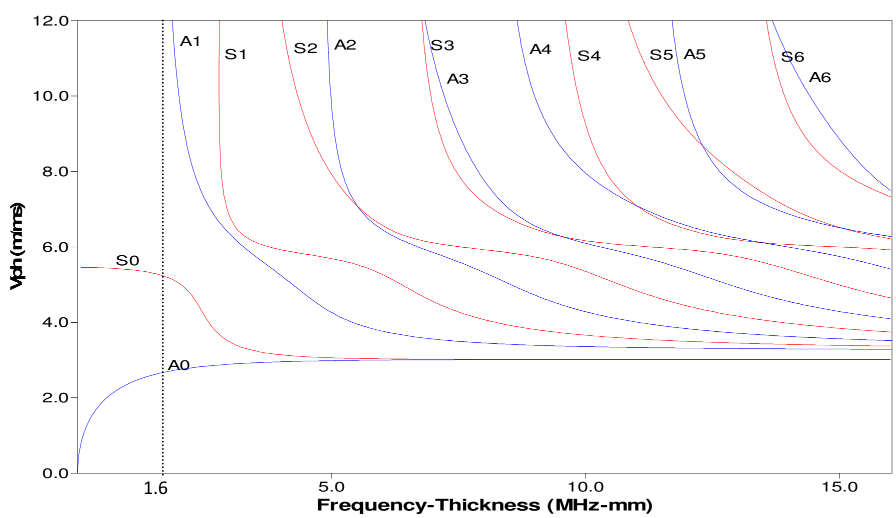

Fig. 5.1: Phase velocity dispersion curve for SS316 strip

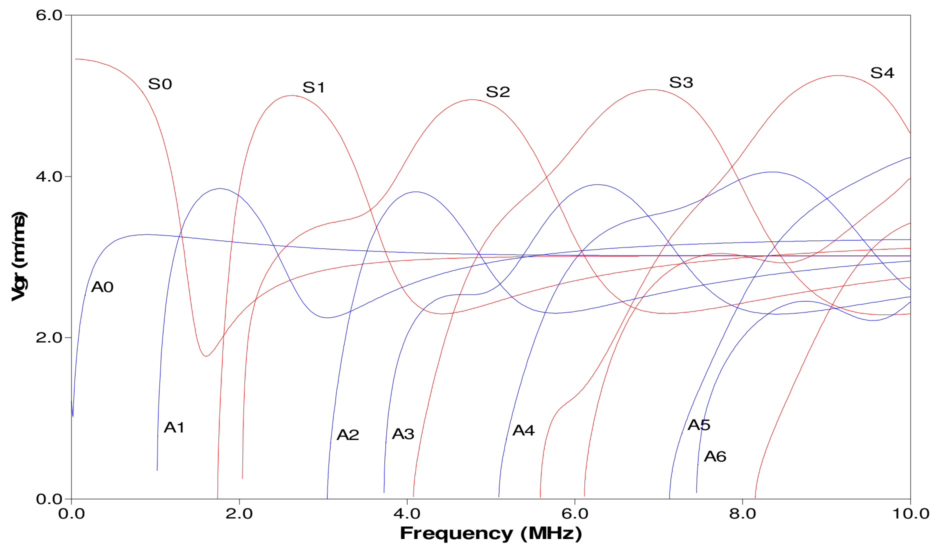

Fig. 5.2: Group velocity dispersion curve for SS316 strip

Wave structure (at 1.6 MHz-mm) for asymmetric (A_0) and symmetric mode (S_0) obtained from DISPERSE is shown in Fig. 5.3. It can be observed from the wave structure of 'A_0' and 'S_0' modes that at the mid point along the thickness Uy is zero for symmetric mode and Ux is zero for asymmetric mode.

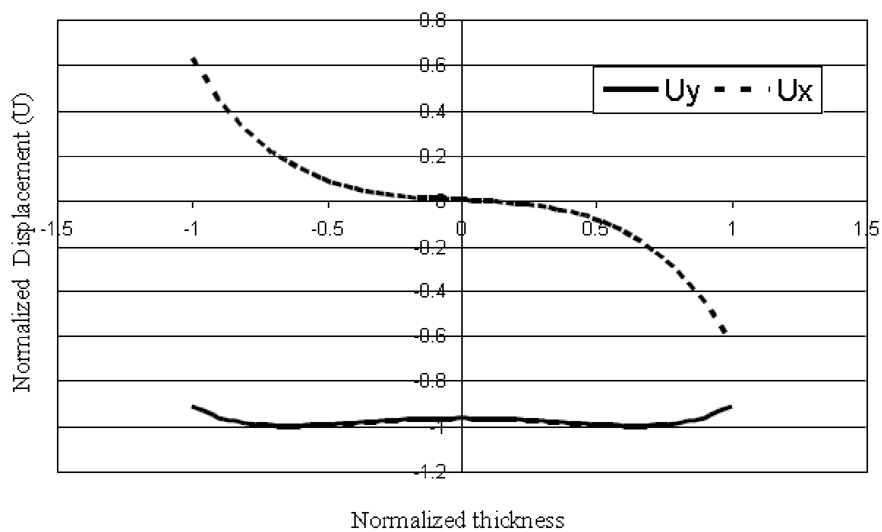

(a)

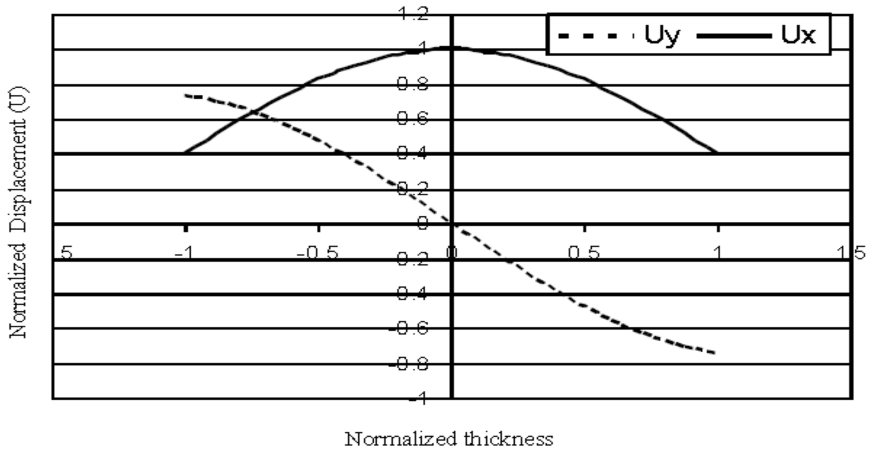

(b)

Fig. 5.3: Wave structure for (a) asymmetric (A_0) and (b) symmetric mode ($S_{0)}$

The 'A_0' Lamb wave mode was selected based on the high out-of-plane displacement component required for enhanced leakage into the liquid sodium from the waveguide. A suitable point on the dispersion curve (1.6 MHz-mm) was chosen for operation (Fig. 5.1). The point was selected in such a way that, it is well away from the highly dispersive region, which allows the energy to propagate long distances in the waveguide with minimum losses and less wave packet spread so as to get better resolution. However, mild dispersion was determined to be desirable in order to have the frequency based beam steering, as explained in detail later. Moreover above 1.6 MHz-mm, there is a chance that higher modes such as 'A_1' also will be generated in the waveguide. Hence a suitable working point for generation of 'A_0' mode for our waveguide design was selected as 1.6 MHz-mm to make single mode 'A_0' generation.

5.3 ‘A_0’ wave mode generation

‘A_0’ Lamb wave modes are generated by exciting a L wave piezo-ceramic element on the specifically designed angle wedge made of Aqualene material [50, 51]. Fig. 5.4 shows the schematic for the generation of ‘A_0’ Lamb wave mode using a piezoceramic element on an Aqualene wedge.

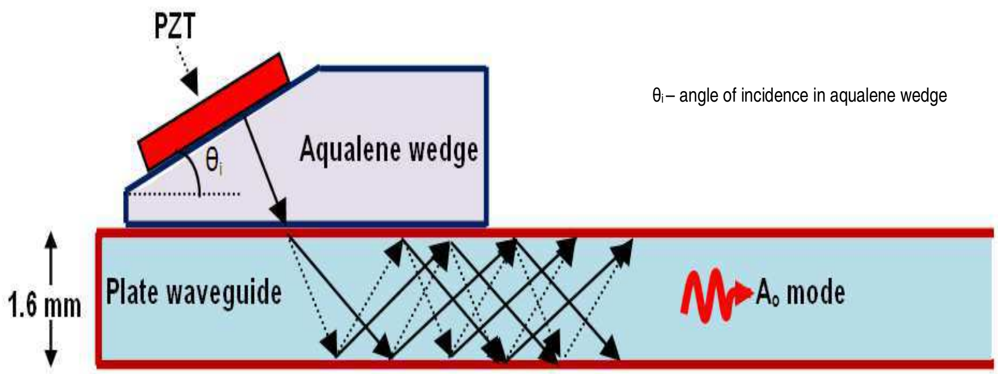

Fig. 5.4: Schematic of generation of ‘A_0’ lamb wave mode using a wedge

Aqualene wedge was procured and machined as per the required angle so as to transmit longitudinal waves through the wedge. The Aqualene is a solid material that possesses acoustical properties that are similar to water and was procured from OLYMPUS NDT (USA). A piezo-ceramic crystal is directly mounted on the wedge. The wedge is then mounted on to the SS strip wave guide using suitable acoustic couplant. Fig. 5.5 shows the crystal and wedge mounted on the waveguide. At the plane of contact of the wedge and the waveguide refraction takes place and longitudinal as well as shear wave modes will be generated in the waveguide. The recombination of different wave modes ends up in generation of a single ‘A_0’ mode that propagates along the waveguide.

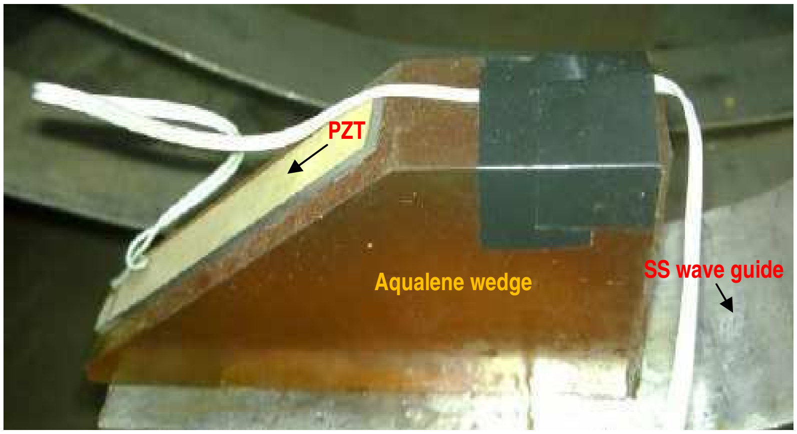

Fig. 5.5: PZT transducer bonded to an Aqualene wedge

5.4 Working principle of waveguide

Lamb wave is generated in the waveguide plate by an excitation from the PZT transducer bonded to an aqualene wedge, where the compression wave is impinging on the waveguide at an angle within the wedge. The generated lamb wave at the end of the plate propagates towards the radiating surface in contact with the liquid sodium. At the radiation surface the lamb wave create a leaky compression wave within the liquid through a mode conversion. The radiated ultrasonic wave is reflected from the target. Reflected ultrasonic waves are received at the wave guide again by mode conversion.

When the PZT crystal is excited, it generates longitudinal wave in the wedge. The ultrasonic waves generated in the wedge, propagates through the wedge and at the surface of waveguide gets converted into a lamb wave in the waveguide. The angle of the wedge for generating the required wave mode is calculated using Snell's law as-

$$\alpha(fd) = Sin^{-1}\left(\frac{v_W}{c_p(fd)}\right) \text{-----(5.1)}$$

Where, 'v_W'is the longitudinal wave velocity in the wedge (aqualene),

'C_p' is the phase velocity in the waveguide at 1.6 MHz-mm. Aqualene material have bulk properties close to that of water with 'ν_w' 1521 m/s and density (ρ) 987 kg/m^3). The value of 'C_p' from the disperse curve is 2515 m/s for 'f' x 'd' of 1.6 MHz-mm. By substituting these values in equation 5.1, the value of 'α' becomes 37^0, which is the wedge angle for generating 'A_0' mode in the waveguide.

The wave generated in the waveguide travels through the material and reaches the radiation end section of the waveguide and the wave is radiated into the surrounding liquid. The angle of emission at the radiation end can be obtained by Snell's law as-

$$\beta(fd) = Sin^{-1}\left(\frac{v_L}{c_p(fd)}\right) \text{----(5.2)}$$

Where, 'v_L'is the longitudinal wave velocity in the surrounding liquid,

'C_p' is the phase velocity in the waveguide at 1.6 MHz-mm.

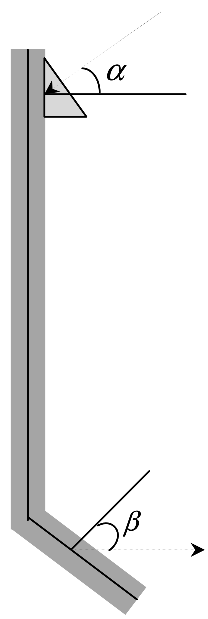

Fig. 5.6: Schematic of waveguide

Since the surrounding medium taken for the study is water, the value of 'v_L' is 1480 m/s. Substituting the value in equation 5.2, the value of 'β' becomes 36^0. So at the radiation end, the waves leak at an angle of $36^0$with the normal to the waveguide. So bending the waveguide at an angle of 36^0 at the bottom radiation end results in leaky lamb waves to travel in the horizontal plane at the waveguide-water interface. The detailed schematic of the waveguide is shown in Fig. 5.6.

5.5 Preliminary studies

A SS316 strip waveguide was machined for the study. For preliminary studies, the length of waveguide is fixed as 10 m and thickness was selected as 1.6 mm. The waveguide was supported on an insulated support stand in the water test setup. Fig. 5.7 shows the waveguide details. The bottom end of the waveguide is provided with a cover tube so as to have only desired contact of the wave guide with the test fluid. The length of the cover tube in the current wave guide configuration is fixed as 1 m. A window is provided at the bottom end of the waveguide which is immersed in the water such that only one face of the plate waveguide is exposed to the liquid. Fig. 5.8 shows the schematic of the waveguide used for the study and Fig. 5.9 shows the experimental test setup.

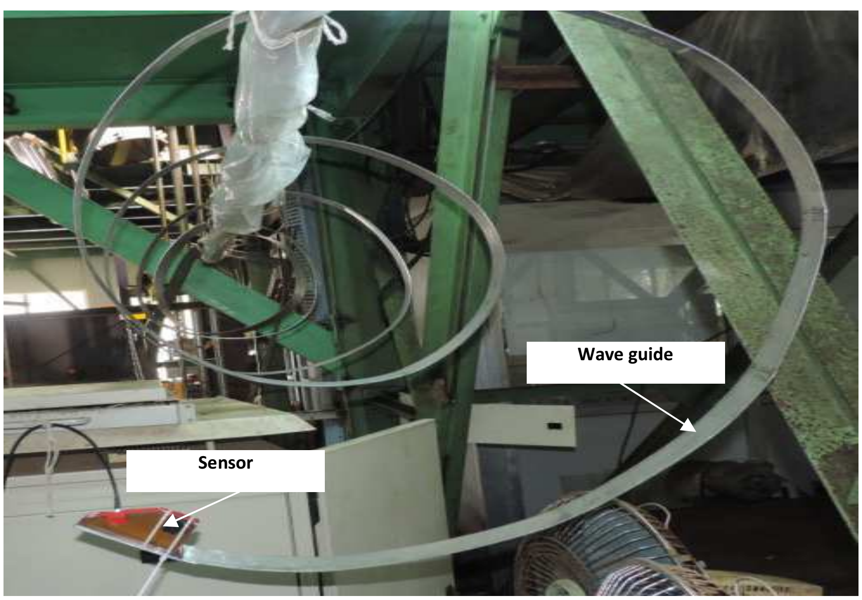

Fig. 5.7: SS Strip waveguide with sensor (10 m long)

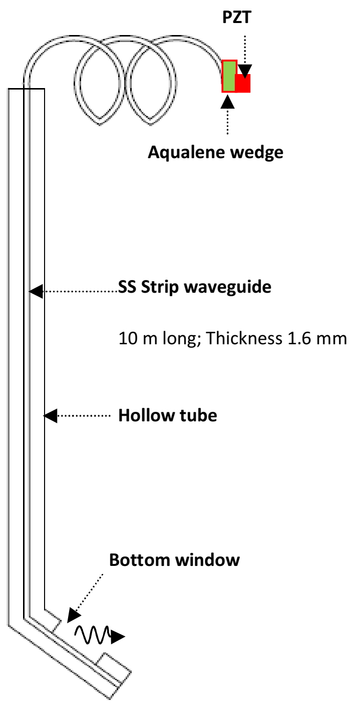

Fig. 5.8: Schematic of waveguide

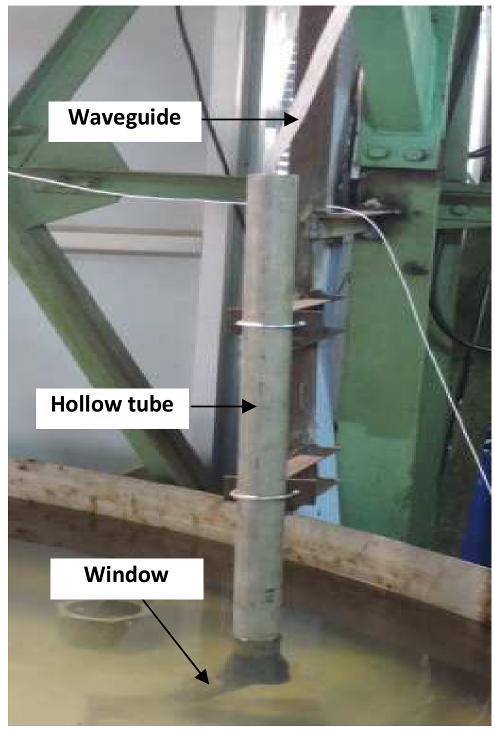

Fig. 5.9: Bottom end of waveguide

5.6 Optimization of the measurement parameters

An ultrasonic pulser-receiver is used to excite the sensor. Ultrasound waves generated in the wave guide is transmitted to the target and the reflected echo from the target is received using the same sensor and are recorded using a high frequency oscilloscope. Various parameters such as crystal excitation frequency, number of cycles, PRF, etc. are varied to obtain an optimum output signal. Fig. 5.10 shows the variation in amplitude of the reflected echo for various input excitation frequencies. It can be clearly observed from the plot that the optimum frequency of operation of the wave guide is 1.10 MHz. Other measurement parameters used for the study are tabulated in Table 5.1.

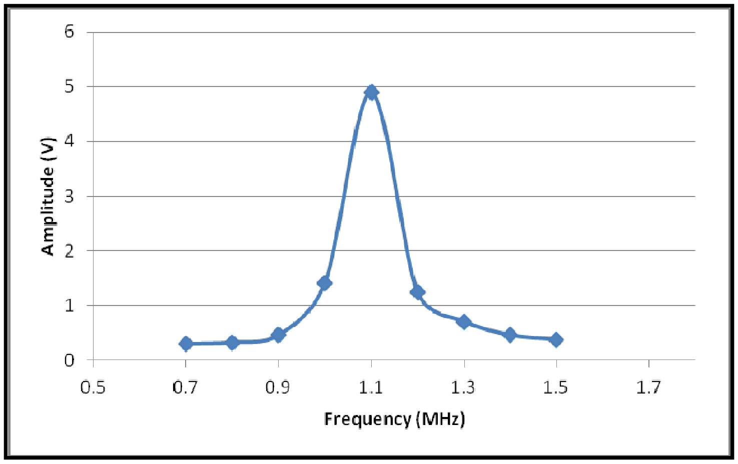

Fig. 5.10: Optimum operation frequency determination

Table 5.1 Optimized measurement parameters

SN.	Parameter	Value
1.	Frequency	1.1 MHz
2.	No. of cycles	20
3.	Control	20
4.	Repetition rate	50
5.	Low pass filter	2.5 MHz
6.	High pass filter	800 kHz
7.	Receiver gain	50 dB

5.7 Time signal representation of waveguide signal

A target plate was fixed at a distance of 3 m away from the end of the waveguide. The crystal is excited at a frequency of 1.1 MHz and the reflected echo from the target was identified in the time domain and was recorded using the digitizer in the conventional pulse echo mode. After transducer ringing signal, the first set of echo observed is the signal reflected from the waveguide end. This echo pulse corresponds to 20 m (to and fro) travel of sound in the waveguide medium. The second echo corresponds to the reflection from the target assembly 3 m away from the waveguide. Ultrasonic waves generated in the wave guide are leaked to the liquid through the window provided at the bottom of the waveguide in water. The generated signal is directed towards the target to obtain echo signals. Time signal recorded from the sensor is shown in Fig. 5.11.

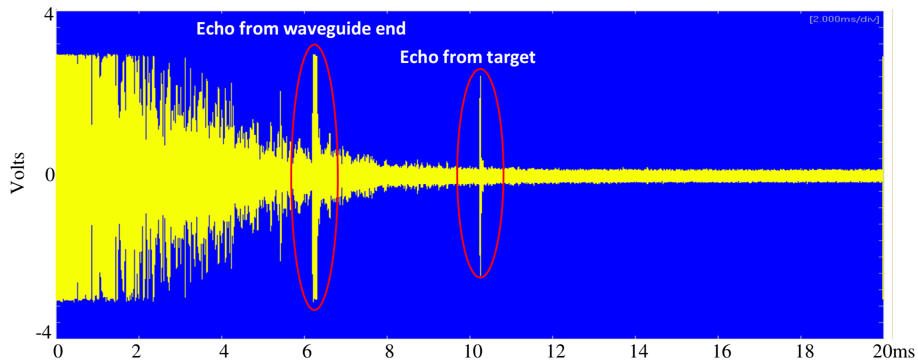

Fig. 5.11: A typical time signal recorded from the wave guide sensor

5.8 Wave guide beam profiling and demonstration of Frequency based beam steering.

In order to understand the beam intensity distribution pattern, beam profiling was carried out using the developed waveguide using a transducer characterization system TraCSS® (provided by Dhvani Research and Development Solutions Pvt Ltd, India) in an immersion mode. The bottom end of the wave guide was inserted inside a water test tub having three axis scanner. A standard commercial pinducer (Valpey Fisher Inc., USA) was used to scan the ultrasonic field intensities from the waveguide sensor. Axial beam profiling and cross sectional beam profiling were carried out. After installing the sensor inside the tub, sensor was excited for different input excitation frequencies using the Tone Burst RITEC RPR 4000 ultrasonic pulser-receiver. For each input excitation frequencies, the pinducer was moved from the centre of the sensor towards the axial direction up to 400 mm to record the axial beam intensity pattern. Fig. 5.12 shows the ultrasonic beam intensity distribution in the axial direction. Good symmetry was observed in the intensity distribution pattern. Moreover, a clear indication of steering of ultrasonic signal for different excitation frequency was observed in the plots.

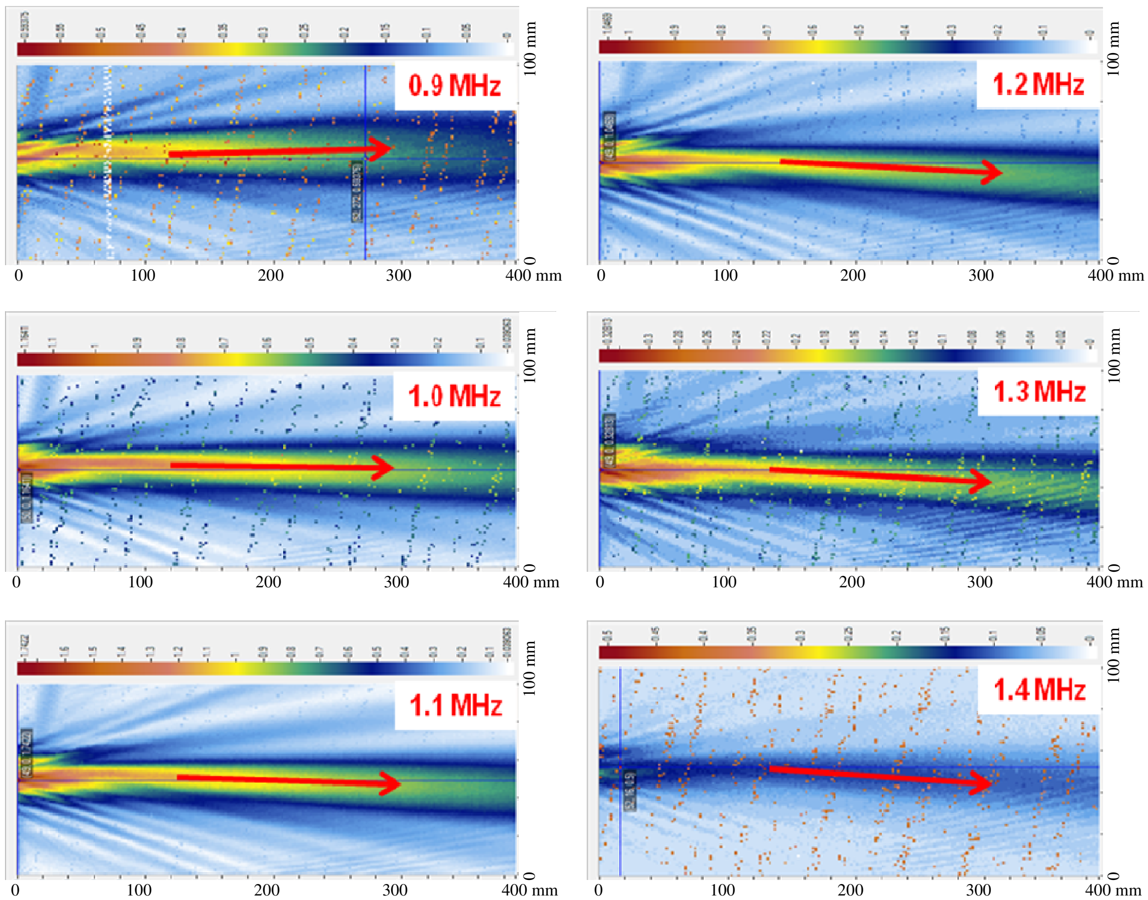

Fig. 5.12: Intensity plot distribution along the axis of the waveguide sensor

After carrying out the axial beam profiling, cross-sectional beam profiling was also carried out using the pinducer. From the sensor surface, pinducer was fixed at a distance of 250 mm. Ultrasonic beam intensity was plotted and is shown in Fig. 5.13. Symmetry of the beam, exit angle deviation etc were verified from the recorded signal. Fig. 5.14 shows the cross-sectional beam intensity variation plots recorded from the sensor surface as well as at an axial distance of 500 mm at an operating frequency of 1.1 MHz. The figure shows the ultrasonic intensity lobes in the waveguide sensors, similar to that in the conventional ultrasonic sensors.

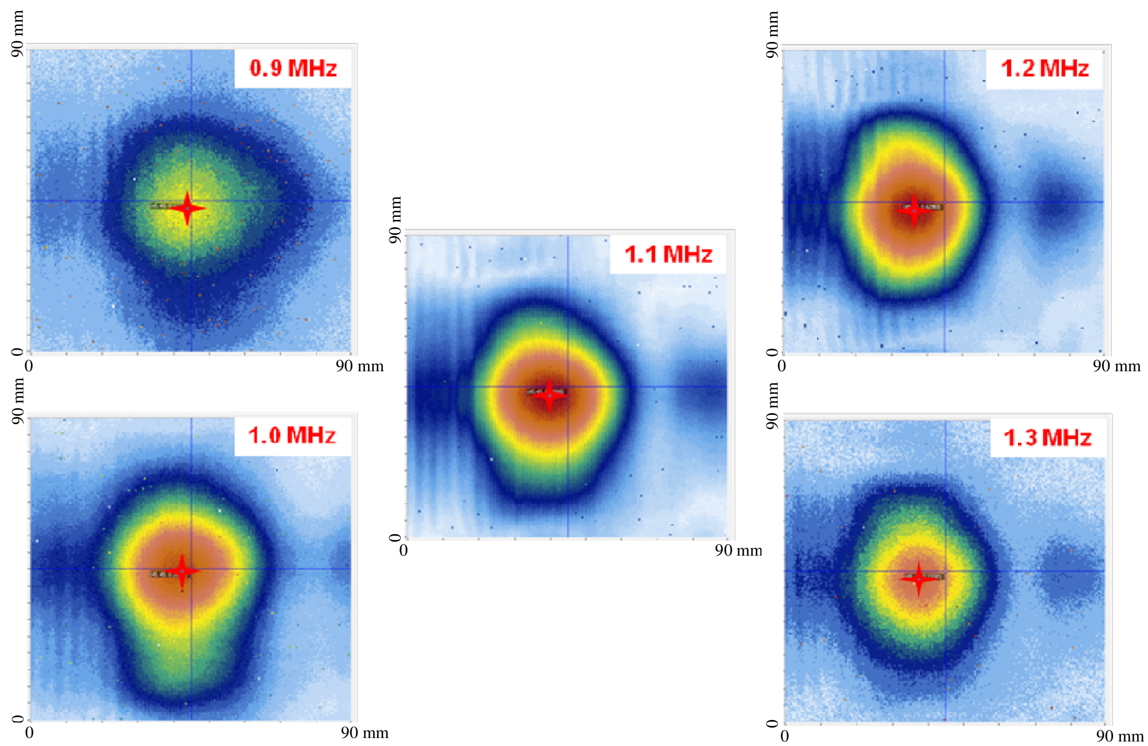

Fig. 5.13: Cross sectional intensity plot distribution at 250 mm

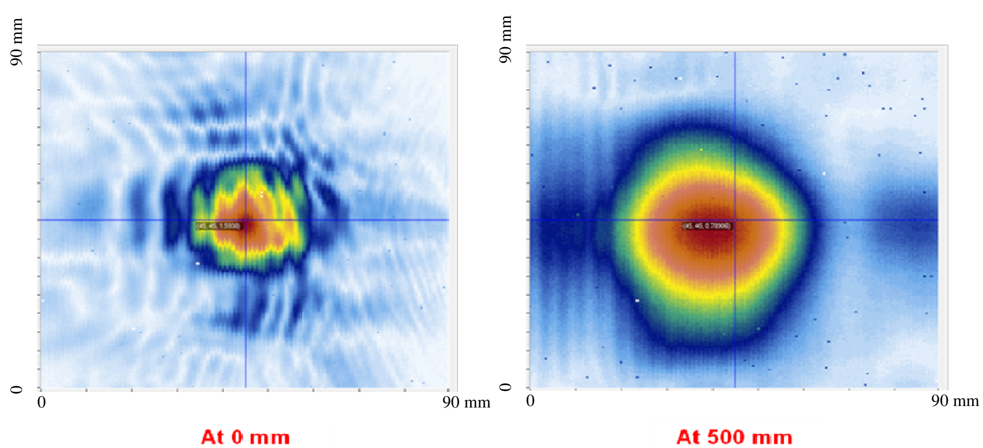

Fig. 5.14: Cross sectional intensity plots comparison at 1.1 MHz

5.9 Beam exit angle measurement

From the measured axial and cross-sectional beam intensity plots, deviation in the beam exit angle is observed. The beam exit angle of the developed waveguide sensor was measured. To measure the variation in beam exit angle, waveguide was operated for different frequencies and the angle at which maximum amplitude falls was measured. Fig. 5.15 shows the beam exit angles measured from the waveguides for different operating frequencies. Even though the measured angles are comparatively small, these studies also revealed the possibility of using the waveguides for beam steering applications [52, 53].

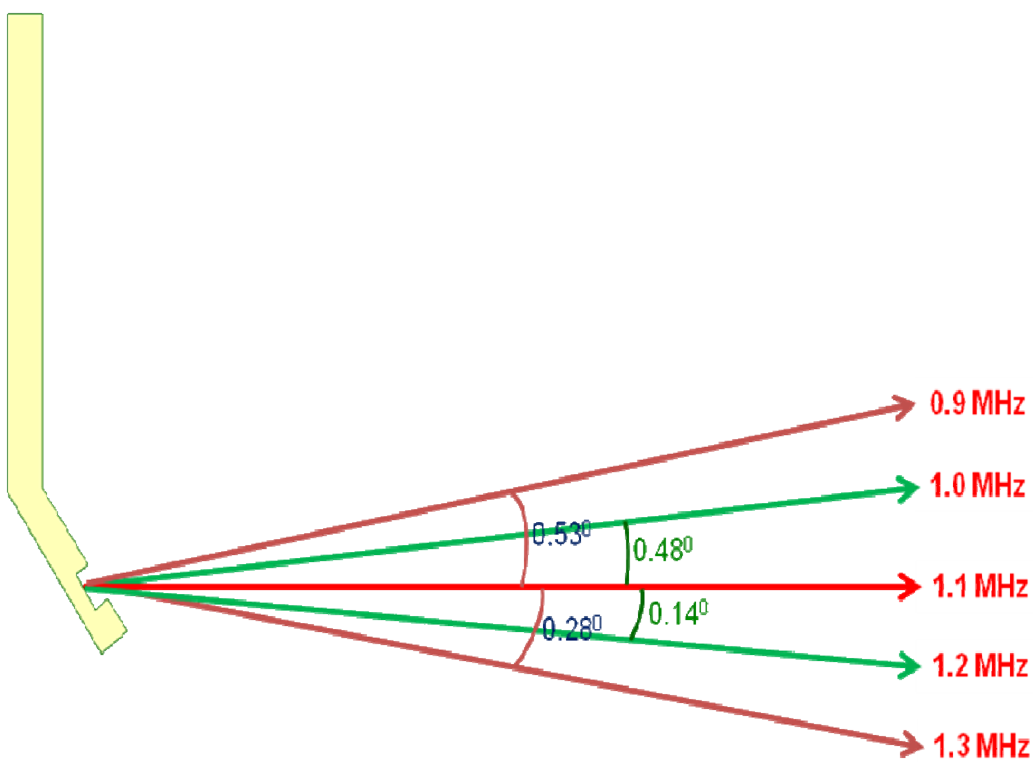

Fig. 5.15: Measured beam exit angle from waveguide

5.10 Vibration studies using the developed waveguide

Towards the end of studies using waveguides, vibration measurements were attempted using various target objects in the test vessel. The schematic of experimental setup is shown in Fig. 5.16. A test vessel of 5 m diameter is used for testing the waveguide (Fig. 5.17) and water is used as the test fluid.

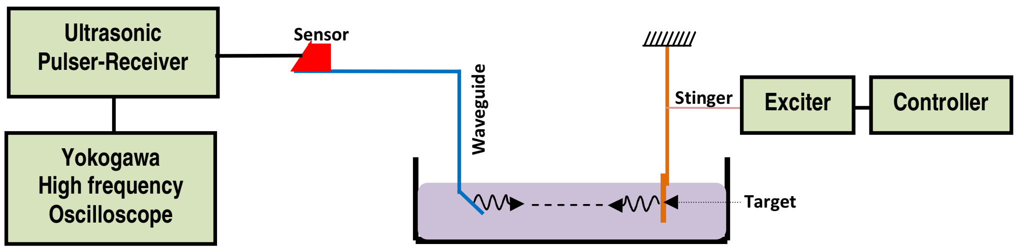

Fig. 5.16: Schematic of experimental test setup

Fig. 5.17: Test vessel used for waveguide testing

For vibration measurement, a target rectangular plate is kept at a distance of 3m from the waveguide. An electro-dynamic exciter is used to excite the target with known frequencies and a reference LVDT (Honeywell make, Model DW7U) is used to measure the amplitude of vibration. The target is connected to the electro-dynamic exciter (B&K make) using a stinger rod (Fig. 5.18). To determine the optimum frequency of operation, the sensor was excited with different frequencies and echo from the target was recorded and the optimum frequency of operation is determined as 1.1 MHz.

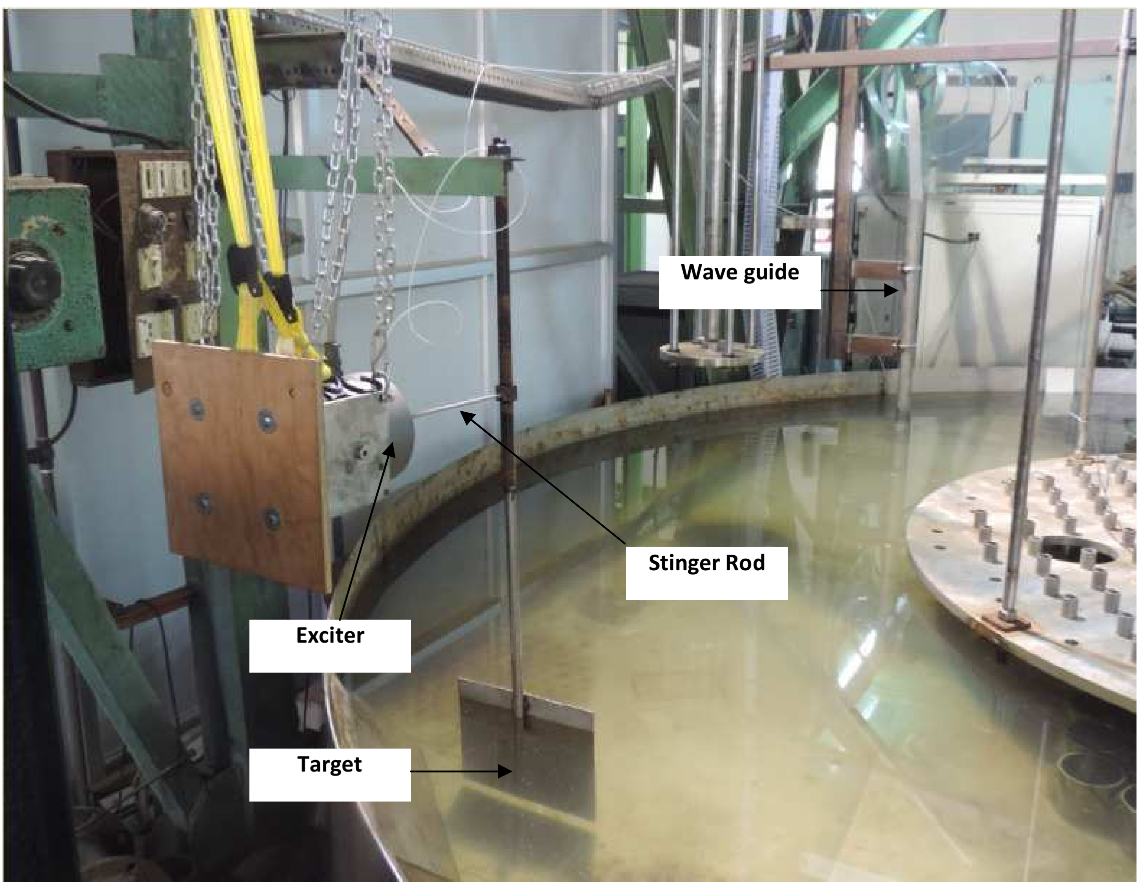

Fig. 5.18: Wave guide focused on the target plate

Ultrasonic waveguide sensor was used in pulse-echo mode at a pulse repetition frequency of 50 Hz for the detection of target vibration. The ultrasound waves emitted by the ultrasonic sensors are focused on the target and measures the time delay between each emitted and echo pulses, to determine the sensor-to-target distance. So continuous triggering of the sensor yields the time of flight corresponding to the target movement. The target plate was excited with a known frequency and the ultrasonic train of pulses from the target for 2 second duration was recorded using the oscilloscope. The recorded data was analyzed and the vibration data from the ultrasonic signal was extracted using the software written in LabVIEW® (National Instruments Inc., USA). Fig. 5.19 and Fig. 5.20 shows the extracted time signal and spectra calculated from the ultrasonic signals for vibration excitation frequencies of 10 Hz and 5 Hz respectively applied to the target plate. The amplitude of vibration measured using the wave guide sensor was compared with that measured using the LVDT. The results indicate that the vibration signals are reliably extracted from the wave guide ultrasonic signal. This developed wave guide technique is promising for its use in remote measurement of vibration of components.

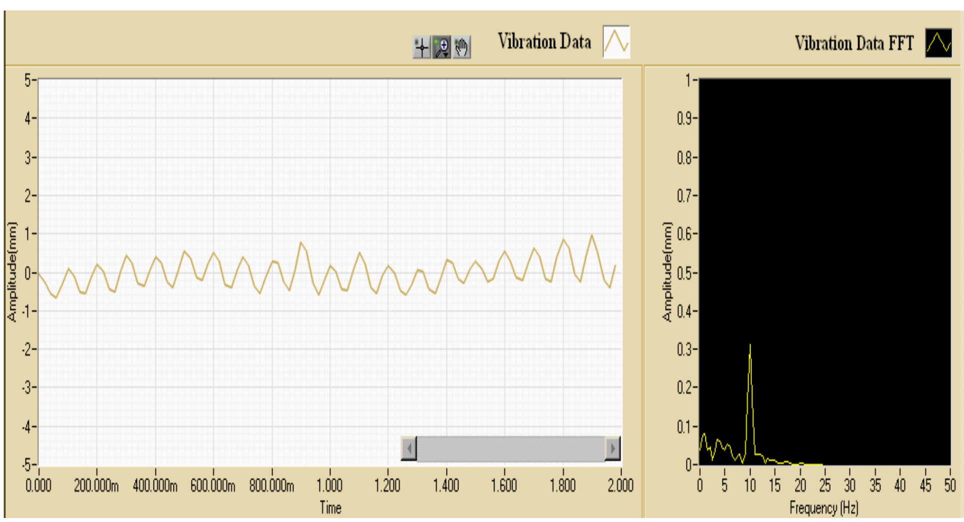

Fig. 5.19: Measured vibration time signal and spectra (10 Hz)

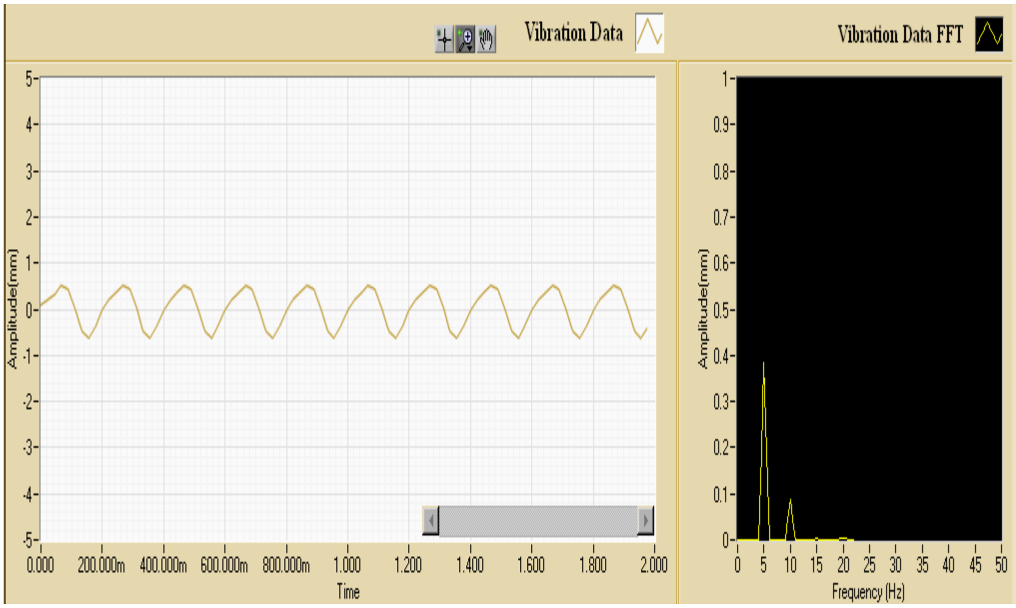

Fig. 5.20: Measured vibration time signal and spectra (5 Hz)

5.11 Applicability of waveguides for sodium measurements

So many parameters need to be considered for developing waveguide system for reactor application, especially when the working fluid is liquid sodium. The major acoustic properties of water and sodium are tabulated in Table 5.2.

Table 5.2 Properties of water and sodium

SN.	Property	Water	Sodium
1.	Velocity (m/s)	1450 at 30^0C	2473 at 200^0C 2420 at 300^0C 2368 at 400^0C 2316 at 500^0C
2.	Density (g/cc)	1	0.8
3.	Acoustic impedence (kg/m^{2}s x 10^6)	1.48	2

The velocity of ultrasonic waves in sodium is around 2316 m/s at 500^0C. Referring the previous section 5.4 regarding the working principle of waveguides, the following equation is used to determine the leaking angle to the surrounding liquid-

$$\beta(fd) = Sin^{-1}\left(\frac{v_L}{c_p(fd)}\right)$$

Considering velocity of ultrasonic waves in sodium at 500^0C, the beam exit angle at the radiation ends turns to be 78.9^0 to the normal to the waveguide. The calculated bend angles of waveguide for various temperatures are tabulated in Table 5.3.

Table 5.3 Bend angles in liquid sodium for SS316

SN.	**Temp. (^{0}C)**	**Phase velocity 'A_0' (m/s)**	**Wave velocity sodium (m/s)**	**Calculated bend angles**
1.	200	2478	2473	86.1^0
2.	250	2460	2446	83.9^0
3.	300	2449	2420	81.2^0
4.	350	2429	2394	80.2^0
5.	400	2409	2368	79.3^0
6.	450	2388	2342	78.6^0
7.	500	2359	2316	78.9^0

This poses a challenge in designing the waveguide with suitable bend angle at the radiation end. Since, bending the waveguide radiation end beyond a certain angle distorts the wave pattern and considering the fact that ultrasonic velocity in liquid sodium is fixed, alternate options such as increasing the velocity of ultrasonic waves in waveguide needs to be carried out. This can be achieved by coating the waveguide with suitable material which is having higher longitudinal wave velocity like Beryllium, which needs further detailed investigation and can be a logical extension of this work.

5.12 Proposed schematic of waveguide Sensor implementation in FBRs

Based on the experimental results, a waveguide design was proposed for its implementation. A typical deployment schematic for reactor application using the developed waveguide is shown in Fig. 5.21. Suitable design of proper guides and drive control systems are required for its practical implementation, similar to that of a SONAR device. This developed waveguide technology is promising and can find application in FBRs for on-line vibration measurement of components like inner vessel, control plug and pump shells, CSRDM and DSRDM, etc. under normal operating conditions at high temperature.

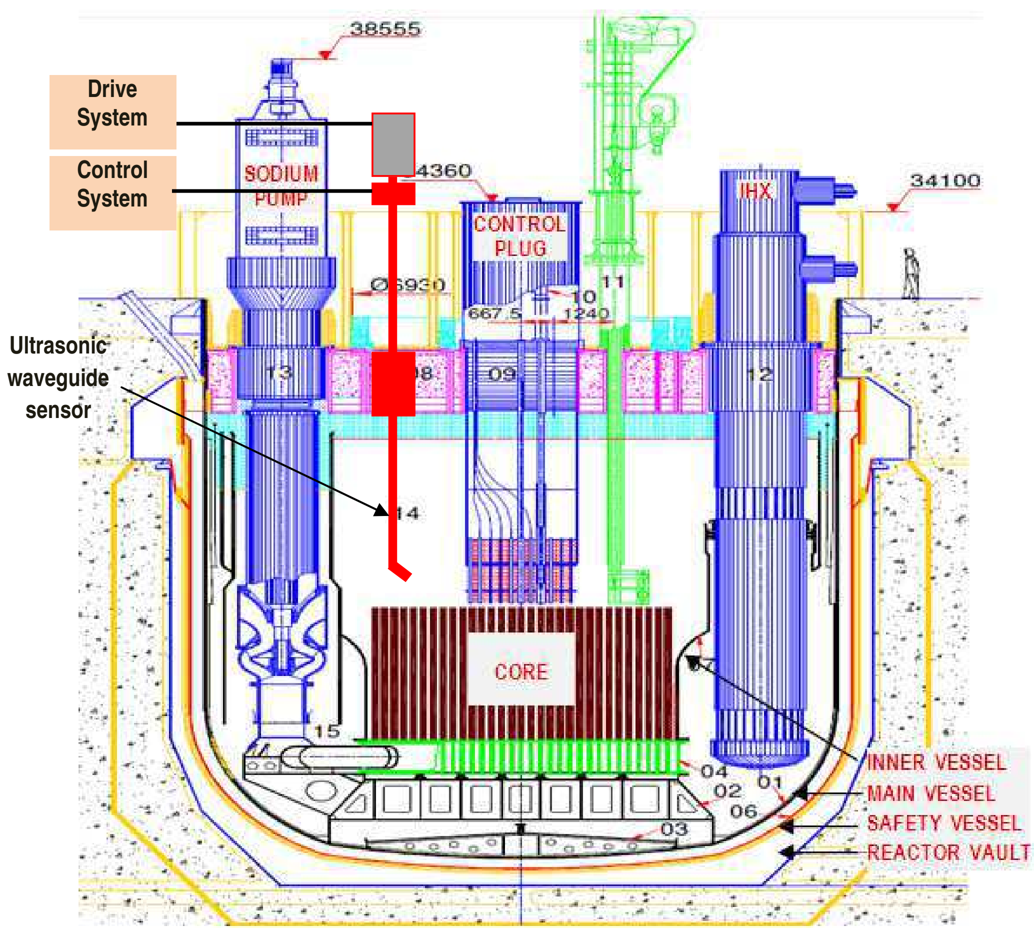

Fig. 5.21: Proposed schematic of waveguide sensor implementation in FBRs

5.13 Summary

- For high temperature applications, a SS316 strip waveguide was developed.
- An ultrasonic waveguide sensor module with aqualene wedge was designed and manufactured.
- Analytical modeling was carried out and A_0 lamb wave mode was selected based on the high out-of-plane displacement component required for enhanced leakage into the liquid sodium.
- The length of the waveguide was fixed as 10 m and thickness as 1.6 mm and operating frequency 1.1 MHz.
- Axial and cross sectional beam profiling studies were carried to optimize the operating parameters of the wave guide.
- Beam exit angle for different operating frequencies were measured and beam steering technique was demonstrated using the waveguide.
- Vibration measurement of a target plate was carried out in water using the developed waveguide sensor.
- A proposed scheme of implementation in FBR is arrived and its applicability to high temperature sodium was discussed.

CHAPTER-6
CONCLUSION AND SCOPE FOR FUTURE WORK

6.1 Conclusion

The important conclusions obtained from the current research studies follows-

- Feasibility of ultrasonic technique for vibration measurement of immersed components in the primary circuit of FBRs established using immersed US sensors.
- Effect of measurement parameters such as PRF, Ultrasonic transducer operating frequency, signal acquisition frequency, etc were discussed.
- No measurable phase shift was observed in the reflected echo with reference to transmitted pulse.
- Ultrasonic sensors for vibration measurement were manufactured in-house and tested using immersion technique.
- Axial and cross sectional beam profiling was carried out to study the symmetry and bonding of the crystal.
- Development of SONAR device with drive mechanism and three US sensors were completed and its testing completed in water.
- Software for drive mechanism and data acquisition and analysis was designed and developed.
- Self vibration of the SONAR device can affect the measured target vibration.
- A horizontal US sensor fixed in the SONAR device measures the amplitude of the self vibration of sonar device, which was used to compensate the measured target vibration.

- Vibration compensation technique was established and it was applied to the measured target vibration to calculate the true vibration of the target.
- Maximum error observed during measurements in comparison with reference LVDT is found to be 5.8% which corresponds to 16 microns.
- For high temperature applications, a SS316 strip waveguide was developed. An ultrasonic waveguide sensor module was designed and manufactured.
- Analytical modeling was carried out and A_0 lamb wave mode was selected based on the high out-of-plane displacement component required for enhanced leakage into the liquid sodium.
- The length of the waveguide was fixed as 10 m and thickness as 1.6 mm and operating frequency 1.1 MHz.
- Axial and cross sectional beam profiling studies were carried to optimize the operating parameters of the wave guide.
- Beam exit angle for different operating frequencies were measured and beam steering technique was demonstrated using the waveguide.
- Vibration measurement of a target plate was carried out in water using the developed waveguide sensor.

6.2 Summary

The research work of this thesis has been focused on vibration measurement of immersed components in the primary pool of FBRs. The main objective of the research is the development of ultrasonic technique for vibration measurement of immersed components in FBRs. Even though ultrasonics finds wide applications in various industries, its application related to FBRs is limited. Sodium is the coolant used in FBRs and is opaque to light. Coolant sodium and high temperature environment poses the challenges of direct vibration measurement techniques, hence calls for alternative solutions like ultrasonic techniques. As part of developing in-service inspection technique, the application of ultrasonic waves is investigated for its usefulness in measuring vibration of sodium-immersed components. In this research work, extensive studies were carried out and a measurement methodology was developed and optimized. Using the developed technique, measurements were carried out using simulated targets and a system named SONAR was developed for PFBR. Studies related to the development of ultrasonic waveguides were also carried out. All the challenging issues were successfully addressed and the end results were found to be very promising for applications in FBRs.

Brief introduction to FBRs, details of PFBR, PFBR primary circuit components, coolant etc. were discussed in detail in the first chapter. Detailed literature survey was carried out on application of ultrasonic techniques in various industries and challenges faced as on today have been identified. Important applications developed using ultrasonic waves are summarized in the first chapter.

The second chapter described the details of internals of PFBR as well as the flow path of coolant in PFBR. Flow induced vibration in FBRs, various FIV mechanisms and its consequences are discussed in details in the second chapter. This chapter also covers FIV studies carried out on PFBR subassembly, similarity criteria followed, test details and its results and discussion. The third chapter discusses the principles and applications of ultrasonic technique. Details of development of ultrasonic technique for vibration measurement were also explained in detail.

Development of SONAR device for vibration measurement of PFBR fuel subassembly was explained in chapter four. The chapter discusses the preliminary experiments carried out, studies using prototype model, optimization of various measurement parameters and development of SONAR device for PFBR. Extensive studies carried out using the device, instrumentation details, vibration compensation techniques and its various test results are discussed in detail in the chapter.

As an extension to the project work, development of ultrasonic waveguide was also carried out. The wave guide is used for the measurement of vibration in hostile high temperature environment. Details of the development of ultrasonic wave guides and its testing is explained in chapter five. A typical scheme of application of waveguide for FBR application was also shown in this chapter. The performance of the waveguide system was satisfactory and encouraging. The technique proved to be very promising for under sodium vibration measurements inside the reactor primary vessel without the use of high temperature sodium immersible ultrasonic sensors.

Ultrasonic technique was studied and implemented for subassembly vibration measurement in PFBR and a measurement device (sonar) was developed for PFBR for subassembly vibration measurement during commissioning. Studies were also carried out for development of ultrasonic waveguide sensors for FBR applications. A waveguide system was developed and tested successfully and was also employed for vibration measurement of a target plate.

6.3 Scope for future work

Development of SONAR device was completed for vibration measurement in PFBR. Development and testing of an ultrasonic waveguide was also demonstrated. These ultrasonic techniques can be used for detecting various anomalies in an operating FBR. Using the developed ultrasonic techniques the following studies can be planned as future works.

6.3.1 Vibration measurements in PFBR using SONAR device

Fuel subassembly vibration measurements are planned in PFBR during commissioning. Measurements will be carried out during the isothermal operation of PFBR at 200^0C with dummy subassemblies in the core. SONAR device is designed and developed for the central canal of control plug of PFBR with proper leak tightness arrangements. By proper rotation of Large Rotatable Plug (LRP) and Small Rotatable Plug (SRP), SONAR device can be positioned on top of any fuel subassembly in the core. Since measurements are planned during isothermal operation, ultrasound velocity will be constant during the measurements.

However effect of gas entrainment in sodium in PFBR primary pool is to be assessed. Entrained gas bubbles in sodium can alter the ultrasound velocity and also attenuate the signal. The effect of entrained gas in sodium on the measurement results can be taken up as a future work. Finite element modeling of ultrasound signal transmission for its application in gas entrainment studies can be carried out as future work.

6.3.2 Design and deployment of waveguide system for future FBRs

A prototype waveguide system for vibration measurement applications in FBR is completed and demonstrated. Further studies in sodium are to be taken up for its completeness and to improve its accuracy. Extension of application of ultrasonic waveguide to study the vibration behavior of primary vessel components such as inner vessel, control plug, pump and IHX shell, CSRDM and DSRDM is planned as future activity. Development of drive system for ultrasonic waveguide and its deployment in FBR also needs to be taken up as a future extension of this activity.

6.3.3 Finite element modeling of waveguide for vibration measurement

Finite element modeling of signal transmission and signal strength obtained at the top of the wave guide during various conditions is to be carried out. In addition to the studies on wave propagation using a single transmitted pulse and its reflected echo, FE modeling of ultrasonic wave transmission coupled with a target in motion needs to be studied as a future activity. Parametric studies by changing the width of the waveguide to optimize the waveguide design and to see its effect on measurement accuracy also can be taken up. Suitable isolation system that is required between wave guide element and outer sheath tube (skirt) so as to isolate the waveguide from surrounding fluid media needs to be studied for high temperature measurements in sodium.

6.3.4 Determination of wave guide operating frequency for different temperatures

During measurements in sodium using the waveguides, depending upon the sodium temperature ultrasound velocity varies and this results in change in the angle of leaky Lamb waves. Hence incident angle of waves on the target, which is supposed to be orthogonal, varies and results in a decrease in amplitude of reflected echo. Since the bend angle of the waveguide element cannot be changed during measurements, correction needs to be done by adjusting the operating frequency of the waveguide. Extensive theoretical studies needs to be carried out considering the material properties at elevated temperatures and variation in sound velocity to determine the leaky Lamb wave exit angle. Experimental validation of the analytical results also can be planned as future work by using specially designed step wedges as target in water and in sodium. Theoretical estimates of beam divergence for water and liquid sodium also helps in determining the range of measurements that can reliably achieved using a waveguide configuration.

REFERENCES

[1] Website, www.amd.gov.in/work/uranium.htm; Atomic Minerals Division.

[2] S.C.Chetal,V.Balasubramaniyan,P.Chellapandi,P.Mohanakrishnan,P.Puthiyavinayagam, C.P.Pillai, S.Raghupathy, T.K.Shanmugham, C.S.Pillai, The design of the prototype fast breeder reactor, Nuclear Engineering and Design, 236(2006), pp 852–860.

[3] Jean-Francois SAUVAGE, EDF-CEA, Phenix- 30 years of history: the heart of a reactor, CEA and EDF, 2004.

[4] J.L. Berton, et. al., Continuous monitoring of the position of two subassemblies heads of Phenix at 350 MWth power and 550^0C temperature, 7th Symposium on reactor surveillance and diagnostics, SMORN-VII, June 1995, Avignon, France.

[5] M.K. Au-Yang, Application of ultrasonic to non-intrusive vibration measurement, Journal of pressure vessel technology, Vol 115, pp 415-419, Nov 1993.

[6] Prakash, V., et al., Experimental qualification of subassembly design for Prototype Fast Breeder Reactor. Nucl. Eng. Des. 241 (2011), 3325–3332.

[7] M. Thirumalai, M. Anandaraj, P. Anup Kumar, V. Prakash, C. Anandbabu, P. Kalyanasundaram, G. Vaidyanathan, Experimental investigation of weir instability in main vessel cooling system of 1/4 FBR model, Nuclear Engineering and Design 240 (2010) 84–91

[8] Website: https://projectgroupf.wordpress.com/vortex-shedding/

[9] Website: http://www.lvdt.co.uk/how-lvdts-work/

[10] Website: http://www.azom.com

[11] Website: http://www.slideshare.net/

[12] Website: https://ecourses.ou.edu

[13] Bruel and Kjaer (B&K) Vibration handbook.

[14] Clarence W. de Silva, Vibration Fundamentals and Practice, CRC Press, Boca Raton London New York Washington, D.C.

[15] http://www.dewetron.nl/dewe_5000/

[16] G. Srinivasan, et.al., The Fast Breeder Test Reactor- Design and Operating Experience, Nuclear Engineering and Design 236, (7-8), pp. 796-811.

[17] M. Anandaraj et. al., Flow induced vibration studies on PFBR fuel subassembly. Second international conference on asian nuclear prospects 2010 (ANUP-2010), Chennai, India

[18] M. Thirumalai et. al., Subassembly hydraulic experiments. THEME Meeting on challenges in Thermal hydraulics of nuclear reactors, TM-CTHNR 2010, Kalpakkam, Tamilnadu, India. Feb 18-19, 2010.

[19] S. Govindarajan, Structural design criteria for irradiated core components, Design document for PFBR, Internal report PFBR/31100/DN/1007/R-0.

[20] J.A. Ryan and L.J. Julyk, FFTF scale model characterization of flow induced vibrational response of reactor internals, IAEA Specialist meeting on LMFBR flow induced vibrations, Argonne, Illinois, USA, Sept 1977.

[21] E.H. Novedsten, F.A.Grochowski, T.M.Yang, J.A.Ryan and T.M.Mulcaly, CRBRP Flow induced vibration programme, IAEA Specialist meeting on LMFBR flow induced vibrations, Argonne, Illinois, USA Sept 1977.

[22] G. Padmakumar, et al, Comprehensive scale model for LMFBR reactor assembly thermal hydraulics, International Journal of Nuclear Energy Science and Technology, Vol. 3, No. 4, 2007, pp. 325-344.

[23] M. Anandaraj et.al., FIV testing of PFBR control plug model, Internal Report: FRTG/CMS/99221/EX/3038.

[24] Jalaldeen, S., Balasubramanian, V., Chellapandi, P., Bhoje, S.B., 1991. Fluid-elastic instability analysis for PFBR main vessel cooling circuit. In: SMiRT 11, vol. E12/3, pp. 353–358.

[25] Aita, S., Tigeot, Y., Saclay, C.E.N., Bertaut, C., Serpantie, J.P., 1986. Fluid elastic instability analysis of a flexible weir: experimental observations. In: ASME PVP 1986 Conference, vol. 104, pp. 41–49.

[26] Website: www.olympus.in

[27] Website: www.nde-ed.org

[28] IAEA-TechDoc- 462, Ultrasonic testing of materials at Level 2, Training manual for non-destructive testing techniques, A technical document issued by the International Atomic Energy Agency, Vienna, 1988.

[29] Website: https://www.classle.net

[30] Datasheet- Olympus make Pulser Receiver: Model 5072 PR

[31] www.ni.com/LabVIEW-basics

[32] J.A. McKnight, et. al., Recent advances in the technology of under sodium inspection in LMFBRs, Liquid Metal Engineering and Technology, BNES, London, pp. 423-430, 1984.

[33] K. Swaminathan, et. al., The development and deployment of ultrasonic under sodium viewing system in the Fast Breeder Test Reactor, IEEE Trans. Nucl. Sci. 37 (5) (1990), pp. 1571-1577.

[34] K. Swaminathan, et. al., An ultrasonic scanning technique for in-situ 'Bowing' measurements of Prototype Fast Breeder Reactor fuel subassembly, IEEE Trans. Nucl. Sci. Feb., Vol. 59, No.1, pp. 174-181.

[35] L.M. Barrett, et. al., Ultrasonic viewing in Fast Reactors, Physics in Technology, 1984, 15(6), pp. 308-314.

[36] R.D. Watkins, et. al., A proposed method for generating and receiving narrow beams of ultrasound in the Fast reactor liquid sodium environment, Ultrasonic, November 1982

[37] J.I. Sylvia, et. al., Ultrasonic imaging of projected components of PFBR, Nuclear Engineering and Design 2013, Vol. 258, pp. 266-274.

[38] G. Seed, In-service inspection and monitoring of CDFR, Nuclear Energy 1986, 24(2), pp. 129-135.

[39] F. Baque, et. al., Review of in-service inspection and repair technique developments for French liquid metal fast reactors, Vol. 150 (1), 2005, pp. 67-78.

[40] N. Uesugi, et. al., An ultrasonic viewing system in liquid sodium, IEEE Nuclear Science Symposium, USA, Oct. 1979.

[41] H.A. Rohrbacher, et. al., Ultrasonic and acoustic detection methods for LMFBR's, Proc. BNES Conf. Fast Reactor Power Stations (London Thomas Telford), 1974, pp.505-514.

[42] Young-Sang Joo, et. al., Development of ultrasonic waveguide sensor for under-sodium inspection in a sodium-cooled fast reactor, NDT&E International 44 (2011) 239–246.

[43] R.D. Watkins, et. al., Ultrasonic waveguide for use in sodium coolant of fast reactors, Nuclear Energy 27 (2) (1988), pp. 85-91.

[44] K.F. Graff, 1991, Wave motion in elastic solids, Dover Publications, New York.

[45] Brian Pavlakovic and Mike Lowe, User's Manual, DISPERSE A system for generating dispersion curves, Version 2.0.16B, 2003, Non-Destructive Testing Laboratory, Imperial College London, UK.

[46] J.L. Rose, Ultrasonic waves in solid media, Cambridge University Press (1999).

[47] B. Pavlakovic et. al., DISPERSE: A general purpose program for creating dispersion curves, Review of Progress in Quantitative NDE 16 (1997), pp. 185-192.

[48] Friedrich Mosera, et. al., Modelling elastic wave propagation in waveguides with the finite element method, NDT&E International 32 (1999), pp. 225-234.

[49] Ivan Bartoli, et. al., Modelling guided wave propagation with application to the long range defect detection in rail road tracks, NDT&E International 38 (2005), pp. 325-334.

[50] T. Hayashi, et. al., Wave structure analysis of guided waves in a bar with an arbitrary cross section, Ultrasonics 44 (2006), pp. 17-24.

[51] M.O. Deighton, et. al., Mode conversion of Rayleigh and Lamb waves to compression waves at a metal-liquid interface, Ultrasonics, November 1981.

[52] Turn Bull, et.al., Beam steering with pulsed two dimensional transducer arrays, IEEE Trans. Ultrason. Ferroelectrics Freq. Contr. 38(4), pp. 320-333.

[53] Y.S. Joo, et. al., Beam steering technique of ultrasonic waveguide sensor for under sodium inspection of Sodium Fast Reactor, ICONE 13-50340, 2005.